A. COMPETITION AND ALLOSTERY GOVERN SUBSTRATE SELECTIVITY OF CYCLOOXYGENASE-2

B. ENZYMATIC OXIDATION OF M_1dG IN THE GENOME

By

Michelle Marie Mitchener

Dissertation

Submitted to the Faculty of the

Graduate School of Vanderbilt University

in partial fulfillment of the requirements

for the degree of

DOCTOR OF PHILOSOPHY

in

Chemistry

December 16, 2017

Nashville, Tennessee

Approved:

Lawrence J. Marnett, Ph.D.

Brian O. Bachmann, Ph.D.

Walter J. Chazin, Ph.D.

Ned A. Porter, Ph.D.

To my family

As promised, you were always just a phone call away.

ACKNOWLEDGEMENTS

First, I would like to thank my mentor, Larry Marnett, for accepting me into his laboratory and guiding me through my graduate studies. Over the entire course of my time here at Vanderbilt, Larry has cared about me both as a person and as a scientist. Importantly, he has believed in me and my abilities when I have not. I would not be the scientist I am today without his leadership and encouragement.

I am also thankful to the many others in leadership positions who have promoted my success as a graduate student. My thesis committee, composed of Larry, Brian Bachmann, Ned Porter, and Walter Chazin, has provided helpful feedback and shown great flexibility with regard to scheduling committee meetings. I would like to thank Larry's administrative team, especially Anne Lara, for scheduling these and other meetings and for answering work-related questions that no one else could.

I have been privileged to work with many talented postdoctoral associates, graduate students, and research assistants during my tenure in the Marnett laboratory. Though I lack room to thoroughly thank each one for his/her contribution to my education, I would like to thank a few members who played key roles in my scientific development. I am grateful to Will Beavers for involving me in his own research early in my graduate studies when I was struggling with my own project. He always believed that I had more potential than I myself thought, and he truly wanted to see me succeed. I would also like to thank Jim Galligan for offering me good experimental ideas and accepting some from me in return. Jim treated

me as a scientific peer despite his academic seniority. I am indebted to Phil Kingsley for teaching me almost everything I know about bioanalytical methodologies. He was also always there to remind me to keep both my scientific successes and failures in perspective. I am thankful that Orrette Wauchope allowed me to join him in studying lipid electrophile-induced DNA damage. Orrette's willingness to collaborate and explain experimental methods eased my transition to the study of DNA adducts. Finally, I must thank Carol Rouzer, not only for editing countless documents for me, but also for essentially serving a second advisor. Carol encouraged and guided me, both broadly speaking and experimentally, during a critical time in my Ph.D. career; I doubt I would have persevered through that time if it were not for her assistance.

Outside of the laboratory, I have had an incredible support network of friends as well. I must thank my roommate, Erin Shockley, for putting up with me for the past five and a half years and for allowing me to play with and occasionally cry on her cat, Leila. I am also grateful to the friends whom I have met through InterVarsity's Graduate Christian Fellowship. In the midst of the busyness and pressure of graduate study, they have helped me distinguish between things of temporal importance and those of eternal significance. My church family at Brook Hollow Baptist Church has also been a constant source of encouragement over the years. They have rejoiced with me in my successes and mourned with me in my failures, but above all they have reminded me to do all that I do to the glory of God.

Lastly, I would like to thank my family, including my extended family, for their prayers and support. Uncle Steve, Aunt Holly, and family deserve special thanks for inviting me to Memphis each Thanksgiving so that I would not have to spend the holiday alone. Above all, I need to thank my parents and my sister. I am who I am and where I am today primarily because of them.

TABLE OF CONTENTS

LIST OF TABLES

LIST OF FIGURES

LIST OF ABBREVIATIONS

α-KG	alpha-ketoglutarate
1-AG	1-arachidonoylglycerol
2-AG	2-arachidonoylglycerol
AA	arachidonic acid
AEA	arachidonylethanolamide
AO	aldehyde oxidase
BSA	bovine serum albumin
CORM	COX-2 Reaction Model
COX	cyclooxygenase
COX-1	cyclooxygenase-1
COX-2	cyclooxygenase-2
$cPLA_2\alpha$	cytosolic phospholipase A_2 alpha
dA	2'-deoxyadenosine
DAG	diacylglycerol
DAGL	diacylglycerol lipase
dC	2'-deoxycytidine
dG	2'-deoxyguanosine
DMEM	Dulbecco's Modified Eagle Medium
DMSO	dimethyl sulfoxide
dsDNA	double-stranded DNA
dT	2'-deoxythymidine
EGF	epidermal growth factor

FBS	fetal bovine serum
GM-CSF	granulocyte/macrophage colony-stimulating factor
hCOX-2	purified human COX-2
IFN-γ	interferon-gamma
IOX1	8-hydroxy-5-quinolinecarboxylic acid
LC-MS/MS	liquid chromatography tandem mass spectrometry
LPS	lipopolysaccharides
LYPLA2	lysophospholipase A2
m1A	1-methyladenosine
M_1dG	3-(2-deoxy-β-D-erythro-pentofuranosyl)pyrimido[1,2-α]purin-10(3H)-one
mCOX-2	purified murine COX-2
MDA	malondialdehyde
N-OG	*N*-oxalylglycine
NAC	*N*-acetylcysteine
NAGly	*N*-arachidonylglycine
NER	nucleotide excision repair
NF-κB	nuclear factor kappa-light-chain-enhancer of activated B cells
NSAID	nonsteroidal anti-inflammatory drug
PBS	phosphate buffered saline
PG	prostaglandin
PG-G	prostaglandin glyceryl ester
PGD_2	prostaglandin D_2

PGE_2	prostaglandin E_2
$PGF_{2\alpha}$	prostaglandin $F_{2\alpha}$
PGG_2	prostaglandin G_2
PGG_2-G	prostaglandin G_2-glycerol
PGH_2	prostaglandin H_2
PGH_2-G	prostaglandin H_2-glycerol
PGI_2	prostacyclin
PIP_2	phosphatidylinositol 4,5-bisphosphate
PLC	phospholipase C
PPHP	5-phenyl-4*E*-pentenyl-1-hydroperoxide
PUFA	polyunsaturated fatty acid
RPM	resident peritoneal macrophage
RPMI	Roswell Park Memorial Institute medium
SILAC	Stable Isotope Labeling by Amino Acids in Cell Culture
ssDNA	single-stranded DNA
TEMPOL	4-hydroxy-2,2,6,6-tetramethylpiperidin-1-oxyl
TxA_2	thromboxane A_2
XO	xanthine oxidase

CHAPTER I

INTRODUCTION

Inflammation

Hallmarks of Inflammation

Inflammation is the immune system's response to infection and injury that serves to protect the host against an invading pathogen or external assault. The acute phase of inflammation is characterized by an influx of neutrophils followed by monocytes that mature into inflammatory macrophages. The migration of immune cells to the region of insult and their subsequent activation by a variety of signaling molecules give rise to the cardinal characteristics of inflammation (Fig. 1). These include redness (due to increased blood flow to the area), pain (via direct small molecule mediator effects and through stretching of sensory nerves due to swelling), heat (due to increased blood flow and greater local cellular metabolism), and swelling (edema due to increased blood flow and immune cell infiltration of the area) (1). Upon removal of the noxious stimulus or clearance of the pathogen, these inflammatory symptoms typically subside in what is known as resolution of inflammation. Failure of resolution gives rise to the final cardinal characteristic of an inflammatory state which is loss of function of the affected tissue and predisposition to disease. In fact, chronic inflammation plays a role in a variety of

diseases, including arthritis, cancer, stroke, diabetes, cardiovascular disease, and neurodegenerative diseases.

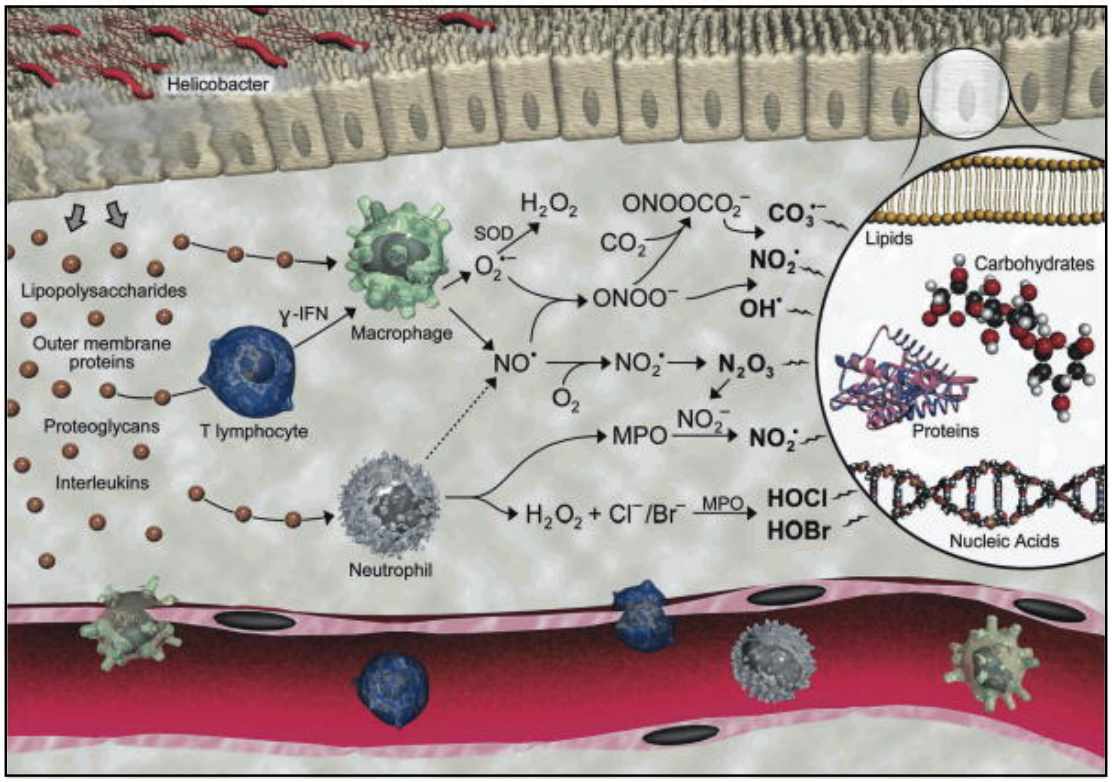

Figure 1. The chemical biology of inflammation. Illustration by Jeff Dixon. Reprinted with permission from Macmillan Publishers Ltd: Taghizadeh, K, *et al. Nature Protocols* **(2008)**, 3; 1287. Copyright 2008 (2).

Oxidation of polyunsaturated fatty acids (PUFAs)—whether enzymatic or non-enzymatic—contributes to the inflammatory response and its associated cellular pathologies. Therefore, the Marnett laboratory has had a longstanding interest in understanding PUFA oxidation in the context of inflammation and in characterizing how it may contribute to disease development and progression. Herein I will briefly introduce one enzymatic pathway and one non-enzymatic

pathway of PUFA oxidation as they relate to the inflammatory response and, in the following sections, delve more deeply into the particulars of each as they relate to my dissertation aims.

Cyclooxygenase-2 induction and prostaglandin formation

Cyclooxygenases (COXs) catalyze the regio- and stereo-specifically controlled autoxidation of PUFAs, particularly arachidonic acid (AA), to give prostaglandin endoperoxides, the precursor molecules to prostaglandins (PGs). PGs are lipid mediators that, in addition to other functions, play a key role in the chemotactic and vasoactive events of inflammation. The COX enzymes carry out the rate-limiting step in PG synthesis by oxidizing AA to yield prostaglandin G_2 (PGG_2), which they also subsequently reduce to prostaglandin H_2 (PGH_2). PGH_2 is then acted upon by a variety of tissue-specific synthases to yield a diversity of prostaglandin products, including prostaglandin E_2 (PGE_2), prostaglandin D_2 (PGD_2), prostacyclin (PGI_2), prostaglandin $F_{2\alpha}$ ($PGF_{2\alpha}$), and thromboxane A_2 (TxA_2) (1).

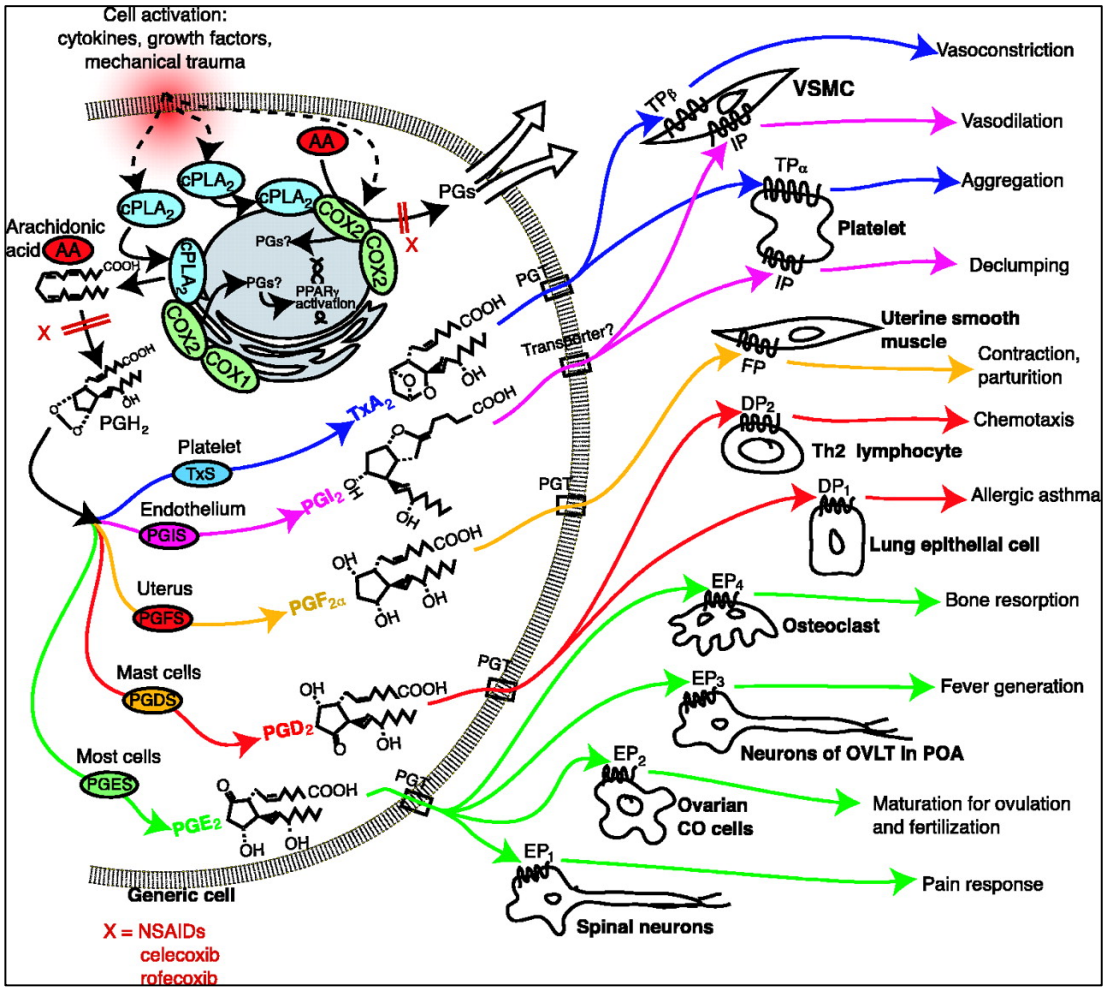

Figure 2. Prostaglandin synthesis and actions. A "generic" cell when activated by mechanical trauma, cytokines, growth factors, or various inflammatory stimuli triggers signaling, including type IV cytosolic phospholipase ($cPLA_2$) translocation to ER and nuclear membranes, AA release from membrane lipids, and metabolism by cyclooxygenase-1 (COX-1) or cyclooxygenase-2 (COX-2) to the intermediate PGH_2. Other PLA_2 subtypes could be involved in AA release for eicosanoid synthesis but are not shown here. *De novo* COX-2 enzyme synthesis can be induced by a host of factors (top) to reinforce PG formation. In a cell type-restricted fashion, a heterogeneous family of PGH_2 metabolizing enzymes can form PGE_2, PGD_2, $PGF_{2\alpha}$, PGI_2, and/or TxA_2. These PGs may undergo facilitated transport from the cell through a known PG transporter (PGT) or other carrier to exert autocrine or paracrine actions on a family of PG receptors EP_1, EP_2, EP_3, EP_4, DP_1, DP_2, FP, IP, TP_α, and TP_β on the cell types indicated. Only a few of the many diverse activities of PGs are shown here. PGs could potentially enter the nucleus and activate nuclear hormone receptors such as PPAR-γ. PGES, PGE synthase; PGDS, PGD synthase; PGFS, PGF synthase; PGIS, prostacyclin synthase; TxS, thromboxane synthase. VSMC is vascular smooth muscle cell. OVLT in POA is the organum vasculosa lamina terminalis at the midline of the preoptic area. CO cells are cells of the cumulus oophorus. X marks the site of inhibition by NSAIDs (aspirin, ibuprofen, indomethacin) and the coxibs celecoxib (Celebrex) and rofecoxib (Vioxx). Reprinted from *Science*, 294(5548), Funk, C.D., Prostaglandins and leukotrienes: Advances in eicosanoid biology, 1871-1875, Copyright (2001), with permission from AAAS (3).

The PG species then exert their effects via their respective G protein-coupled receptors, which include PGE_2 receptors 1-4, PGD_2 receptors 1-2, PGI_2 receptor, $PGF_{2\alpha}$ receptors A and B, and thromboxane receptors α and β (Fig. 2). Typically, one or two PGs are produced per cell type, and they act locally as autocrine and paracrine lipid mediators to modulate the inflammatory response and/or maintain local homeostasis.

One of the two COX isoforms, COX-2, is preferentially induced in response to a variety of inflammatory stimuli and is largely thought to be responsible for the plethora of PG molecules involved in inflammatory signaling. The first molecules to be identified as inducers of COX-2 expression in macrophages were lipopolysaccharides (LPSs) that are present in the cell walls of all gram-negative bacteria (4). LPSs bind to toll like-receptor 4 (TLR4) and activate the nuclear factor kappa B signaling pathway to induce COX-2 transcription (5). LPS signaling through TLR4 also leads to the phosphorylation of cAMP-responsive element-binding protein, another central regulator of COX-2 transcription (6). Furthermore, a variety of pro-inflammatory cytokines, including interleukin-1 and interferon- γ (IFN-γ), as well as growth factors, such as insulin-like growth factor, transforming growth factor-α, and epidermal growth factor (EGF), induce COX-2 expression (5). The role of PGs in promotion of pain, fever, and inflammation, is affirmed by the clinical efficacy of structurally distinct non-steroidal anti-inflammatory drugs (NSAIDs), all of which inhibit COXs and therefore PG synthesis (7). Inhibitor and knockout studies in mice also attest to the importance of COX-2 in acute inflammation and its resolution (8).

Reactive species and lipid autoxidation

Concomitant with the enzymatic oxidation of lipids to yield signaling molecules, such as PGs, for recruitment of other inflammatory cells, vasoconstriction, inflammation resolution, and wound healing, immune cells also release a variety of small molecule reactive oxygen and nitrogen species (Fig. 1). The production of these toxic metabolites may be viewed as an attempt to defend the body against an invading pathogen via a sort of “chemical warfare” limited to the region of initial infection. For example, activation of macrophages and neutrophils results in increased O_2 consumption by NADPH oxidase yielding increased levels of superoxide (O_2^-) (9). The coupled reduction of O_2 and oxidation of arginine by nitric oxide synthase (NOS) yields nitric oxide (NO) (10). NO can react with O_2^- at an approximately diffusion-limited rate to give peroxynitrite ($NOOO^-$) (11), which when protonated forms the strong oxidant peroxynitrous acid (NOOOH) (12). $NOOO^-$ can also couple with CO_2 to form peroxynitrosocarbonate ($NOOOCO_2^-$) (2). Further homolytic breakdown of each of these products produces highly reactive oxygen and nitrogen species that can not only wreak havoc on the invading pathogen but also invoke collateral damage on the cell’s own macromolecules. PUFAs, preferentially located at the *sn*-2 position of membrane glycerophospholipids, are especially prone to oxidation due to the presence of two or more allylic hydrogen atoms (13). Hydrogen abstraction produces a carbon-centered radical that then couples with O_2 to form a peroxyl radical (Fig. 3). This peroxyl radical may abstract another hydrogen atom from a neighboring PUFA, thus propagating the radical reaction.

Such chain reactions proceed until two lipid radical species react with each other or until a membrane-bound antioxidant, principally vitamin E, reacts with a lipid peroxyl radical to terminate autoxidation and prevent further membrane damage (14). The fatty acid hydroperoxides generated during PUFA autoxidation are subject to chemical breakdown to yield a variety of electrophilic species that can modify nucleophilic residues on proteins and DNA and potentially alter their functions. One such electrophilic molecule, malondialdehyde (MDA), will be the focus of a later section.

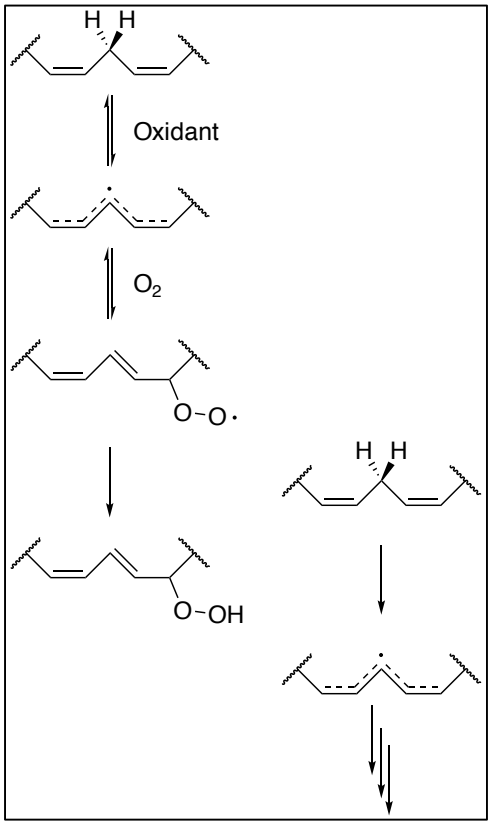

Figure 3. Generalized schematic of PUFA autoxidation. Abstraction of a *bis*-allylic hydrogen atom results in a pentadienyl radical (initiation), which reacts with O_2 to form a peroxyl radical. The peroxyl radical can then abstract a *bis*-allylic hydrogen atom from a neighboring PUFA thereby generating a new pentadienyl radical (propagation) while terminating itself to the fatty acid hydroperoxide (termination).

Enzymatic PUFA oxidation by COX-2

COX structure and function

The COX enzymes carry out the bis-dioxygenation of AA to give PGG_2 at their cyclooxygenase active site and the subsequent reduction of PGG_2 to PGH_2 at a distinct peroxidase active site (15-17). PGH_2 then serves as a substrate for a variety of PG synthases that convert the molecule to an array of cell-type specific signaling species, including PGE_2, PGD_2, $PGF_{2\alpha}$, PGI_2, and TxA_2, as aforementioned (3). In addition to AA, the COX enzymes can also oxygenate a panoply of PUFAs and AA amide and ester derivatives, albeit with reduced catalytic efficiency that varies between the two isoforms. The products of these reactions range from hydroxyl fatty acids to PG analogs depending on the number and arrangement of double bonds in the substrate (18-21).

As the COX enzymes carry out the rate-limiting step in PG synthesis, they have, perhaps not surprisingly, become targets for pharmacological intervention. In fact, COXs are the target of an array of popular NSAIDs designed to suppress pain, fever, and inflammation, including ibuprofen (Advil), naproxen (Aleve), and aspirin. There are two isoforms of the enzyme, COX-1 and COX-2. COX-1 is constitutively expressed in many tissues and consequently has been assumed to play a housekeeping role in most cells. COX-2 is not expressed or expressed at low levels in most tissues, but its expression can be induced by a variety of inflammatory stimuli (22-24). The apparent homeostatic versus inflammatory function of COX-1 and COX-2, respectively, led to the development and release of

COX-2-selective inhibitors celecoxib (Celebrex) and rofecoxib (Vioxx) onto the pharmaceutical market in the early 2000s. However, information regarding potential cardiovascular risks of the drugs surfaced, reducing enthusiasm for their clinical application (25-29).

The two COX isoforms share 60% sequence identity and are very similar in their overall folding (30-33). Both are homodimers, composed of sequence-equivalent subunits of 70 kDa each, and both enzymes require one molecule of heme per dimer for full catalytic activity (34-36).

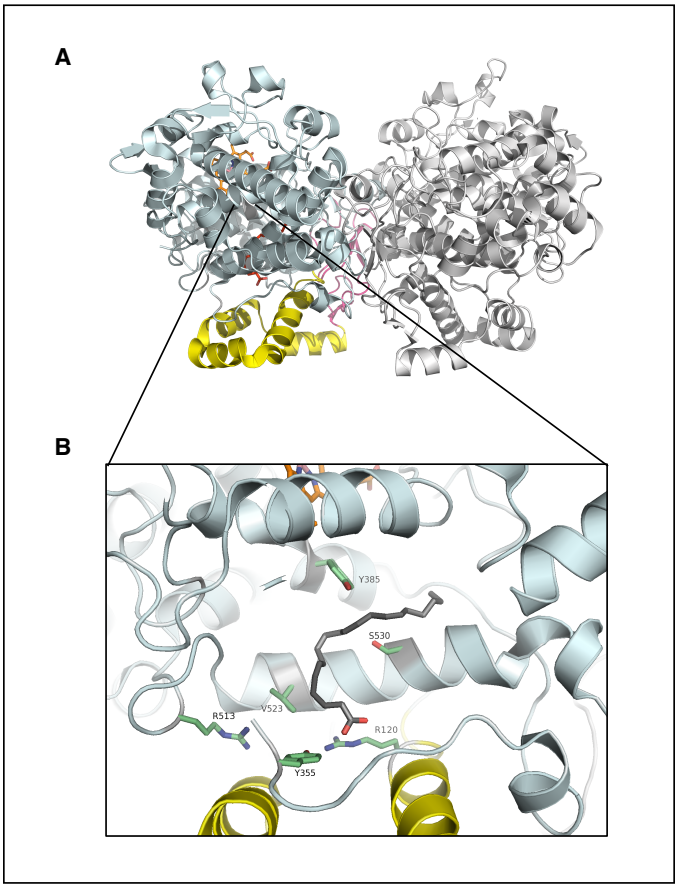

Figure 4. COX-2 structure. (*A*) Sequence homodimer with catalytic (colored) and allosteric (gray) subunits. Pictured are the EGF domain (pink), membrane-binding domain (yellow), and catalytic domain (pale blue) with heme cofactor (orange). (*B*) Close-up of the COX active site showing bound AA (black) and select amino acid residues (green). Figure generated with the kind help of Shu Xu.

Each subunit contains an EGF domain, the function of which is largely unknown; a membrane-binding domain, with which to tether itself to one face of a membrane bilayer; and a catalytic domain, which contains the non-covalently associated heme that is requisite for both the cyclooxygenase and peroxidase activities of the enzyme and is shared between the two respective active sites (30-32, 37) (Fig. 4*A*). Immunoelectron microscopy experiments and western blot analysis of subcellular fractions have revealed that COX localizes to the lumen of the endoplasmic reticulum and to the inner and outer membranes of the nuclear envelope (38).

COX mechanism

Initial experiments confirming the catalytic activity of COXs involved incubation of radiolabeled AA with homogenates of ram seminal vesicles, wherein the researchers ultimately obtained radiolabeled PGE_2 product (upon spontaneous breakdown of radiolabeled PGH_2), thereby confirming fatty acids were the biosynthetic precursors of PGs (39, 40). This discovery ignited interest in exploring the mechanism for this reaction. Further experiments with stereospecifically isotopically labeled substrate revealed selective enzymatic removal of the carbon-13 *pro*-(*S*)-hydrogen (41). These studies, combined with previously established chemistry regarding PUFA autoxidation, led Hamberg and Samuelsson to propose a free radical mechanism for the oxygenation of AA by COX (41-43). This mechanism, with added insight gained from studies of the relationship between the cyclooxygenase and peroxidase activities of the COX

enzymes, spectral studies of the heme iron oxidation state, and electron paramagnetic resonance studies characterizing the free radicals in COX catalysis, led to our current understanding of the overall mechanism of COX activation and catalysis (Fig. 5).

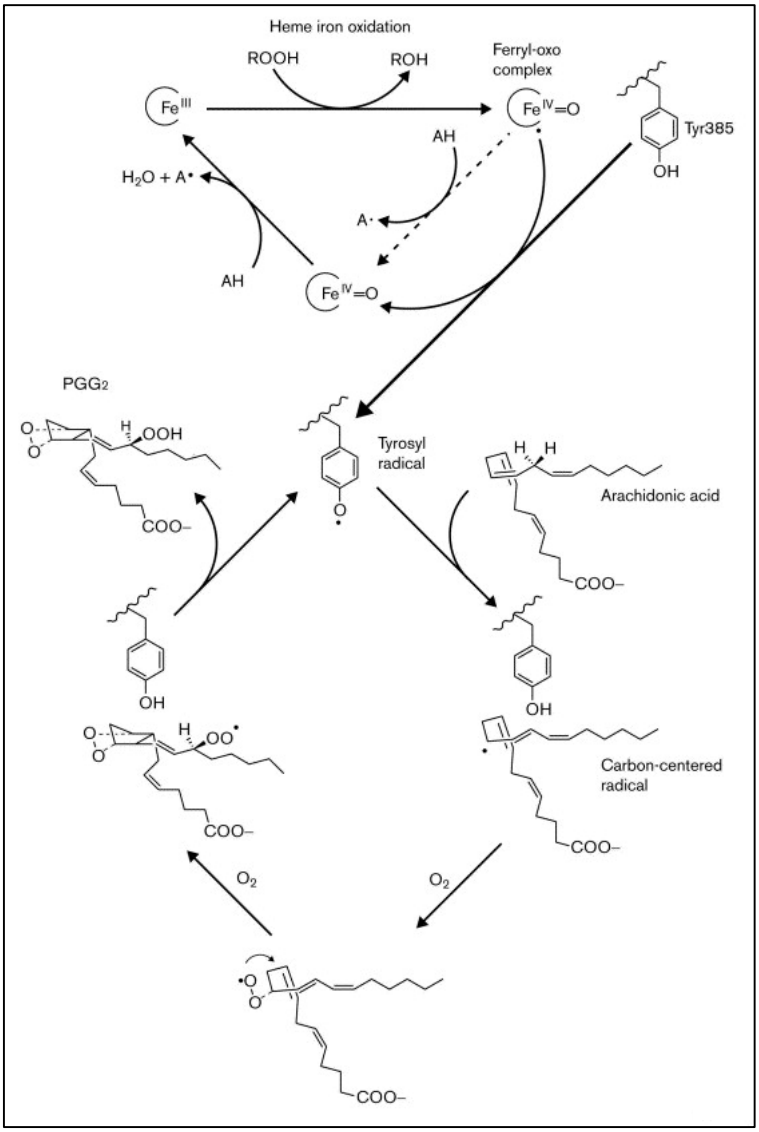

Figure 5. Mechanism of COX activation and catalysis. A hydroperoxide oxidizes the heme prosthetic group to a ferryl-oxo derivative that can be reduced in the second step of the peroxidase catalytic cycle or can oxidize Tyr385 to a tyrosyl radical (upper half of figure). The tyrosyl radical then abstracts the 13-*pro*-(*S*) hydrogen of AA to initiate the cyclooxygenase catalytic cycle (lower half of figure). Reprinted from *Curr Opin Chem Biol.*, 4(5), Marnett, L.J., Cyclooxygenase mechanisms, 545-552, Copyright (2000), with permission from Elsevier (44).

In this model, COX enzymes are synthesized and exist in cells as mature but inactive proteins that must first react with a hydroperoxide activator before they can initiate catalysis. In test tube experiments, this is likely an autoxidation product of the PUFA being assayed, since commercial preparations commonly contain 0.5-1% hydroperoxide impurities as a result of autoxidation during storage. Whereas the identity of the hydroperoxide activator in cells is less certain and probably varies by cell type, some evidence suggests NOOOH might serve such a role in inflammatory cells (such as monocytes, macrophages, and neutrophils) (45-47).

Hydroperoxide oxidation of the heme prosthetic group initiates the peroxidase cycle (upper half of Fig. 5) via generation of a ferryl-oxo complex. This complex can react sequentially with two molecules of peroxidase reductant (AH), such as phenol, to regenerate Fe(III) heme (35, 48, 49). Alternatively, the ferryl-oxo complex can abstract a hydrogen atom from the nearby Tyr-385 (Fig. 4*B*), forming the catalytic tyrosyl radical (50, 51) that will initiate the cyclooxygenase cycle (lower half of Fig. 5). The tyrosyl radical abstracts the 13-*pro*-(*S*)-hydrogen from AA to give a carbon-centered radical. This species reacts with a molecule of oxygen to form a peroxyl radical, which then cyclizes intramolecularly to form an endoperoxide followed by rearrangement to form the characteristic five-carbon prostanoid ring structure. The new carbon-centered radical will then react with a second molecule of oxygen followed by abstraction of a hydrogen atom from Tyr-385 to yield the final PGG_2 product and regenerate the catalytic tyrosine. The newly formed PGG_2 molecule subsequently can serve

as a hydroperoxide activator for another COX homodimer, leading to its own reduction to the alcohol PGH_2 at the peroxidase active site of that enzyme.

As one might anticipate, based upon the need for hydroperoxide activation prior to catalysis, the time-course of COX reactions *in vitro* exhibits a lag phase (52-55) (Fig. 6). The reaction also ceases prematurely, that is, before all of the available substrate is consumed, indicative of enzyme inactivation.

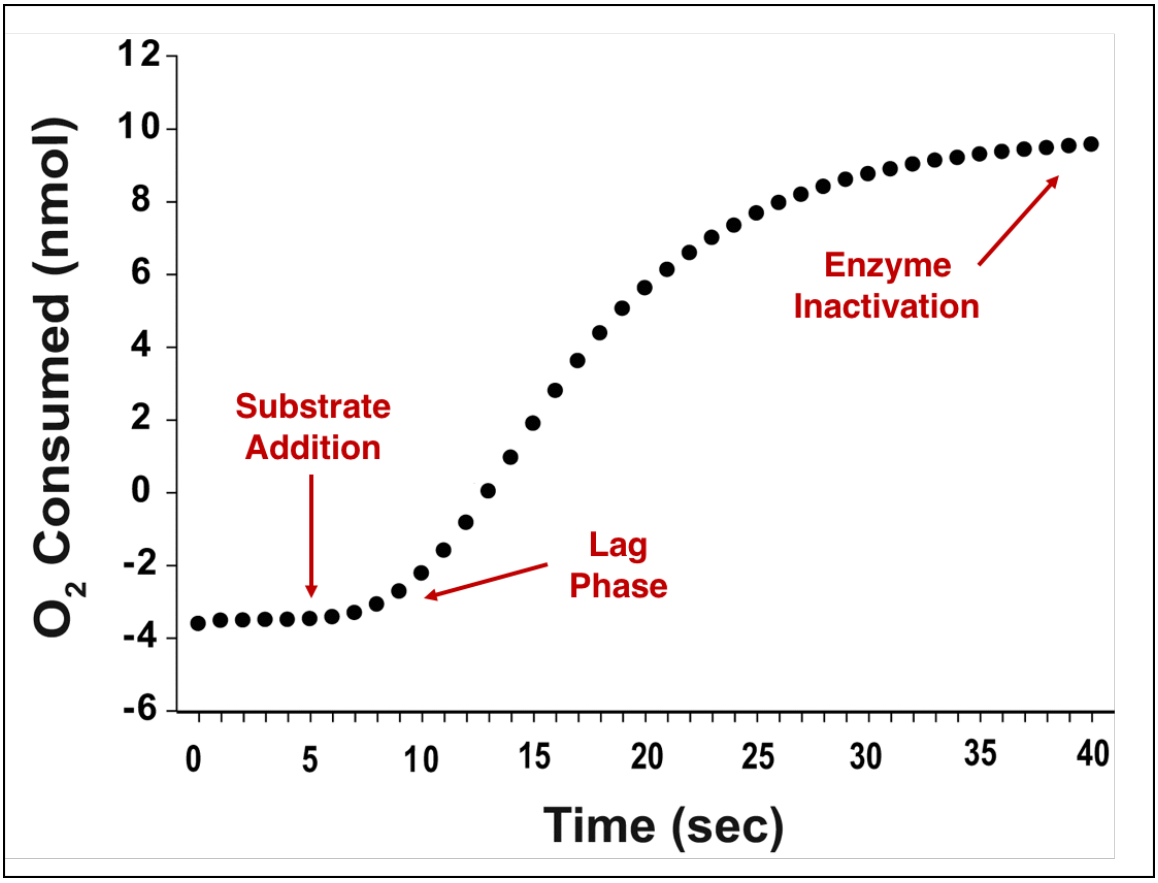

Figure 6. Oxygen electrode response in the oxygenation of AA by COX-2. Modified from *J Biol Chem.*, 286(21), Dong, L. et al., Human cyclooxygenase-2 is a sequence homodimer that functions as a conformational heterodimer, 19035-19046, Copyright (2011), with permission from the American Society for Biochemistry and Molecular Biology (56).

Several groups demonstrated that enzyme inactivation was dependent on the presence of both oxygen and hydroperoxide (57-59). Further studies revealed that COX inactivation begins instantaneously and occurs in a time- and concentration-dependent manner (60). Studies by Lecomte et al. with radiolabeled AA revealed 40% of the radiolabel ended up bound to COX post-reaction, suggesting COX itself was being covalently modified during the reaction (61). Mass spectrometric studies of COX-2 post-reaction with AA revealed lysyl-levuglandin Schiff base adducts present on the enzyme (62). While it is unknown whether these adducts contribute to enzyme inactivation, high levels of adducts were formed within 100 s after addition of AA to COX-2.

Differences between COX isoforms

Though both COX isoforms share a common overall structure, function, and mechanism, subtle differences between the two result in some important physiological consequences. The first difference, as noted above, is that they differ in temporal expression; COX-1 is typically consitutively present in cells whereas COX-2 expression is inducible in response to an array of inflammatory stimuli (22-24, 33). A second difference is the relative size of their active sites; COX-2 has a somewhat larger active site (394 $Å^3$) than COX-1 (316 $Å^3$) (32). This is primarily due to a substitution of Val in COX-2 for Ile in COX-1 at amino acid 523, which generates a “side pocket” in COX-2 that is absent in COX-1. Additional amino acid substitutions lending greater volume to the COX-2 active site include R513H and V434I (COX-2→COX-1) (32). These slight structural

differences between isoforms allowed for the development of COX-2-selective inhibitors (31).

Another consequence of an enlarged active site is that COX-2 shows greater substrate promiscuity than COX-1. While both enzymes metabolize AA most efficiently, purified human COX-2 (hCOX-2) metabolizes dihomo-γ-linolenic acid with about 30-50% the efficiency of AA (18). COX-2 metabolizes linoleic acid, α-linolenic acid, γ-linolenic acid, and eicosapentaenoic acid with greater efficiency than COX-1 (18). In addition, COX-2 also more efficiently oxygenates amide and ester analogs of AA. Of particular interest is COX-2's relative selectivity for the ability to oxygenate the two known endocannabinoids, arachidonylethanolamide (AEA) and 2-arachidonoylglycerol (2-AG) (19, 20) (Table 1).

Table 1. Steady-state kinetic parameters for COX-2-mediated metabolism of AA and alternative substrates. Reprinted from *Biochem Biophys Res Commun.*, 338(1), Rouzer, C.A. and Marnett, L.J., Structural and functional differences between cyclooxygenases: fatty acid oxygenases with a critical role in cell signaling, 34-44, Copyright (2005), with permission from Elsevier (63).

	k_{cat} (s^{-1})	K_m (μM)	k_{cat}/K_m (s^{-1} μM^{-1})
Human COX-2			
AA	15 ± 1	6.1 ± 0.6	2.4
2-AG	17 ± 1	4.4 ± 0.9	4.0
Murine COX-2			
AA	21 ± 2	8.2 ± 1.6	2.5
2-AG	11 ± 1	4.7 ± 0.8	2.3
AEA	0.1	24	0.0042
NAGly	6.3 ± 1.1	12 ± 1	0.54

AEA and 2-AG are bioactive lipids that bind cannabinoid 1 receptors (primarily in the brain) and cannabinoid 2 receptors (primarily in the periphery) (64-66), the same receptors that mediate the psychotropic effects of Δ^9-tetrahydrocannabinol, the active component of marijuana (67, 68). COX-2 can also selectively oxygenate the lipoamino acid *N*-arachidonylglycine (NAGly) (21). Site-directed mutagenesis studies have suggested that the R513H (COX-2→COX-1) substitution, located at the base of the side pocket in COX-2, is the key residue enabling COX-2 to oxygenate AA amides and esters with greater efficiency than COX-1. However, slight effects of the other two differential residues were observed in the case of the triple mutant (V523I/R513H/V434I) (69).

Biosynthesis and metabolism of 2-AG

As evident in Table 1, COX-2 utilizes 2-AG as a substrate with approximately the same catalytic efficiency as it does AA (19). The biosynthesis of 2-AG begins when activation of phospholipase C (PLC) catalyzes the hydrolysis of phosphatidylinositol 4,5-bisphosphate (PIP_2) to give diacylglycerol (DAG). Since PLCs favor substrates with AA, and PIP_2 is enriched with AA at the *sn*-2 position, most of the product DAGs contain AA. Hydrolysis of these AA-containing DAGs by DAG lipases (DAGLs) yields 2-AG (70, 71). 2-AG itself is then subject to direct hydrolysis by various monoacylglycerol lipases (such as MAGL, ABHD6, and ABHD12 in mouse brain) (72) or non-specific esterases (such as CES1 and CES2 in THP1 cells) (73). COX-2 metabolism of 2-AG yields prostaglandin G_2 glyceryl ester (PGG_2-G), a glyceryl ester analog of PGG_2, that

is subsequently reduced by the COX-2 peroxidase site to give its respective alcohol product (PGH_2-G) (19). Likewise, PGH_2-G is acted upon analogously by the respective PG synthases (with the exception of thromboxane synthase), and with approximately similar rates, to yield an array of PG-G species (74, 75) (Fig. 7).

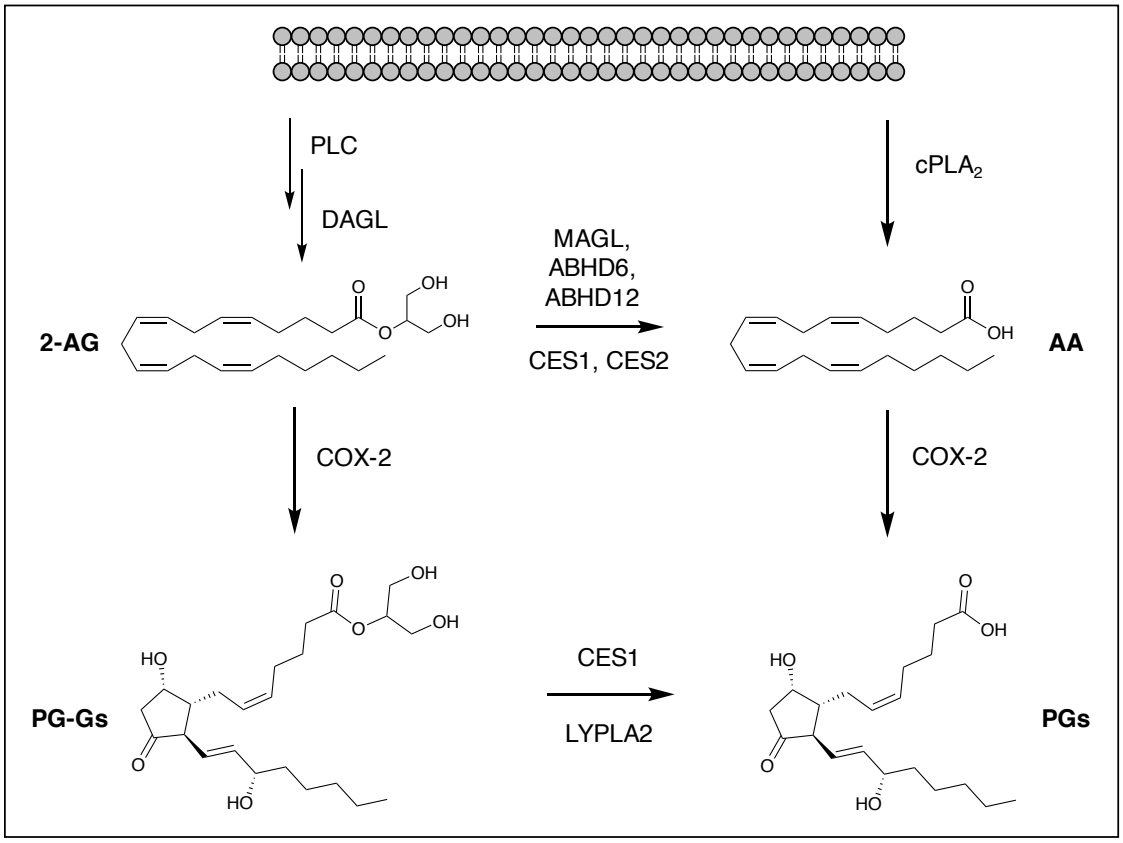

Figure 7. Biosynthesis and metabolism of 2-AG and AA. PG products depicted from COX-2 oxygenation of 2-AG and AA, respectively, are PGD_2-G and PGD_2. These are the primary PG products formed in activated RAW264.7 macrophages.

Whereas the existence of COX-2 oxygenation products of 2-AG *in vitro* is undisputed, debate remains over the biological relevance of such species *in vivo*. Despite similar catalytic efficiencies of COX-2 with AA and 2-AG, levels of PGs

far exceed (up to 1000x) levels of PG-Gs in cells and *in vivo*. Relative levels of substrates can partly account for this (levels of free AA exceed those of 2-AG by 10:1 in some cell lines), but even resident peritoneal macrophages (RPMs) treated with 1 μM 2-AG synthesized more PGs than PG-Gs (75). In RPMs, some of the PG synthesis could be attributed to 2-AG hydrolysis to AA followed by COX-2 oxygenation to PGs (75). Another possible explanation for the discrepancy in product levels arises from that fact that COX-2 requires activation by hydroperoxides, and higher concentrations of hydroperoxides are required to maintain 2-AG oxygenation than AA oxygenation (76). In addition, compartmentalization of the substrate within the cell might explain the poor utilization of 2-AG. Furthermore, PG-Gs can be hydrolyzed to PGs. In fact, PG-Gs are hydrolyzed quite rapidly to PGs in both rat and human plasma (74). In THP1 cells, CES1 accounts for 80-95% of PG-G hydrolysis to PGs (73). More recently, our lab found lysophospholipase A2 (LYPLA2) to be the major PG-G hydrolase in human cancer cells (77).

Despite their low abundance, PGI_2-G and PGE_2-G have been detected in RPMs pretreated with LPS to induce COX-2 expression followed by zymosan treatment to invoke endogenous substrate release (75). Likewise, PGD_2-G and PGE_2-G form in RAW264.7 macrophages treated with LPS and IFN-γ followed by ionomycin (19). In these cells, PGE_2-G causes calcium mobilization in the picomolar to nanomolar concentration range, as well as induction and phosphorylation of extracellular signal-regulated kinases 1 and 2, while PGE_2 does not (78). Studies suggest PG-Gs bind at distinct receptors from PGs (78),

with a recent study suggesting PGE_2-G serves as an endogenous agonist for the pyrimidinergic receptor P2Y6 (79). Thus, while progress is being made to understand the biological function of PG-Gs, including the first *in vivo* detection of PG-Gs in rat hind paw homogenates (80), the verdict regarding their physiological importance, especially in light of their low abundance, remains to be determined.

Heterodimeric nature of COXs

Another area of COX biochemistry that remains rife for exploration lies in the fact that the enzyme, while a structural homodimer, operates as a functional heterodimer. On the one hand, the idea that the monomeric subunits of COX are not identical is not new. Early studies assessing the stoichiometry of heme binding to dimer revealed not only that one heme is required for full activity of the dimer, but also that the two COX subunits possess different affinities for heme, and thus, even without bound ligand, are not fully identical (34). Crystal structures of either AA or 1-arachidonoylglycerol (1-AG) bound to purified murine COX-2 (mCOX-2) reveal that the orientation of the substrate varies between the COX subunits; for example, in the crystal structure of the mCOX-2:AA complex, in one subunit, substrate is bound in a productive binding conformation (poised for H atom abstraction at the C-13 position), while in the other subunit, substrate is bound in a nonproductive conformation (upside-down) (37, 81). Furthermore, COX heterodimers consisting of one catalytically inactive (Y385F) subunit and one catalytically active (native COX-2) subunit display comparable enzymatic

activity as native COX-2 homodimers (82). These findings suggest half-of-sites activity of the enzyme, where the heme-bound COX subunit functions as the catalytic site and the unbound subunit serves as an allosteric site.

More recent support for the notion of COXs acting as functional heterodimers stems from the work of Prusakiewicz et al. who showed that many weak, competitive inhibitors of AA oxygenation by COX-2 are potent, time-dependent inhibitors of 2-AG oxygenation, an observation consistent with potential inhibitor binding to one or both subunits of the enzyme (83). Additional studies with inhibitors revealed that binding of celecoxib to one subunit of the enzyme was sufficient to inhibit binding of aspirin in the second (84). Yuan et al. extended this study from inhibitors to other fatty acid molecules, revealing that binding of some non-substrate fatty acids to the allosteric site of COX could potentiate oxygenation of AA in the catalytic site (85). These initial findings were supported by work from Duggan et al. who demonstrated that certain inhibitors could selectively prevent COX-2 oxygenation of 2-AG, but not AA, via binding to the allosteric subunit of the enzyme (86). Alternatively, non-substrates such as 13-methylarachidonic acid can act as positive allosteric modulators to selectively potentiate COX-2 oxygenation of 2-AG (87). Collectively, these studies provide strong support for the idea of allosteric regulation of the COX enzymes via a sort of “cross-talk” between subunits of the COX homodimer, and they suggest that the effects of that cross-talk can vary dependent on the substrate being oxygenated.

Non-enzymatic PUFA oxidation and DNA damage

Formation and carcinogenicity of MDA

As mentioned briefly before, fatty acid hydroperoxides generated during PUFA autoxidation are subject to chemical breakdown to yield a variety of electrophilic species (Fig. 8). MDA is an endogenous product of lipid peroxidation as well as a product of enzymatic and non-enzymatic breakdown of PGH_2 (introduced in the previous section) (41, 88).

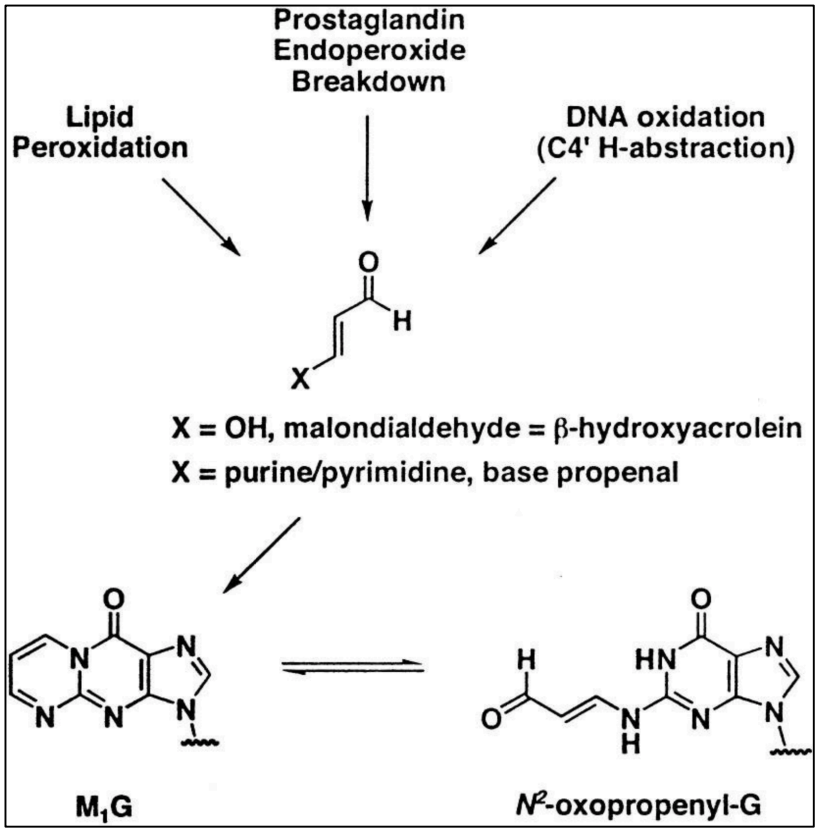

Figure 8. Endogenous generation of the M_1dG adduct. M_1dG exists in equilibrium with its ring-opened form, N^2-(3-oxo-1-propenyl)-dG. Ring-opening occurs at basic pH, and spontaneously when M_1dG is opposite dC in DNA. Reprinted from *PNAS*, 100(24), VanderVeen, L.A., Hashim, M.F., Shyr, Y., and Marnett, L.J., Induction of frameshift and base pair substitution mutations by the major DNA adduct of the endogenous carcinogen malondialdehyde, 14247-14252, Copyright (2003), with permission from the National Academy of Sciences (89).

Mukai and Goldstein first reported the mutagenicity of MDA in *Salmonella typhimurium* (90). Since some strongly mutagenic impurities can be generated during preparation of MDA, Basu and Marnett confirmed these initial findings using three distinct methods for preparing highly purified MDA (91). MDA was also shown to be mutagenic in a murine lymphoma cell line (92) as well as carcinogenic in a 2-year rodent bioassay performed by the National Institute of Environmental Health Sciences that reported MDA to induce thyroid tumors in rats but not mice (93).

Given its documented carcinogenic potential as well as its electrophilicity, one could postulate that MDA exerts its mutagenic effect through direct modification of DNA. Indeed, MDA forms adducts with 2'-deoxyguanosine (dG), 2'-deoxyadenosine (dA), and 2'-deoxycytidine (dC), with the primary DNA adduct being 3-(2-deoxy-β-D-erythro-pentofuranosyl)pyrimido[1,2-α]purin-10(3H)-one (M_1dG) (94-96) (Fig. 8). Reaction of MDA with plasmid DNA followed by replication in *E. coli* revealed similar mutations at dG, dA, and dC, which resulted largely in base-pair substitutions (76%; dG→dT, dA→dG, dC→2'-deoxythymidine (dT)) and frameshift mutations (97). Additional studies revealed that M_1dG could also be formed from reaction of dG with base propenals (98) resulting from oxidative damage to the deoxyribose ring of DNA (99).

Endogenous M_1dG and correlation with oxidative stress

M_1dG has been detected in genomic DNA isolated from a plethora of different tissues from healthy humans and rodents, including human leukocytes (100-102), pancreas (103), bronchial tissue (104), and liver (105), rat spleen (106), brain (107), and liver (105, 108-110), and mouse liver (111). Perhaps unsurprisingly given its mechanism of formation, M_1dG levels have also been positively correlated with oxidative stress. Table 2 below provides a brief summary of the literature to this effect:

Table 2. Correlation of genomic M_1dG levels with oxidative stress.

Subject	Organ	Description	Reference
human	blood	1.7-fold elevation in M_1dG levels in asbestos workers (versus control)	(112)
human	larynx	1.7-fold elevation in MDA-DNA adducts in smokers (versus non-smokers)	(113)
human	bronchial tissue	1.5-fold elevation in MDA-DNA adducts in current smokers (versus never smokers)	(104)
human	white blood cells	3.6-fold elevation in MDA-DNA adducts in subjects fed a PUFA-rich diet (versus subjects fed a monounsaturated fatty acid-rich diet)	(100)
human	normal breast tissue	2.5-fold elevation in M_1dG levels in cancer patients (versus non-cancer controls)	(114)
rat	brain	3-fold increase in M_1dG levels in older (18-month) rats (versus 6-month old rats)	(107)
rat	liver	Dose-dependent increase in M_1dG levels upon chronic exposure to polychlorinated biphenyls (versus vehicle)	(110)

M_1dG mutagenicity

The specific mutagenicity of M_1dG was assessed by the generation of site-specific M_1dG adduct-containing vectors that were subsequently replicated in *E. coli* or mammalian cells. In *E. coli*, M_1dG served as a replication block and premutagenic lesion (115). In COS-7 cells, M_1dG resulted in base-pair substitutions. In both cell lines, M_1dG caused frameshifts in reiterated DNA sequences (89). In sum, M_1dG displayed a mutation frequency of approximately 2% of replication events. Rationale for this surprisingly “low” mutagenic potential came from Mao et al., who reported the conformation(s) of M_1dG in duplex DNA (116). When M_1dG is positioned across from dC but not dG in a duplex, it ring-opens to form its corresponding oxopropenyl derivative (116-118). This finding illuminated previous observations that M_1dG is five times more mutagenic when positioned opposite dT (ring-closed adduct) than dC (ring-opened adduct) (115).

Fate of M_1dG

Initial M_1dG mutagenicity studies also shed light on potential pathways for removal of the adduct. Studies in *E. coli* strains deficient in functional UvrA protein, which is essential for nucleotide excision repair (NER), showed higher mutational frequencies, suggesting M_1dG might be repaired by this pathway (115). Additional studies of both M_1dG and a structurally similar adduct, propanodeoxyguanosine, in an *E. coli* strain deficient in NER repair also showed higher mutational frequencies and/or replication strand bias ((119), 112678323).

Removal of adducts via NER results in short, single-stranded DNA oligomers that are then hydrolyzed to give free nucleosides (Fig. 9). In fact, analysis of human urine revealed the presence of free M_1dG in levels of approximately 12 fmol/kg/day (120). Administration of free M_1dG to rats revealed a short half-life of the nucleoside *in vivo* (~10 min in plasma) and conversion to a single detectable metabolite—6-oxo-M_1dG (121). Incubation of M_1dG with rat liver cytosol gave 6-oxo-M_1dG, the levels of which were reduced in the presence of allopurinol and menadione (121), suggesting a role for xanthine oxidase (XO) and aldehyde oxidase (AO), respectively, in this oxidation. Further experiments in rats administered [^{14}C]-labeled M_1dG, revealed that a portion of the radiolabeled material ended up in both the urine (primarily M_1dG) and feces (primarily 6-oxo-M_1dG), with approximately 45% of the administered dose having been converted to 6-oxo-M_1dG in the process (122, 123). When [^{14}C]-labeled 6-oxo-M_1dG was administered, approximately 97% of it was recovered unchanged, suggesting this compound is relatively stable (123). 6-oxo-M_1dG has also been detected in the feces of untreated rats, where it appears to be excreted at a rate of 350-1893 fmol/kg/day (124).

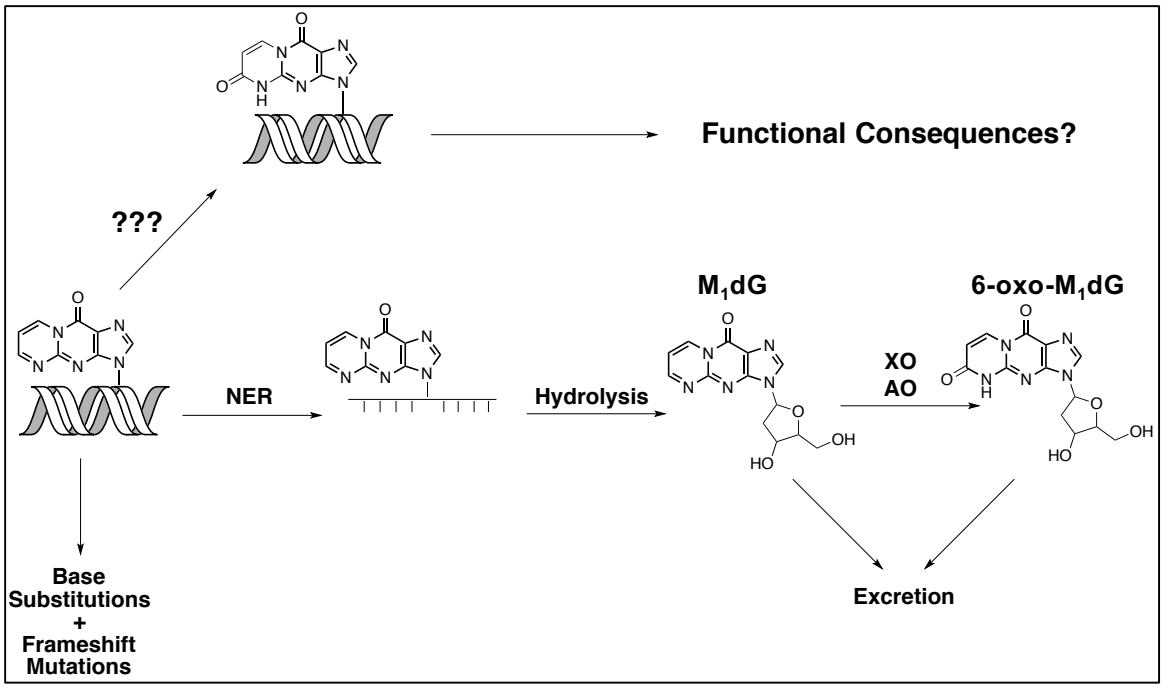

Figure 9. Fate of M_1dG in dsDNA.

Interestingly, Singh et al. recently demonstrated that M_1dG and other structurally related exocyclic guanosine adducts can be oxidatively repaired by AlkB, an Fe(II)/α-ketoglutarate (α-KG)-dependent dioxygenase, in both single- and double-stranded DNA (125). This led our lab to speculate whether M_1dG might also be oxidized in genomic DNA to 6-oxo-M_1dG. In fact, we recently reported the oxidation of M_1dG to 6-oxo-M_1dG in genomic DNA in multiple cell lines at a rate that appears to exceed that of repair (126). We simultaneously reported the presence of the oxidizing activity in the nuclear lysates from one such cell line, an activity that was ablated upon heat treatment. The search for the identity of the responsible activity/enzyme is ongoing.

Dissertation Aims

This dissertation is composed of two distinct projects, which are presented in chapters II and III, respectively.

Chapter II details studies to determine whether COX-2 substrates AA and 2-AG allosterically regulate each other's turnover by the enzyme and if there is evidence of such a phenomenon in intact cells. Significant effort was made to develop optimal conditions for fixed-timepoint kinetics studies of COX-2, a technical challenge due to the aforementioned peroxide activation and self-inactivation of the enzyme. Furthermore, mass spectrometric analysis of products was required, as oxygen consumption measurements (via traditional oxygen electrode methodologies) do not distinguish between oxygenated substrates. A systems biology approach to understanding the complex interplay between both substrates and the two enzyme subunits was employed in order to interpret the kinetic data. The methodology developed is applicable not only to COX-2 but to other multimeric enzymes as well.

Chapter III examines the nature of the oxidation of M_1dG to 6-oxo-M_1dG in the genome. Evidence is presented that suggests the oxidation reaction is indeed enzymatic. Cofactor and inhibitor studies, both *in vitro* and in intact cells, suggest a nuclear Fe(II)/α-KG-dependent enzyme is likely responsible. Chapter III closes with promising data obtained from experiments involving substrate competition with a broad-spectrum inhibitor-based photoaffinity probe for protein identification.

CHAPTER II

COMPETITION AND ALLOSTERY GOVERN SUBSTRATE SELECTIVITY OF CYCLOOXYGENASE-2

Introduction

As noted above, COX-2 utilizes 2-AG and AA with similar kinetic efficiencies *in vitro* (19); however, PG-G production in intact cells is much lower than would be expected based on the relative bulk amounts of cellular AA and 2-AG available upon appropriate stimulation (127). These observations, coupled with the growing evidence for allosteric regulation of COX-2, led us to hypothesize that differential interactions of AA and 2-AG at the allosteric site of COX-2 might result in a complex interplay between the substrates when both are present. Here, I present evidence that modulation of AA levels inversely affects biosynthesis of PG-Gs both in intact cells and *in vitro*. Mathematical modeling of COX-2 oxygenation kinetics that explicitly incorporates the dynamics of all the chemical intermediates in the reaction network was used to analyze the data. The model employed a novel Bayesian parameter inference formalism to characterize the multiple reaction pathways that exist between the two substrates, the enzyme subunits, and their products and reveals probability distributions, given our experimental data, for kinetic constants rather than single best-fit values. This approach provides a systems-level understanding of multiple competing interactions in the reaction network and accurate confidence estimates for fitted values. The presented methods are generalizable to other kinetic systems that, like COX-2, can appear

deceptively simple. The findings support the hypothesis that a combination of competition and allosteric regulation controls the selective use of substrates by COX-2 and provide the first evidence of the physiologic relevance of this phenomenon in live cells.

Materials and Methods

***Materials*.** The expression and purification of recombinant mCOX-2 from Sf9 insect cells were performed as previously described (128). AA, 2-AG, 5-phenyl-4*E*-pentenyl-1-hydroperoxide (PPHP), PGE_2-d_4, AA-d_8, and 2-AG-d_8 were purchased from Cayman Chemical (Ann Arbor, MI). PGE_2-G-d_5 was synthesized as described previously using chemicals from Sigma-Aldrich (St. Louis, MO) (19). RAW264.7 cells were obtained from the American Type Culture Collection (Rockville, MD). Cell culture reagents were purchased from Life Technologies (Gaithersburg, MD). Fetal bovine serum (FBS) was purchased from Atlas Biologicals (Fort Collins, CO). Fatty acid-free bovine serum albumin (BSA), LPS, zymosan B, ionomycin, and IFN-γ were purchased from Sigma-Aldrich. Granulocyte/macrophage colony-stimulating factor (GM-CSF) was purchased from R&D Systems (Minneapolis, MN). Giripladib was synthesized in the Lindsley laboratory as described (129).

AA and 2-AG Kinetics with mCOX-2. For kinetic analyses, the desired concentration of mCOX-2 was reconstituted with 2 equivalents of heme per subunit in 195 µL of 100 mM Tris-HCl buffer, pH 8, with 500 µM phenol. Following a 3 min pre-incubation at 37 °C, 5 µL of dimethyl sulfoxide (DMSO) containing the specified

amounts of AA, 2-AG, and PPHP (final concentrations of 0-16 μM for each substrate and 1 μM for PPHP) was added to the tube and, after thorough mixing, the reaction was allowed to proceed for 10 s. The reaction was quenched by adding 200 μL of ethyl acetate containing 0.5% glacial acetic acid and internal standards, PGE_2-d_4 and PGE_2-G-d_5. Tubes were frozen, and the organic layer was separated and evaporated to dryness under nitrogen gas. The samples were then reconstituted in 200 μL of methanol and analyzed using liquid chromatography-tandem mass spectrometry (LC-MS/MS) as described below. Initial velocities, estimated on the basis of the total product synthesized in 10 s, were plotted versus substrate concentration. In the case of incubations containing a single substrate, kinetic parameters (k_{cat}, K_m, and K_I) were determined by data fitting to the Michaelis-Menten model (for AA) or a substrate-inhibition model (for 2-AG) using GraphPad Prism 6 software. The concentration of enzyme was selected to maintain substrate consumption below 20%. This varied with enzyme preparation, likely due to the presence of variable amounts of inactive enzyme. Accordingly, some variability in k_{cat} was also noted between enzyme preparations.

Kinetic Modeling: Competitive Inhibition. Data simulations were carried out with KinTek Explorer Version 4.0 Student Edition software (130-132) using the following model:

$E + AA \rightleftharpoons E{\cdot}AA$	$k_f = 1000\ s^{-1}\mu M^{-1}$	$k_r = 830\ s^{-1}$
$E{\cdot}AA \longrightarrow E + PG$	$k_f = 1.3\ s^{-1}$	$k_r = 0\ s^{-1}$
$E + 2\text{-}AG \rightleftharpoons E{\cdot}2\text{-}AG$	$k_f = 1000\ s^{-1}\mu M^{-1}$	$k_r = 760\ s^{-1}$
$E{\cdot}2\text{-}AG \longrightarrow E + PG$	$k_f = 1.2\ s^{-1}\mu M^{-1}$	$k_r = 0\ s^{-1}$

$E{\cdot}2\text{-}AG + 2\text{-}AG \rightleftharpoons E{\cdot}2\text{-}AG{\cdot}2\text{-}AG$ $k_f = 1000\ s^{-1}\mu M^{-1}$ $k_r = 63000\ s^{-1}$

$E{\cdot}2\text{-}AG{\cdot}2\text{-}AG \longrightarrow E{\cdot}2\text{-}AG + PG\text{-}G$ $k_f = 0\ s^{-1}\mu M^{-1}$ $k_r = 0\ s^{-1}$

The model assumes that each substrate establishes a rapid, reversible equilibrium with the catalytic site prior to forming product, and that binding of 2-AG to the allosteric site results in substrate inhibition. The experimental values of K_m for AA and 2-AG (0.83 μM and 0.76 μM, respectively) were assumed to be reasonable estimates of the binding affinity of each substrate for the enzyme's catalytic site. Similarly, the values of K_I for 2-AG at the allosteric site and k_{cat} for the formation of PG and PG-Gs were all obtained from the experimental data (Fig. 6 and Fig. 4, respectively). The KinTek program does not allow for entry of equilibrium constants, so values for the rate constants of the forward and reverse reactions were entered to simulate the appropriate rapid, reversible equilibrium for the formation of each enzyme-substrate complex. Simulations were performed using 15 nM enzyme and all combinations of AA and 2-AG (0.5 to 16 μM) used in the experiment described in the legend to Fig. 4, with reactions carried out for 10 s incubation times.

Kinetic Modeling: Uncompetitive Inhibition. The effects of AA on the production of PG-Gs from 2-AG by COX-2 were evaluated using classical models of uncompetitive, noncompetitive, and mixed inhibition. In all cases, competition of each substrate with the other at the active site and substrate inhibition of 2-AG were included. The general equation was:

$$V = \frac{V_{max}[AG]}{K_{mAG}\left(1 + \frac{[AA]}{K_{mAA}} + \frac{[AA]}{K_{I1}}\right) + [AG]\left(1 + \frac{[AG]}{K_I} + \frac{[AA]}{K_{I2}}\right)}$$

In this equation, K_{mAG} and K_{mAA} were the experimental values obtained for 2-AG and AA, respectively (Fig. 6). V_{max} was the experimental value for PG-G formation obtained from the experiment described in the legend to Fig. 4. K_I was the experimental value for substrate inhibition of 2-AG oxygenation (Fig. 6*B*). The model assumes that binding of either AA or 2-AG to the allosteric site creates an inactive complex. Curve fitting was carried out using the data generated in the experiment described in the legend to Fig. 4. For noncompetitive inhibition K_{I1} was set equal to K_{I2}. For mixed inhibition, the two values were fit independently. For uncompetitive inhibition, the term including K_{I1} was removed.

Kinetic Modeling: Explicit Catalytic and Allosteric Sites. The COX-2 reaction model (CORM) was implemented as a Python program that when executed, generates a set of BioNetGen rules that, in turn, generate thirteen ordinary differential equations using the mass-action kinetics formalism, within the PySB models-as-programs Python modeling framework (133). Bayesian statistical sampling of possible model parameter values was then performed using the Markov Chain Monte Carlo algorithm DREAM$_{(z)}$ (134) in the Python package Python PyMC (135). Experimentally measured parameters were fixed. Fitted parameters included both K_D and k_{cat} values. Because the ordinary differential equations used to derive CORM require rate constants instead of K_D values, fitted K_D values were converted into rate parameters (k_r/k_f). The reaction k_f was then assumed to be diffusion-limited while the k_r was allowed to vary to yield a particular K_D. Parameter prior probabilities were specified as normal distributions, with means set at the parameter values fitted using the uncompetitive inhibition model

and standard deviations of approximately an order of magnitude, reflecting a relative lack of knowledge about likely parameter values. A model likelihood function measured model simulation fit to experimental data as has been described in previous work (136). Additionally, four thermodynamic cycles present in the interaction network (Fig. 9) provided another measure of model likelihood, as the relative values of these parameters must be consistent with energy conservation. The thermodynamic cycles are shown below:

E + AA ⇌ E·AA + AA ⇌ AA·E·AA ⇌ AA + AA·E ⇌ E + AA

E + 2-AG ⇌ 2-AG·E + AA ⇌ 2-AG·E·AA ⇌ 2-AG + E·AA ⇌ E + AA

E + AA ⇌ AA·E + 2-AG ⇌ AA·E·2-AG ⇌ AA + E·2-AG ⇌ E + 2-AG

E + 2-AG ⇌ E·2-AG + 2-AG ⇌ 2-AG·E·2-AG ⇌ 2-AG + 2-AG·E ⇌ E + 2-AG

The fit of model simulations to experimental data and the extent to which tested parameters were consistent with energy conservation was measured using the probability density function for a normal distribution:

$$f(x, \mu, \sigma) = \frac{1}{\sigma\sqrt{2\pi}} e^{-\frac{(x-\mu)^2}{2\sigma^2}},$$

where *x* is the simulated value, μ is the observed average value, and σ is the standard deviation. When measuring goodness of fit to experimental data, the average and standard deviation for each experimental measurement were used. When measuring energy conservation, perfect energy conservation (i.e. a ratio of 1:1 for the product of K_Ds on each side of a thermodynamic cycle) was used as the average and 0.001 as a standard deviation to allow small deviations from this ideal

value. This function was minimized during our parameter scans to find probable parameter values given the network interactions and the experimental kinetics.

The DREAM$_{(Z)}$ algorithm was initialized with five chains in random locations in parameter space drawn from prior parameter probability distributions. Sampling was performed for 2.5 million iterations; 100,000 samples were discarded as burn-in, and sample matrixes were thinned by a factor of 10. All chains converged to a limiting distribution as assessed by both the Geweke score (137) and Gelman-Rubin convergence criterion (138). Ninety-five percent credible intervals for each parameter were then estimated by determining the narrowest interval that encompasses 95 percent of the sample distribution. Fig. 13 *A*-*D* was plotted using the Python package seaborn (http://stanford.edu/~mwaskom/software/seaborn/). All code used to build the model and fit the model parameters is freely available in the Lopez laboratory GitHub repository (https://github.com/LoLab-VU/CORM).

RAW 264.7 Cell Culture. Low passage number RAW 264.7 cells were maintained in Dulbecco's Modified Eagle Medium (DMEM) + GlutaMAX containing 10% heat-inactivated FBS. For studies of the effects of AA enrichment on PG-G biosynthesis, cells were plated at 5 x 10^5 cells/dish onto 35 mm plates and incubated with AA complexed with BSA and 20 ng/mL GM-CSF for 20 h as described previously (139). The cells were then transferred to fresh DMEM/heat-inactivated FBS with LPS (100 ng/mL, *E. coli* 011:B4), IFN-γ (10 ng/mL), and GM-CSF (20 ng/mL). Cultures were incubated for 5 h and then washed in phosphate-buffered saline and overlaid in fresh serum-free DMEM. Zymosan was added (160 μg/dish), and cells were incubated for 1 h or 2 h prior to harvesting for analysis of

AA and 2-AG or PGs and PG-Gs, respectively.

For studies of the effects of inhibition of AA release, RAW264.7 cells were plated at 3 x 10^6 cells/dish onto 100 mm plates and incubated for 24 h. The medium was then removed and replaced with serum-free DMEM with LPS (1 μg/mL, E. coli 011:B4) and IFN-γ (10 ng/mL). Cultures were incubated for 6 h and then washed and overlaid with fresh serum-free DMEM containing either DMSO or 1 μM giripladib in DMSO. Fifteen minutes later, ionomycin was spiked into the medium to a final concentration of 5 μM, and cells were incubated for an additional 45 min.

LC-MS/MS Analysis. Following cell treatments as described above, the culture medium was removed and extracted with 2 volumes of ethyl acetate containing PGE_2-d_4 and PGE_2-G-d_5. The cells were scraped into 1 mL of ice-cold methanol containing internal standards (AA-d_8 and 2-AG-d_8) and added directly into the ethyl acetate solution. The solution was vigorously mixed, and the organic layer was then removed and dried under a stream of nitrogen gas. The resultant film was reconstituted and analyzed for AA and 2-AG levels using a Luna C18(2) column (50 x 2 mm, 5 μm) (Phenomenex, Torrance, CA) with a gradient elution of 83 to 99% solvent B over 2 min at a flow rate of 300 μL/min (solvent A: 80 μM silver acetate, 0.1% acetic acid in water; solvent B: 118 μM silver acetate, 0.1% acetic acid in methanol). MS/MS analysis was conducted on a QTrap 3200 (AB SCIEX, Framingham, MA) operated in positive ion mode utilizing selected reaction monitoring for the following transitions: *m/z* 519→409 for AA, *m/z* 527→417 for AA-d_8, *m/z* 485→411 for 2-AG, and *m/z* 493→419 for 2-AG-d_8 (140). PGs and PG-Gs were quantified in a similar manner with a gradient elution of 25 to 98% solvent

B over 4 min at a flow rate of 300 µL/min (solvent A: 5 mM ammonium acetate, pH 3.6; solvent B: acetonitrile with 6% solvent A) with selected reaction monitoring for the following transitions: *m/z* 370→317 for PGE_2/D_2, *m/z* 374→321 for PGE_2-d_4, *m/z* 444→391 for PGE_2/D_2-G, and *m/z* 449→396 for PGE_2-G-d_5 (141). This method of PG and PG-G analysis was also applied to kinetic studies with purified mCOX-2 as described in the corresponding methods section.

Results

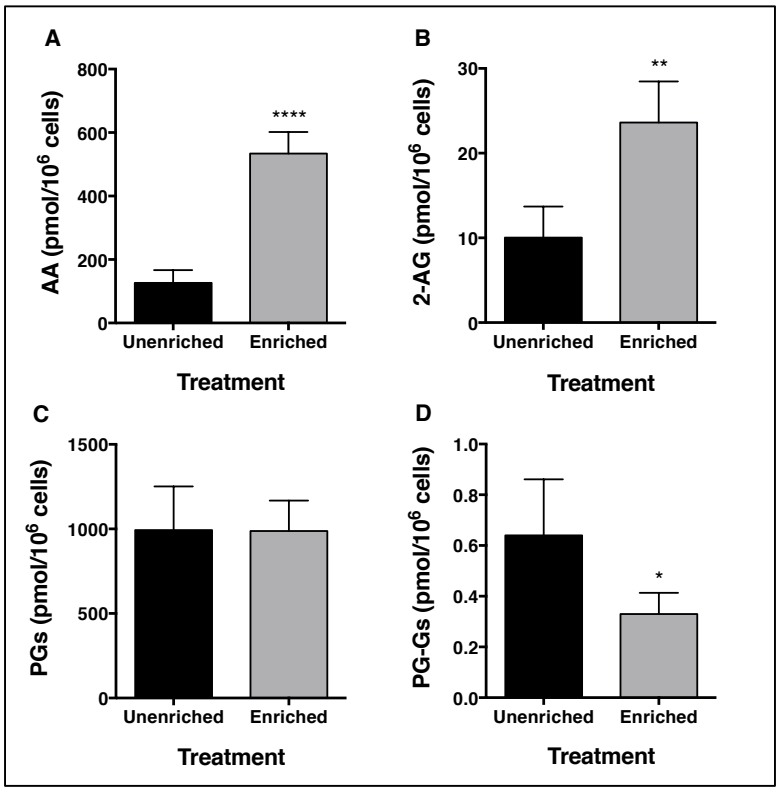

Figure 1. AA enrichment leads to reduced PG-G levels in zymosan-stimulated RAW264.7 cells. Cells (5 x 10^5) were enriched with AA, incubated with LPS and IFN-γ to induce COX-2 expression, and then stimulated with zymosan to trigger release of AA (*A*) and 2-AG (*B*) and biosynthesis of PGs (*C*) and PG-Gs (*D*). Data are the mean ± S.D. of four independent experiments, each performed in triplicate. Statistical significance was determined by Student's t-test (* $p < 0.05$, ** $p < 0.01$, **** $p < 0.0001$ compared to unenriched).

AA Enrichment Suppresses 2-AG Oxygenation in RAW264.7 Cells. RAW264.7 murine macrophage-like cells exhibit COX-2-dependent PG-G biosynthesis (19). Incubation of RAW264.7 cells overnight with AA complexed to BSA increases their cellular phospholipid AA content by ~100% (139). We utilized this enrichment to examine the impact of endogenously released AA on the production of PGs and PG-Gs following zymosan stimulation. AA enrichment resulted in a 4.2-fold (Fig. 1*A*) and 2.4-fold (Fig. 1*B*) increase in peak zymosan-

stimulated AA and 2-AG release, respectively. However, despite the substantial increase in available substrate, AA-enriched cells produced no more PGs (Fig. 1*C*) than unenriched cells in response to zymosan, and the quantity of PG-Gs produced by the AA-enriched cells was reduced by ~50% (Fig. 1*D*). Thus, AA enrichment in stimulated RAW264.7 cells results in increased release of both AA and 2-AG in response to zymosan, but reduced production of PG-Gs.

Inhibition of Endogenous AA Release Results in Elevated PG-G Levels. We next employed a pharmacologic approach to manipulate the levels of AA in RAW264.7 cells. The major route for the release of AA for PG biosynthesis in macrophages is hydrolysis at the *sn*-2 position of AA-containing phospholipids by cytosolic phospholipase A_2 alpha (cPLA$_2$α) (142-145). Consequently, we explored the effects of giripladib, a selective inhibitor of cPLA$_2$α (146), on AA release and PG biosynthesis in ionomycin-stimulated RAW264.7 cells. As seen in Fig. 2*A* and *C*, giripladib exposure led to an 89% and 93% decrease in AA release and PG biosynthesis, respectively. Giripladib treatment also resulted in an approximately 1.6-fold increase in PG-G levels (Fig. 2*D*) with no change in the levels of 2-AG (Fig. 2*B*). When ionomycin-stimulated RAW264.7 cells were incubated with 5 μM PGE$_2$-G-d$_5$ under the same conditions as described in the legend to Fig. 2, there was no difference in the recovery of the added PG-G between cells incubated in the absence (92 ± 1%) or presence (89 ± 1%) of giripladib, indicating that the observed increase in endogenously produced PG-Gs was not due to an off-target suppression of PG-G hydrolysis by the inhibitor.

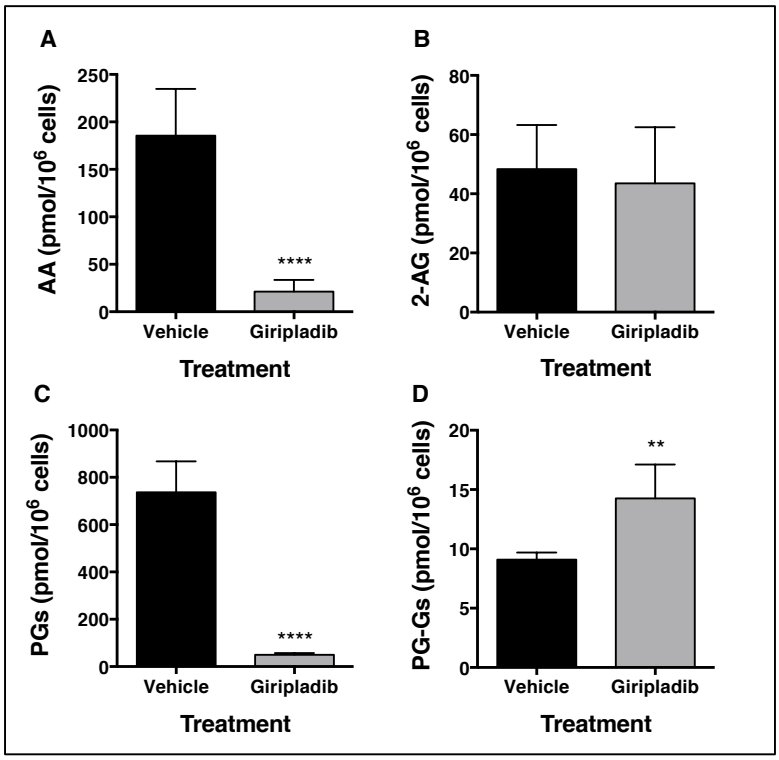

Figure 2. Inhibition of cPLA$_2\alpha$-dependent AA release by giripladib results in increased PG-G biosynthesis in RAW264.7 cells. Cells (3 x 10^6) were preincubated with LPS and IFN-γ and then stimulated with ionomycin in the presence or absence of giripladib (1 μM). Data show AA (*A*) and 2-AG (*B*) levels along with amounts of PGs (*C*) and PG-Gs (*D*) formed. Results are the mean ± S.D. of six determinations. Statistical significance was determined using Student's t-test (** $p < 0.01$, **** $p < 0.0001$ compared to vehicle).

AA Suppresses 2-AG Oxygenation by COX-2 in Vitro. One possible explanation for these cellular observations is that AA suppresses COX-2-dependent 2-AG oxygenation when both substrates are present. To examine this possibility, we characterized the kinetics of oxygenation of AA and 2-AG by purified mouse COX-2 with both substrates present in the reaction mixture. Kinetic analysis of COX activity is complicated by the requirement for product hydroperoxide activation, which results in an early lag phase, and enzyme self-inactivation, which leads to premature termination of the reaction. Consequently, the enzyme does not exhibit a true initial rate, and monitoring oxygen consumption using the

maximal rate achieved at the end of the lag phase has been the approach used in most kinetic studies (147). While multiple previous investigations have yielded kinetic parameters for COX-2 using this approach, it cannot be used to explore the simultaneous metabolism of two COX-2 substrates since oxygen consumption occurs with both. Hence, we utilized LC-MS/MS to distinguish the oxygenation products of AA and 2-AG, necessitating a fixed time-point assay. To approximate a true initial rate as closely as possible, substrate-enzyme incubations were limited to ten seconds, the shortest time point that yielded reproducible data. The brief incubation period minimized substrate consumption and COX-2 self-inactivation; however, it also increased the likelihood that rates would be underestimated due to incomplete peroxide-dependent activation. This potential problem was eliminated by the inclusion of PPHP in the substrate mixtures. At a concentration of 1 μM, PPHP maximized COX-2-dependent oxygenation, particularly in the case of 2-AG (Fig. 3).

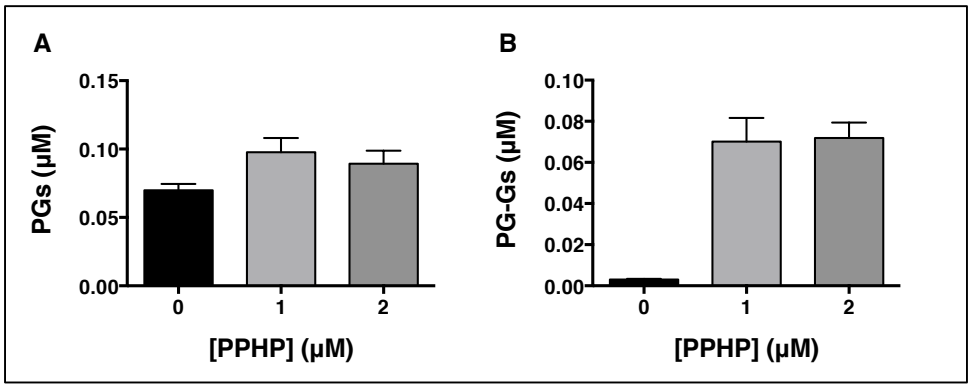

Figure 3. Effect of PPHP on the oxygenation of AA and 2-AG by mCOX-2. Reaction mixtures consisted of mCOX-2, the indicated concentrations of PPHP, and 0.25 μM AA (*A*) or 0.25 μM 2-AG (*B*). Results shown are the mean (± S.D.) of triplicate determinations.

Under the LC-MS/MS assay conditions, AA inhibited 2-AG oxygenation by mCOX-2 in a concentration-dependent manner, reaching >80% inhibition at the highest concentrations of AA tested (Fig. 4*A* and Fig. 5*A*). The IC_{50} for inhibition of 2-AG oxygenation was approximately 0.5 μM AA, regardless of the concentration of 2-AG. 2-AG also suppressed AA oxygenation, but to a lesser extent, never achieving >40% inhibition (Fig. 4*B* and Fig. 5*B*).

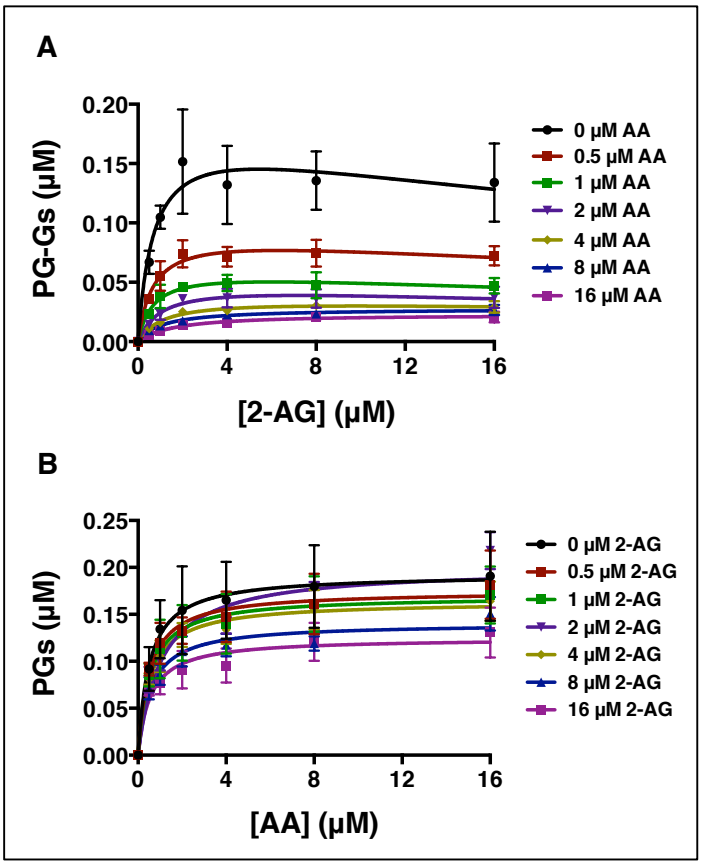

Figure 4. AA suppresses 2-AG oxygenation by mCOX-2 *in vitro*. The indicated concentrations of premixed 2-AG and AA with 1 μM PPHP were incubated with 15 nM mCOX-2 (monomeric concentration) for 10 s. PGs and PG-Gs were quantified by LC-MS/MS. Results are depicted as PG-G formation as a function of increasing 2-AG concentration in the presence of various amounts of AA (*A*) and PG formation as a function of increasing AA concentration in the presence of various amounts of 2-AG (*B*). Results are the mean ± S.D. of triplicate determinations. Kinetic parameters for oxygenation of 2-AG in the absence of AA were: K_m = 0.71 ± 0.37 μM, k_{cat} = 1.2 ± 0.2 s^{-1}, K_I = 42 ± 38 μM. Kinetic parameters for oxygenation of AA in the absence of 2-AG were: K_m = 0.51 ± 0.18 μM, k_{cat} = 1.3 ± 0.1 s^{-1}.

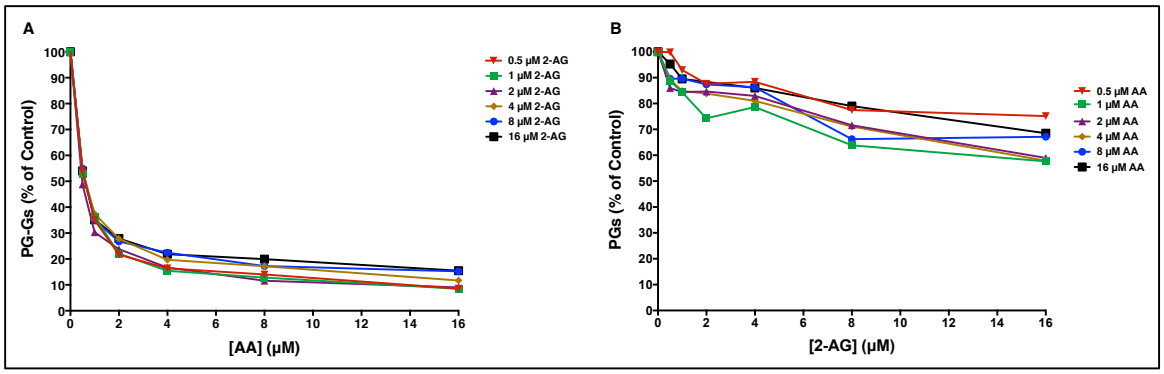

Figure 5. Replot of the data in Figure 4 showing the inhibition of PG-G (*A*) and PG (*B*) synthesis at the indicated substrate concentrations and increasing concentrations of AA and 2-AG, respectively.

Classic Models of Enzyme Inhibition Fail to Explain the Interaction Between AA and 2-AG. The data presented in Fig. 4 and Fig. 5 suggest that the interaction between the two substrates, which have apparently similar catalytic efficiencies with mCOX-2 (Fig. 6, (19)), is inconsistent with simple competition between the substrates for a single active site. We tested this hypothesis by using KinTek Explorer software to simulate the results that would be expected from the experiment depicted in Fig. 4 if the two substrates compete with each other for the catalytic site with affinities estimated by their respective experimental K_m values (Fig. 6). The model also incorporated substrate inhibition in the case of 2-AG (Fig. 6*B*) (87). As shown in Fig. 7 *A*-*F*, experimental levels of PGs far exceeded those predicted by substrate competition alone. Conversely, experimental levels of PG-Gs were much lower than expected based on the competitive model (Fig. 7 *G*-*L*).

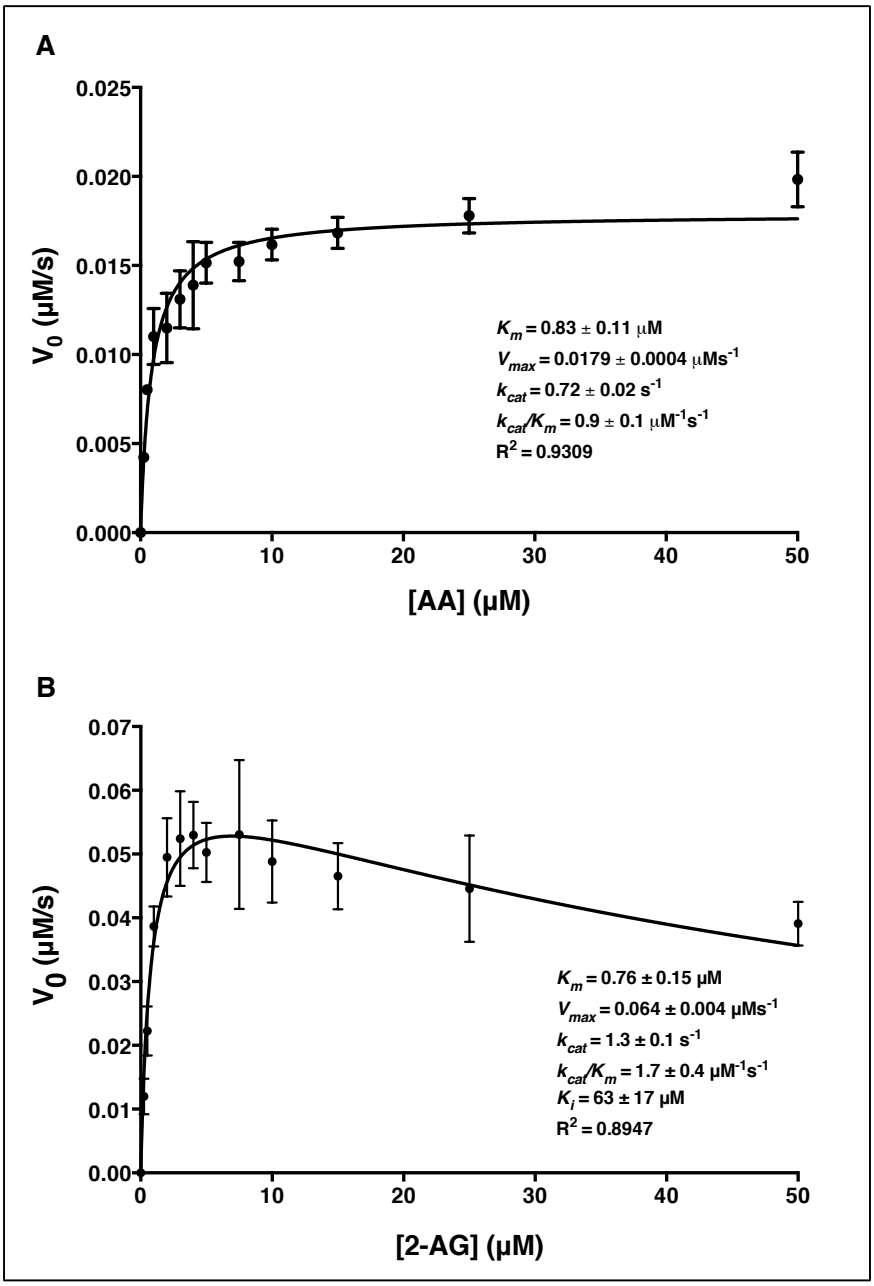

Figure 6. Kinetics of oxygenation of AA and 2-AG by mCOX-2. (*A*) Kinetic determinations for AA were conducted using 25 nM mCOX-2, and the initial velocity plot is reflective of PGs formed during a 10 s incubation, as determined by LC-MS/MS. (*B*) Kinetic determinations for 2-AG were conducted in the presence of 1 μM PPHP using 50 nM mCOX-2, and the initial velocity plot is reflective of PG-Gs formed during a 10 s incubation as determined by LC-MS/MS. The data were analyzed using GraphPad Prism 6 software according to the Michaelis-Menten model for AA and a model for substrate inhibition for 2-AG. Results for AA and 2-AG oxygenation are the mean ± S.D. for one or three independent experiments, respectively, each performed in triplicate.

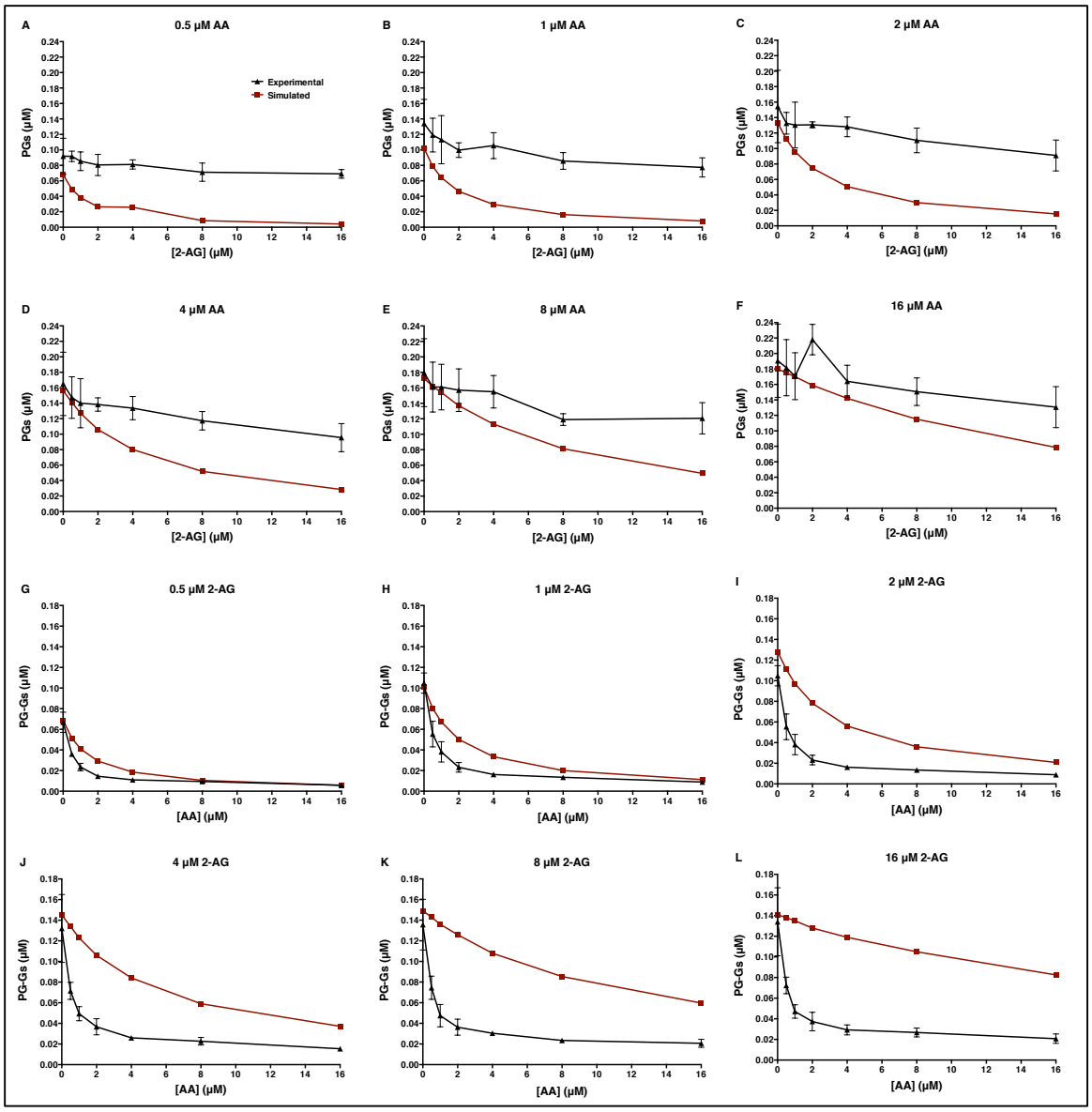

Figure 7. Expected production of PGs and PG-Gs by mCOX-2 incubated with the indicated combinations of AA and 2-AG assuming only a competitive interaction of substrates at the catalytic site of COX-2 and substrate inhibition in the case of 2-AG. The simulated data were obtained using KinTek Explorer software. The experimental data are those obtained from the experiment described in the legend to Fig. 4. Data shown are PGs produced for various concentrations of AA in the presence of increasing concentrations of 2-AG (*A-F*) and PG-Gs produced for various concentrations of 2-AG in the presence of increasing concentrations of AA (*G-L*).

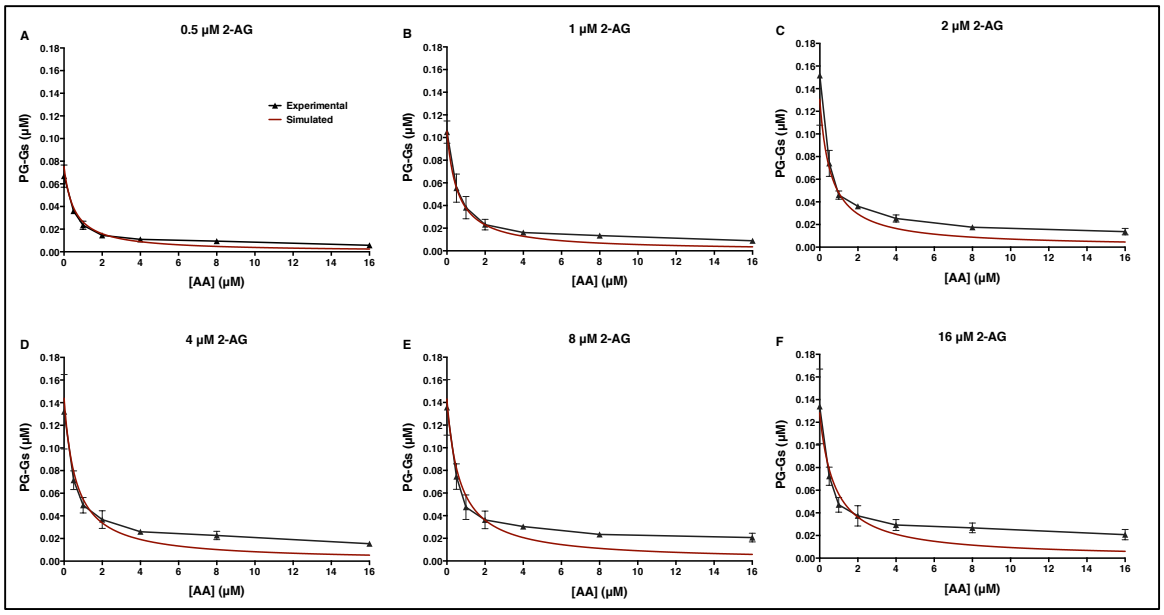

Figure 8. Analysis of the effects of AA on 2-AG oxygenation using classical models of inhibition. The model incorporated classical uncompetitive inhibition based on binding of AA to the allosteric site of COX-2 along with competition between the two substrates for the catalytic site and substrate inhibition of 2-AG. The data points are values obtained in the experiment described in the legend to Fig. 4, and the curves in red are the result of nonlinear regression analysis performed using GraphPad Prism 6 software.

We next tested the hypothesis that the observed results might be explained on the basis of classical models for uncompetitive, noncompetitive, or mixed inhibition of 2-AG oxygenation resulting from binding of AA to the allosteric site. These models also assumed competition between the substrates at the active site and substrate inhibition in the case of 2-AG. The best fit was achieved with a model of uncompetitive inhibition of 2-AG oxygenation by AA, which yielded a K_I value of 0.52 μM for AA at the allosteric site (R^2 = 0.88). The classic uncompetitive model, however, assumes that binding of AA at the allosteric site completely inhibits 2-AG oxygenation, ultimately leading to total blockade of PG-G formation at high AA concentrations. This is inconsistent with the experimentally observed failure of AA

to completely suppress PG-G formation (Fig. 8). Furthermore, similar efforts to model the modest inhibitory effects of 2-AG on AA oxygenation were unsuccessful.

AA Allosterically Curbs 2-AG Oxygenation by COX-2. To better explain the effects of combining AA and 2-AG on the oxygenation of each substrate, we hypothesized that both substrates can bind to either the catalytic or the allosteric subunit or both, and that the binding of a substrate in the allosteric subunit modulates, but does not necessarily eliminate, the activity of the catalytic subunit. To test this hypothesis, we created the COX-2 Reaction Model (CORM), a rule-based ordinary differential equation model encompassing all of the potential binding interactions of each substrate at both the catalytic and allosteric sites of the enzyme (Fig. 9). As some kinetic parameters in CORM are not easily accessible for direct measurement, we used a Bayesian statistics inference approach to determine whether CORM could explain the experimental data and estimate parameter distributions within a probability framework. Bayesian approaches can model systems with parametric uncertainty in order to interpret observed behavior within constraints of existing knowledge (148). To reduce the number of values to be derived computationally, the experimental K_m for each substrate was used to approximate its K_D for binding to the catalytic site when no ligand is present in the allosteric site, and the K_D for binding of 2-AG to the allosteric site in the presence of 2-AG at the catalytic site was fixed at the experimentally determined K_I value for substrate inhibition (Fig. 6). The catalytic constants for product formation when each substrate is bound only to the catalytic site were fixed to the experimentally determined k_{cat} values (Fig. 4), and the catalytic constant for

the enzyme with 2-AG in both sites was set to zero, as assumed in the model for substrate inhibition. The forward rate constants for formation of the remaining reversible intermediate complexes were fixed at diffusion-limited values. All remaining parameters were fitted to experimental data using a Bayesian Markov Chain Monte Carlo walk, which samples possible parameter values to probabilistically determine the combinations that fit the experimental data (136). Equilibrium constants for intermediate complexes were then calculated from the relevant rate constants. This approach generates both a parameter set of the most probable values and a probability distribution (Fig. 10) for the value of each parameter that indicates its level of constraint, given the experimental data. The 95% credible intervals, which are calculated from the probability distributions, contain the true parameter with a 95% probability (Table 1).

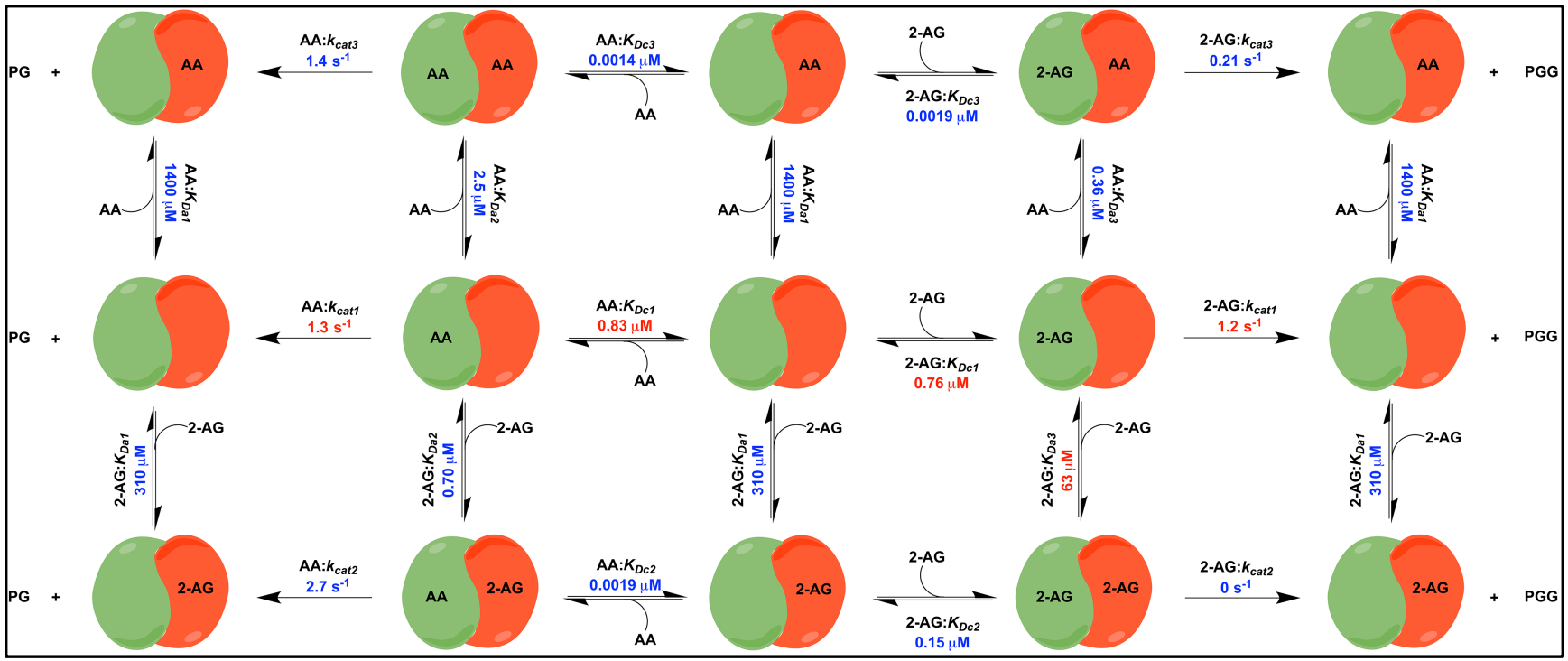

Figure 9. COX-2 Reaction Model (CORM) for the interaction of substrates AA and 2-AG with COX-2, a functional heterodimer comprising a catalytic subunit (left, green) and an allosteric subunit (right, red). The model provides values for the equilibrium constants of all intermediate complexes and rate constants for product-forming steps as indicated. Constants depicted in red were fixed to experimentally determined values. Specifically, K_m values, which varied little between experiments, were based on the data in Fig. 6. In order to optimize fitting to the data in Fig. 4, k_{cat} values obtained from those data were used. Values depicted in blue are the most probable values for those parameters, based upon computational results.

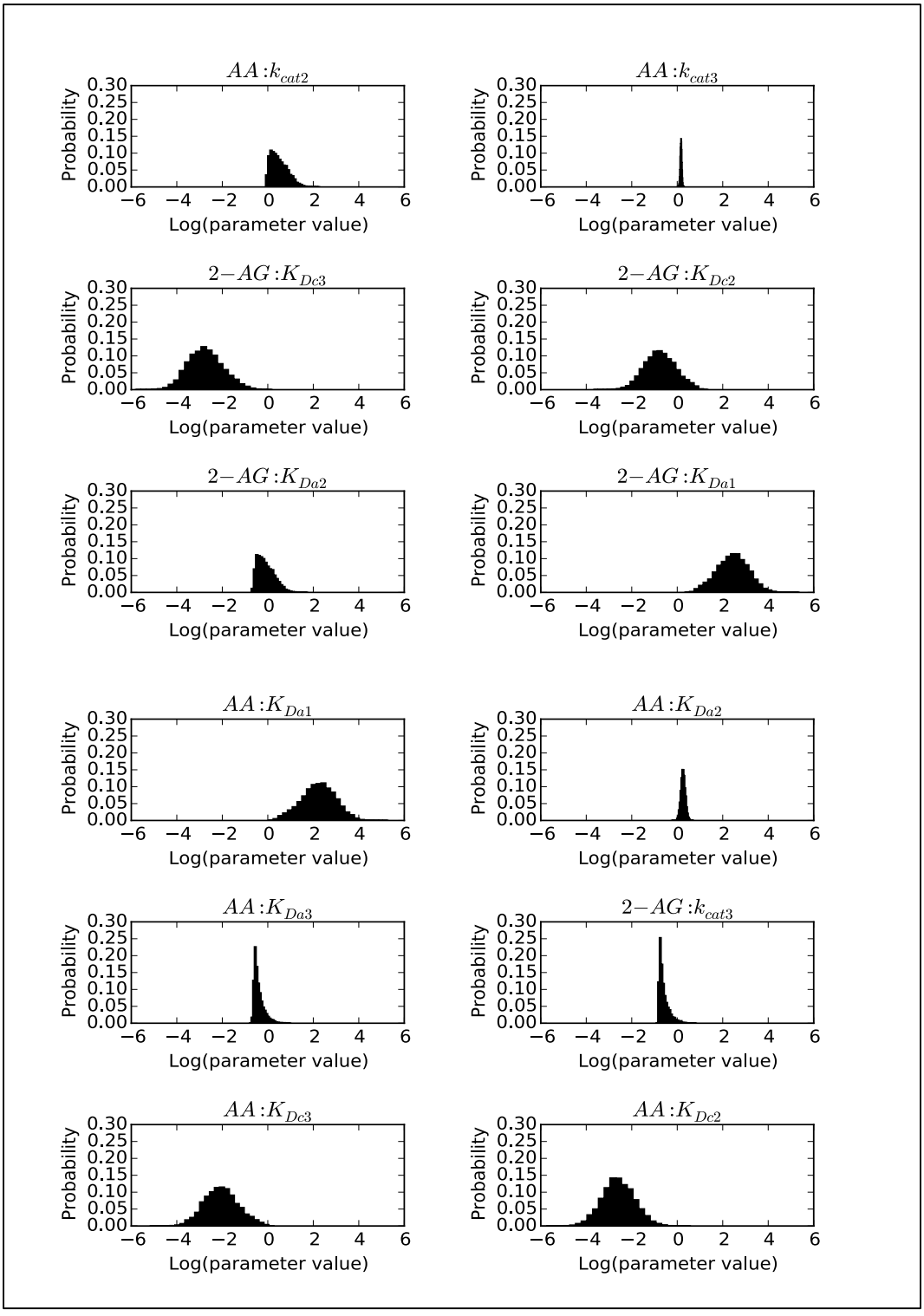

Figure 10. CORM parameter posterior probability distributions. Distributions were obtained using Bayesian Markov Chain Monte Carlo sampling of parameter values as described in the Methods.

As seen in Fig. 10, the coefficients of variation for the parameter distributions vary substantially across the model fit, so that some distributions are quite narrow whereas others are much broader. The presence of broad distributions reflects the fact that our current knowledge of the system is insufficient to result in a tight convergence of all values. Those parameters with broad distributions are less likely to play a significant role in the overall kinetics of the system, whereas those with a narrow distribution more strongly affect the observed kinetic behavior. These considerations suggest that the most influential parameters of those modeled computationally are the dissociation constants for the binding of AA in the allosteric site after either AA or 2-AG has bound in the catalytic site, and the rate constants for the formation of PGs or PG-Gs, respectively, from those resulting doubly bound complexes.

Table 1. CORM 95% credible intervals and most probable parameter values obtained from sampling. These represent the minimum width credible intervals enclosing the region of highest posterior probability density. All k_{cat} parameter values are expressed in units of s^{-1}, and all K_D parameters are in μM.

Parameter	Lower Bound	Most Probable Value	Upper Bound
AA:k_{cat2}	0.90	2.7	17
AA:k_{cat3}	1.3	1.4	1.7
2-AG:k_{cat3}	0.14	0.21	0.77
AA:K_{Dc2}	0.0	0.0019	0.060
AA:K_{Dc3}	0.0	0.0014	0.25
2-AG:K_{Dc2}	0.0091	0.15	4.2
2-AG:K_{Dc3}	0.0	0.00019	0.063
AA:K_{Da1}	5.2	1400	4300
AA:K_{Da2}	1.2	2.5	2.9
AA:K_{Da3}	0.20	0.36	1.3
2-AG:K_{Da1}	11	310	5000
2-AG:K_{Da2}	0.22	0.70	4.4

The most probable K_D and k_{cat} values obtained computationally are shown in Fig. 9 and Table 1. Fig. 11 and Fig. 12 provide a comparison of the experimental data with those predicted by the model. Clearly, CORM provides a better fit to the experimental data than was observed for any of the classic kinetics models tested, supporting the hypothesis that the COX-2 reaction occurs through the formation of multiple complexes via a variety of pathways.

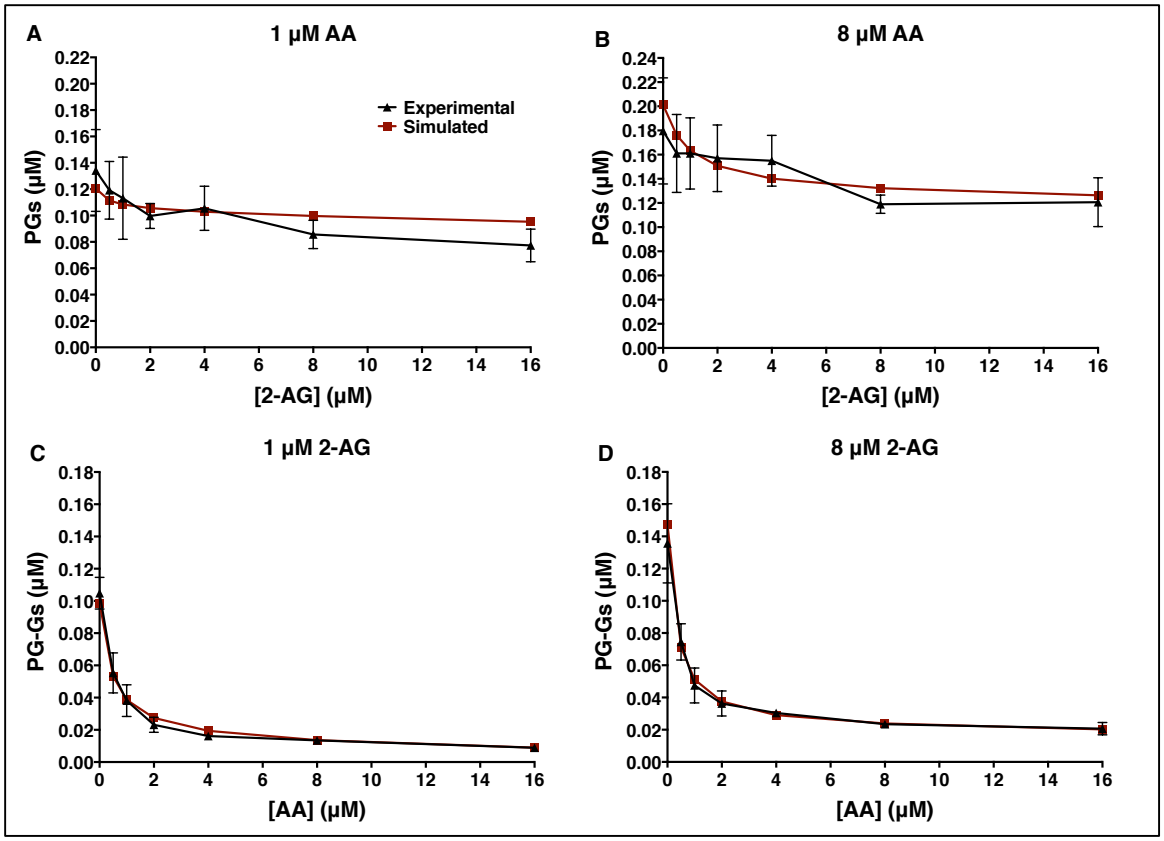

Figure 11. Computational modeling of both the catalytic and allosteric sites of COX-2 enables data fitting. Graphed are the actual data from the experiment described in the legend to Fig. 4 versus those simulated using parameters generated by CORM shown in Fig. 9. Data shown are PG levels produced from low (1 μM) and high (8 μM) concentrations of AA in the presence of increasing concentrations of 2-AG (*A* and *B*) and PG-G levels produced from low and high concentrations of 2-AG in the presence of increasing concentrations of AA (*C* and *D*). For results from the entire set of data, see Fig. 12.

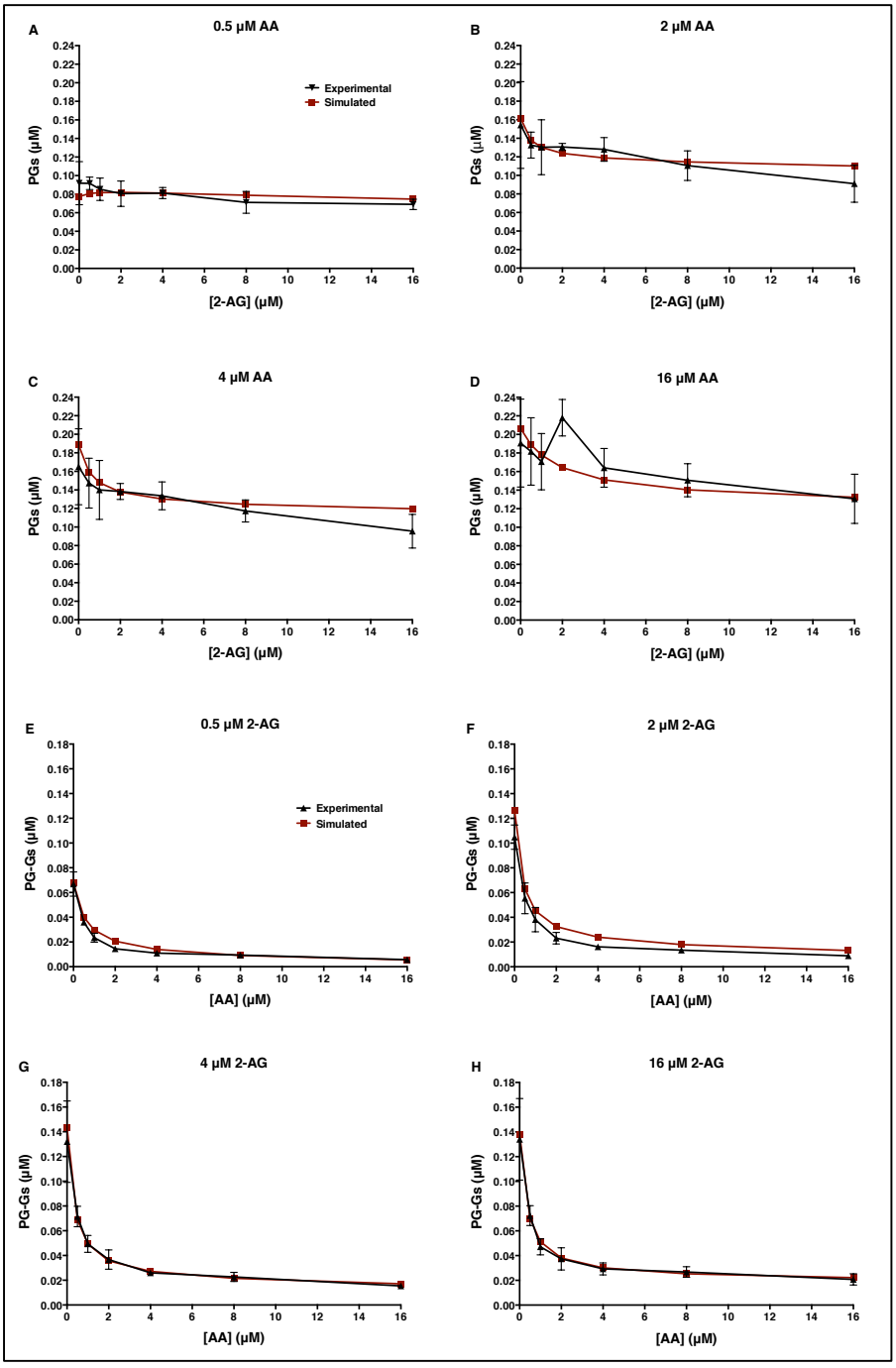

Figure 12. Modeling of both the catalytic and allosteric sites of COX-2 enables data fitting. Experimental results versus those simulated using the computational parameters derived from CORM (Fig. 9 and Table 1) are presented. Data shown are PG levels produced from the indicated concentrations of AA in the presence of increasing concentrations of 2-AG (*A-D*) and PG-G levels produced from the indicated concentrations of 2-AG in the presence of increasing concentrations of AA (*E-H*).

A more detailed analysis of CORM's parameters suggests that binding of either substrate to the allosteric site is favored only if a ligand is present in the catalytic site. When AA is present alone, the doubly bound complex is favored over the singly bound one at concentrations above approximately 1.5 μM whereas for 2-AG, the singly bound complex predominates except at very high concentrations (Fig. 13 *A* and *B*). When both substrates are present over a wide range of concentrations, complexes with two different ligands are favored over those in which the same molecule is bound to both sites (Fig. 13 *C* and *D*). Notably, CORM predicts that the catalytic constant for conversion of 2-AG to PG-Gs when AA is present in the allosteric site is reduced when compared to the catalytic constant associated with 2-AG turnover in the absence of a ligand in the allosteric site; based on the kinetic rate distributions returned by CORM, there is a 98% probability that the turnover of 2-AG with no ligand in the allosteric site is greater than when AA is present in the allosteric site. In contrast, the catalytic constant for AA oxygenation by COX-2 is predicted to be higher when 2-AG occupies the allosteric site than when AA or no ligand is present in that site; there is an 85% probability that the 2-AG bound-complex turns over AA more quickly than the complex with no allosteric ligand. Thus, allosteric interactions between substrates and COX-2, as revealed through kinetic modeling, provide a rational explanation for the observed *in vitro* experimental results.

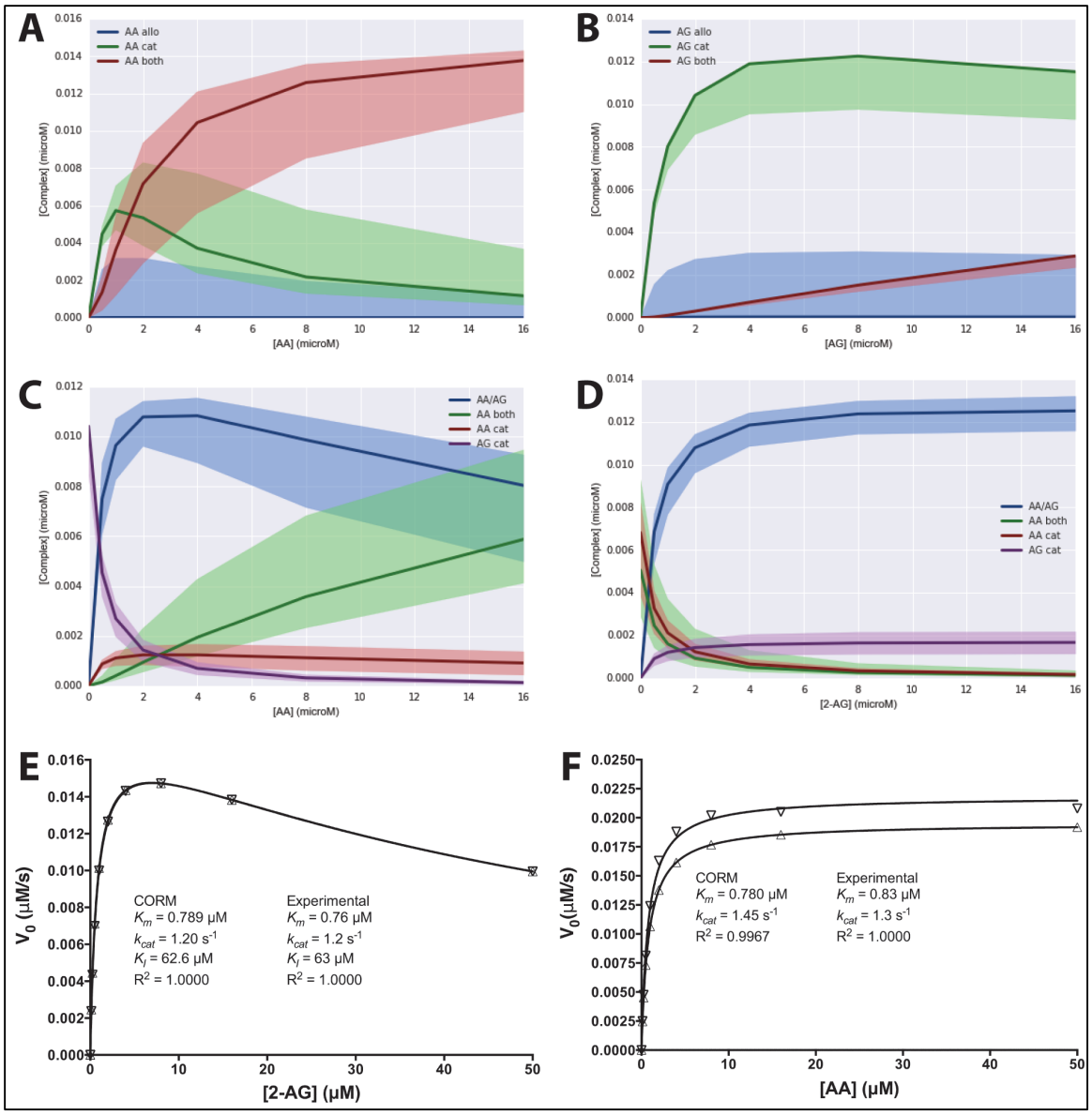

Figure 13. CORM-based predictions of COX-2, AA, and 2-AG complex formation. (*A* and *B*) Steady state levels of AA- or 2-AG-containing complexes formed in the absence of the other substrate. Blue, green, and red lines indicate predicted concentrations of COX-2 with AA or 2-AG bound in only the allosteric site, only the catalytic site, or in both sites, respectively, when simulated at the most probable values returned by CORM calibration. Shaded regions delineate possible complex formation as predicted by the entire calibrated parameter ensemble consistent with experimental data. (*C* and *D*) Levels of prominent complexes as AA concentration varies in the presence of 2 μM 2-AG (*C*) or as 2-AG concentration varies in the presence of 2 μM AA (*D*). Blue, green, red, and purple lines indicate predicted concentrations of COX-2 with both AA and 2-AG bound, with AA bound to both catalytic and allosteric sites, with AA bound only to the catalytic site, and with 2-AG bound only to the catalytic site, respectively. Other low abundance complexes were present at less than 0.0009 μM at all concentrations and are not shown. Lines indicate most probable value simulations, and shaded regions delineate predictions based on the entire parameter set as in (*A*) and (*B*). All simulations were performed in the presence of 15 nM COX-2. (*E* and *F*) Simulated substrate concentration versus initial velocity curves for the COX-2 enzyme behaving as predicted by CORM. The most probable parameter values derived from CORM (Fig.

9 and Table 1) were used to predict the initial velocity of reaction using 15 nM COX-2 and the indicated concentrations of 2-AG (*E*) or AA (*F*) (▽). The resulting values of K_m, k_{cat}, and K_I generated by curve fitting using the substrate inhibition model (*E*) or Michaelis-Menten model (*F*) are shown. Also shown for comparison are the corresponding curves generated from the substrate inhibition model (*E*) or the Michaelis-Menten model (*F*) using the experimental parameters that were employed in the generation of CORM (△).

Discussion

COX-2 as an Allosteric Enzyme. In 1997, Swinney et al. reported that COX-1 behaves as an allosteric enzyme with a Hill coefficient of 1.3 (149). Their interpretation of this apparent cooperativity was later disputed by Chen et al., who explained the phenomenon on the basis of COX's requirement for product hydroperoxide to activate the enzyme's active site (150). Since that time, researchers have generally agreed that the COX isoforms do not behave as allosteric enzymes with regard to AA. However, as outlined above, recent evidence strongly supports the concept that the enzymes are functional heterodimers and that activity is modulated by binding of nonsubstrate ligands to the allosteric subunit (56, 87, 151). Here, we report that AA and 2-AG, despite similar catalytic efficiencies with COX-2 when measured individually *in vitro*, differ markedly in their rate of oxygenation in the presence of the other substrate. Furthermore, we present data consistent with the hypothesis that this modulation of COX-2 activity not only occurs with purified protein but also in intact cells.

CORM Explains the Complex Interplay of COX-2 Substrates. To explain our experimental observations, we hypothesized that AA and 2-AG can bind to both the catalytic and allosteric sites of the enzyme, and that binding in the allosteric site modulates the activity of the catalytic site. This hypothesis is

described by CORM, which provides assessments of the affinity of each substrate for COX-2's catalytic and allosteric sites and the k_{cat} values associated with each catalytically competent complex. We used a Bayesian statistical approach to characterize CORM within a probabilistic framework that uses prior knowledge to constrain plausible biochemical mechanisms of COX-2 reaction dynamics. To the best of our knowledge, this is the first attempt to use this conditional probability approach to infer mechanisms for small biochemical model systems such as the COX-2 reaction network. CORM suggests that the two substrates compete for the enzyme's allosteric site. Binding of AA to that site likely results in a decrease in the enzyme's catalytic efficiency for oxygenation of 2-AG while having little effect on the oxygenation of AA. CORM also suggests that binding of 2-AG to the allosteric site of COX-2 in the presence of AA in the catalytic site increases the enzyme's catalytic efficiency for oxygenation of AA. These results explain why the suppression of 2-AG oxygenation by AA and the suppression of AA oxygenation by 2-AG are greater and lesser, respectively, than predicted based upon competition at the catalytic site alone. Thus, our mechanistic model and parameter inferences reveal a complex enzyme-substrate interaction that cannot be construed from classical kinetic analyses.

It is important to note that a number of assumptions were made when constructing CORM, including that the forward rate constant for formation of all intermediate complexes is diffusion-limited, that the affinity of each substrate binding alone to the catalytic site can be approximated by its experimental K_m, that the respective experimental k_{cat} value should apply to product formation

specifically from this complex, and that the affinity of 2-AG at the allosteric site can be approximated by its experimental K_I. The latter assumptions are reasonable in the case of 2-AG oxygenation, as the experimental values obtained for that substrate were derived from a substrate inhibition model that accounts for binding of 2-AG in both the catalytic and allosteric sites. Consequently, it is not surprising that CORM predicts initial rate values for oxygenation of 2-AG in the absence of AA that are indistinguishable from those predicted from the substrate inhibition model using the same experimentally derived parameters (Fig. 13*E*). In the case of AA oxygenation, however, the K_m and k_{cat} values used to derive CORM were obtained from the Michaelis-Menten model, which assumes only a single binding site for substrate. The presence of a catalytically active complex containing AA in both the allosteric and catalytic sites, as modeled in CORM, calls into question how well the Michaelis-Menten model applies to this scenario. As seen in Fig. 13*F*, initial velocities predicted by the most probable values returned by CORM fit the Michaelis-Menten equation remarkably well. However, the resulting K_m and k_{cat} values are lower and higher, respectively, than the corresponding experimental parameters applied during the generation of CORM. These results indicate that an enzyme exhibiting the behavior predicted by CORM will appear to follow Michaelis-Menten kinetics, as COX-2 does experimentally; however, the K_m and k_{cat} values returned will reflect the activity of all catalytically competent complexes rather than any single one. Consequently, some error has likely resulted from the use of experimental K_m and k_{cat} values to estimate the affinity and activity of the complex containing AA bound only to the catalytic site during the derivation of CORM.

Structural Basis of Allostery. Previously reported data suggest that the two sequence-identical subunits of COX-2 are distinguished by the presence of heme in the catalytic site and its absence in the allosteric site (56). This difference is not recapitulated in the currently available crystal structures of the holoenzyme, which show heme bound to both subunits. Nevertheless, crystal structures of complexes of the holoenzyme with either AA or 1-AG, a more stable isomer of 2-AG, show different conformations for the binding of the substrate in each subunit (37, 81). In both cases, only one subunit contains a productively bound conformation of the substrate. These observations suggest a functional difference between the two subunits even when heme is bound in both sites. They also confirm that both AA and 2-AG retain affinity for the allosteric site, albeit in a different binding pose than what is observed in the catalytic site. Thus, there is a structural foundation for the allosteric regulation of COX-2 activity by both substrates. Our kinetic model suggests that binding of either AA or 2-AG in the allosteric site is inhibitory to 2-AG oxygenation and mildly stimulatory to AA oxygenation, reinforcing literature reports that AA oxygenation is relatively unaffected by the presence of many non-substrate modulators (both inhibitory and stimulatory) at concentrations that markedly affect 2-AG oxygenation (83, 86, 87). We currently do not know the basis for these differences between the substrates, but crystal structure data of 1-AG in the COX-2 active site reveal that binding requires movement of the side chain of leucine-531 that is not required for binding of AA (81). It is possible that the flexibility required to accommodate 2-AG in the active site is highly sensitive to the presence of ligands in the allosteric site.

Role of Allostery in Intact Cells. Our findings that AA inhibits 2-AG oxygenation *in vitro* and that cellular AA and PG-G levels are inversely correlated lead one to question the degree to which allosteric control modulates PG-G synthesis in cells. Most studies of cellular PG-G production have employed stimuli that trigger the release of high concentrations of free AA, only a portion of which is converted to PGs. In most cases, the ratio of AA to 2-AG in whole cell lysates is at least 10:1, but the ratio of PGs to PG-Gs has been in the range of 500 to 1000:1 (75, 127). In the experiments reported here, the PG:PG-G ratio was from 20- to 100-fold higher than the AA:2-AG ratio (Figs. 1 and 2). These findings are consistent with our new evidence that AA suppresses 2-AG oxygenation by COX-2. However, allosteric regulation is likely only one of a number of factors contributing to the high PG:PG-G ratio found in cells. Others include the kinetics of release of AA and 2-AG, the local concentrations of each substrate, and the hydroperoxide tone in the immediate vicinity of the enzyme.

Although the heterodimeric nature of COX enzyme function has been described, the impact of substrate binding in the allosteric site on catalytic efficiency or inhibitor potency has not been thoroughly explored. Previous work from Smith and colleagues has revealed that non-substrate fatty acids, such as palmitic acid, oleic acid, stearic acid, and 20:1ω9, potentiate COX-2 oxygenation of AA (85) and palmitc acid and 20:1ω9 potentiate COX-2 oxygenation of 2-AG (152). Palmitic acid, oleic acid, and stearic acid, which increase COX-2 activty toward AA oxygenation when present in 20-fold excess of the substrate, are the most abundant non-esterified fatty acids in RAW264.7 cells, where palmitic

acid:AA ratios range from 5-60 (153). These data suggest that non-substrate fatty acids may modulate AA and/or 2-AG oxygenation in physiological settings. Additional work from our laboratory by Kudalkar et al. has revealed that 13-methylarachidonic acid allosterically potentiates COX-2 oxygenation of 2-AG by increasing the enzyme's catalytic efficiency and relieving substrate inhibition (87). This finding raises the possibility that there may be unidentified endogenous modulators of 2-AG oxygenation by COX-2 present in cells.

Our current findings extend these previous studies to include COX-2 substrates as modulators of the enzyme's catalytic acitivity. The data presented herein demonstrate that binding of AA or 2-AG in the allosteric site of COX-2 leads to changes in the efficiency of oxygenation of both substrates in the catalytic site, effects that are not easily appreciated through kinetic studies using individual substrates. Our findings also indicate that both substrates are theoretically capable of competing with inhibitors for either site. Clearly future considerations of the kinetic behavior of the COX enzymes must take into account the potential for substrate and inhibitor binding, and the associated functional consequences, in both subunits of the enzyme.

CHAPTER III

ENZYMATIC OXIDATION OF M_1dG IN THE GENOME

Introduction

As described above, oxidative damage to PUFAs and the deoxyribose ring of DNA give rise to MDA and base propenals, respectively (99, 154). Both MDA and base propenals react with DNA *in vitro* to give primarily the exocyclic pyrimidopurinone adduct, M_1dG (98, 155), which has been shown to induce base-pair substitutions and frameshift mutations in both bacterial and mammalian cells (115, 156), unless it is first removed from DNA via NER (115, 157). Recent evidence suggests M_1dG is converted to 6-oxo-M_1dG, a novel genomic DNA adduct of uncharacterized mutagenicity. Whereas oxidation of free M_1dG nucleoside to free 6-oxo-M_1dG is catalyzed by cytosolic XO or AO, oxidation of genomic M_1dG to 6-oxo-M_1dG is carried out by an unidentified nuclear enzyme. Herein I describe my progress toward identifying this enzyme.

Materials and Methods

***Materials*.** All chemicals were obtained from commercial sources and used without further purification unless otherwise noted. Adenine propenal was prepared as previously described (158). Single-stranded 21-mer DNA with sequences 5'-AATAAATCGCGCGCGTAAATA-3' or 5'-TATTTACGCGCGCGATTTATT-3' was purchased from Eurofins MWG Operon

(Huntsville, AL). Rats were purchased from Charles River Laboratories (Wilmington, MA). RAW264.7, HepG2, HEK293, and RKO cells were obtained from the American Type Culture Collection (Rockville, MD). Cell culture reagents were purchased from Life Technologies (Gaithersburg, MD). Fetal bovine serum (FBS) was purchased from Atlas Biologicals (Fort Collins, CO). DNase I and phosphodiesterase I from *Crotalus adamanteus* venom were purchased from Worthington Biochemical Corporation (Lakewood, NJ). Nuclease P1 from *Penicillium citrinum* was purchased from Wako Chemicals USA (Richmond, VA). RNase A from bovine pancreas and Proteinase K were purchased from Takara Bio USA (Mountain View, CA). Alkaline phosphatase from bovine intestinal mucosa and RNase T from *Aspergillus oryzae* were purchased from Sigma-Aldrich (St. Louis, MO). [$^{15}N_5$]-dG, [$^{12}C_6{}^{14}N_4$]-L-arginine, [$^{12}C_6{}^{14}N_2$]-L-lysine, [$^{13}C_6{}^{15}N_4$]-L-arginine, and [$^{13}C_6{}^{15}N_2$]-L-lysine were purchased from Cambridge Isotope Laboratories, Inc. (Andover, MA). Purified AlkB, ALKBH2, ALKBH3, and 1-methyl-2'-deoxyadenosine (m1A)-containing ssDNA were generous gifts from Dr. Deyu Li (University of Rhode Island). The photoaffinity probe, DR025, was provided by the Vanderbilt Institute of Chemical Biology, Chemical Synthesis Core, Vanderbilt University, Nashville, TN 37232-0412.

Preparation of M_1dG-containing double-stranded oligonucleotides. Double-stranded 21-mer oligonucleotide was prepared by combining equimolar amounts of complementary single-stranded DNA in DNase-free water. This solution was heated to 95°C in a heat block for 10 min, at which point the heat block was turned off and the samples allowed to cool gradually to room

temperature. The resulting double-stranded DNA (dsDNA) was subsequently treated with a 10-fold molar excess of adenine propenal for 24 h at 37°C to induce formation of M_1dG adducts. Following reaction, the DNA was precipitated by the sequential addition of 1/10th volume of 3 M sodium acetate (pH 5.5) and then 2 volumes of ice-cold ethanol (absolute) followed by centrifugation at 10,000 *g* for 20 min at 4°C. Precipitated DNA was washed, resuspended in DNase-free water, and quantified spectrophotometrically based upon its characteristic absorption at 260 nm. An aliquot of this oligonucleotide was digested, as described below, to confirm the presence of M_1dG.

DNA digestion and LC-MS/MS analysis of products. Prior to digestion, isotopically labeled internal standards [$^{13}C^{15}N_2$]-M_1dG and [$^{15}N_5$]-6-oxo-M_1dG were added to the samples for ultimate use in absolute quantitation of M_1dG adducts. DNA samples were digested to single nucleosides in a series of three incubation steps with digestive enzymes: (1) 500 U DNase I in 15 mM $MgCl_2$ and 10 mM MOPS (pH 7.9) for 1.5 h, (2) 15 U nuclease P1 in 1 mM $ZnCl_2$ for 2.5 h, and (3) 50 U alkaline phosphatase and 8 U phosphodiesterase I in 50 mM MOPS (pH 7.9) for 15 h at 37°C. Listed quantities of digestion enzymes are for digestion of 1 mg of DNA and were scaled accordingly depending on the DNA content of the sample. Digestion reactions were quenched by addition of ice-cold ethanol and then centrifuged to pellet insolubles. The supernatant was then evaporated to near-dryness under nitrogen and the resulting residue resuspended in water for LC-MS/MS analysis. Digested nucleosides were chromatographed on a Phenomenex 4 µm Synergi Polar-RP column (Torrance, CA) with mobile phases consisting of

0.1% formic acid in water (solvent A) and 0.1% formic acid in a 1:1 methanol/acetonitrile mixture (solvent B) at a flow rate of 400 µL/min. The 5 min gradient consisted of the following: 0−0.50 min, 5% B; 0.5−3.50 min, 5→60% B; 3.50−3.51 min, 60→98% B; 3.51−5.00 min, 98% B. Mass analysis was performed on a 6500 QTrap mass spectrometer (AB Sciex Systems) equipped with an electrospray ionization source with detection in positive ion mode. M_1dG and its isotopically labeled standard, [$^{13}C^{15}N_2$]-M_1dG, were detected with selected reaction monitoring with the following transitions, *m/z* 304→188 and *m/z* 307→191, respectively. 6-oxo-M_1dG and its isotopically labeled standard, [$^{15}N_5$]-6-oxo-M_1dG, were detected with selected reaction monitoring using the following transitions, *m/z* 320→204 and *m/z* 325→209, respectively. These transitions correspond to the cleavage of the glycosidic bond and neutral loss of the deoxyribose moiety (−116 Da), with the positive charge remaining on the base.

Western blot. Samples were denatured in 2x Laemmli sample buffer (Bio-Rad, Hercules, CA) with 6% β-mercaptoethanol and heated at 95°C for 15 min. Proteins were resolved via SDS-PAGE and transferred to nitrocellulose membranes. Membranes were blocked with Odyssey Blotting Buffer (LI-COR Biosciences, Lincoln, NE) for 1 h at room temperature and then incubated with primary antibodies overnight at 4°C as follows: H3K27me3 (Millipore, Temecula, CA, 1:2000); pan-trimethyllysine (PTM Biolabs Inc., Chicago, IL, 1:2000); Sod1 (Cayman Chemical, Ann Arbor, MI, 1:1000); H3 (Cell Signaling Technology, Danvers, MA, 1:1000); XO (Abcam, Cambridge, MA, 1:1000); actin (Santa Cruz Biotechnology, Dallas, TX, 1:5000). Blots were washed three times with Tris-

buffered saline + 0.1% (v/v) Tween-20 (TBST) and then incubated with IRDye® secondary antibodies or IRDye®-streptavidin (LI-COR Biosciences) (1:5000) in blocking buffer for 1 h. Following three additional washes with TBST, blots were developed using the Odyssey Infrared Imaging System (LI-COR Biosciences).

Preparation of rat liver nuclear lysates. All animal care and experimental procedures involving rats were approved by the Vanderbilt University Medical Center Institutional Animal Care and Use Committee and were performed in accordance with relevant guidelines and regulations. Rats were sacrified by isofluorane anesthesia and cervical dislocation. Livers were removed, rinsed in cold phosphate-buffered saline (PBS), cut into small pieces, and subjected to Dounce homogenization in ice-cold hypotonic lysis buffer, consisting of 10 mM HEPES (pH 7.9), 1.5 mM $MgCl_2$, 10 mM KCl, and 0.5% (v/v) IGEPAL with 0.2% (v/v) each of protease and phosphatase inhibitor cocktail followed by lysis on ice for 30 min. Cell lysates were then centrifuged at 1000 *g* for 10 min at 4°C to pellet nuclei. The resulting nuclei were washed twice more with hypotonic lysis buffer, before they were lysed in an isotonic nuclear resuspension buffer, consisting of 50 mM HEPES (pH 7.9), 150 mM NaCl, and 1% (v/v) IGEPAL with 1% (v/v) each of protease and phosphatase inhibitor cocktail. Lysis was promoted by drawing the sample through a 27-gauge needle multiple times and sonicating it with a series of ten, one-second pulses. Insolubles were pelleted via centrifugation at 10,000 *g* for 10 min at 4°C. The resulting supernatant was used as rat liver nuclear lysate in subsequent experiments.

Reaction of M_1dG-containing dsDNA with rat liver nuclear lysates. A volume of nuclear lysate, prepared as described above, containing 750 µg of total protein was incubated with an amount of double-stranded oligonucleotide containing 150 pmol of M_1dG in a total volume of 100 µL for approximately 24 h at 37°C. In experiments involving the addition of small molecules, the indicated compounds were added concomitantly with M_1dG-containing oligonucleotide. Following incubation, the DNA was precipitated by the sequential addition of 1/10th volume of 3 M sodium acetate (pH 5.5) and then 2 volumes of ice-cold ethanol (absolute) followed by centrifugation at 10,000 *g* for 20 min at 4°C. Precipitated DNA was washed once with additional ethanol and then resuspended in DNase-free water for subsequent digestion and LC-MS/MS analysis, as described above.

Cell culture. RAW264.7 cells were cultured in DMEM + GlutaMax supplemented with 10% FBS at 37°C and 5% CO_2. RKO, HepG2, and HEK293 cells were cultured in Roswell Park Memorial Institute (RPMI) medium supplemented with 10% FBS at 37°C and 5% CO_2. Cells purposed for nuclear lysate experiments were scraped into the existing medium and harvested via centrifugation at 1000 *g* at 4°C. The supernatant medium was then removed and cell pellets stored at -20°C. Cells harvested for genomic DNA analysis were washed twice with Ca^{2+}/Mg^{2+}-free Dulbecco's Phosphate Buffered Saline (DPBS) prior to storage at -20°C.

Preparation of cell nuclear lysates. Cell pellets were thawed on ice and lysed in ice-cold hypotonic lysis buffer, consisting of 10 mM HEPES (pH 7.9), 1.5 mM $MgCl_2$, 10 mM KCl, and 0.5% (v/v) IGEPAL with 0.2% (v/v) each of protease

and phosphatase inhibitor cocktail. Cells were resuspended vigorously via pipette and allowed to lyse on ice for 30 min. Cell lysates were then centrifuged at 1000 *g* for 10 min at 4°C to pellet nuclei. The resulting nuclei were washed twice more with hypotonic lysis buffer before they were lysed in an isotonic nuclear resuspension buffer, consisting of 50 mM HEPES (pH 7.9), 150 mM NaCl, and 1% (v/v) IGEPAL with 1% (v/v) each of protease and phosphatase inhibitor cocktail. Nuclear lysates were sonicated with a series of ten, one-second pulses, and then insolubles were pelleted via centrifugation at 10,000 *g* for 10 min at 4°C. The resulting supernatant was used as cell nuclear lysate in subsequent experiments. Cell nuclear lysates were always prepared fresh from cell pellets on the day of the experiment.

Reaction of M_1dG-containing dsDNA with cell nuclear lysates. A volume of nuclear lysate, prepared as described above, containing 500 μg of total protein was incubated with an amount of double-stranded oligonucleotide containing 250 pmol of M_1dG for approximately 20 h at 37°C. In experiments involving the addition of small molecules, the indicated compounds were preincubated with the nuclear lysates for 15 min at 37°C prior to the addition of M_1dG-containing oligonucleotide. Following incubation, the DNA was precipitated by the sequential addition of 1/10th volume of 3 M sodium acetate (pH 5.5) and then 2 volumes of ice-cold ethanol (absolute) followed by centrifugation at 10,000 *g* for 20 min at 4°C. Precipitated DNA was washed once with additional ethanol and then resuspended in DNase-free water for subsequent digestion and LC-MS/MS analysis, as described above.

Treatment of RKO cells with α-KG-dependent enzyme inhibitors. RKO cells were plated at a density of 5 x 10^6 cells/150 mm plate in RPMI + 10% FBS and incubated for 24 h at 37°C and 5% CO_2. The existing medium was removed 24 h later and replaced with serum-free RPMI, and the cells were allowed to incubate at 37°C for an additional 24 h. Once again, the existing medium was removed and replaced with fresh serum-free RPMI containing 400 μM adenine propenal. Cells were incubated at 37°C for 1 h, at which point the adenine propenal-containing medium was removed and replaced with fresh serum-free RPMI containing vehicle or inhibitor. Cells were harvested, as described above, at various times following the addition of inhibitor.

Isolation of genomic DNA. Cell pellets were lysed in hypotonic lysis buffer (10 mM HEPES (pH 7.9), 1.5 mM $MgCl_2$, 10 mM KCl, 0.5% (v/v) IGEPAL) containing 0.2% (v/v) protease and phosphatase inhibitor cocktails. Nuclei were isolated by centrifugation at 1000 *g* and 4°C for 10 min. Nuclear pellets were washed twice with hypotonic lysis buffer prior to lysis in enzyme buffer (10 mM MOPS (pH 7.9), 100 μM deferoxamine, 5 mM EDTA) plus addition of SDS to a final concentration of ~1% (v/v). Samples were vortexed at moderate speed for 1 min to lyse nuclear membranes, followed by treatment with RNase A (100 μg) and RNase T (16 U) for 15 min at 37°C. Samples were subsequently subjected to Proteinase K (200 μg) treatment for at least 3 h at 37°C, with gentle mixing at regular intervals. Genomic DNA was precipitated with the sequential addition of a NaI solution (7.6 M NaI, 40 mM MOPS (pH 7.9), 20 mM EDTA, 100 μM deferoxamine) (mixed well) and a 2x volume of isopropanol. The DNA was washed

twice with 75% ethanol prior to resuspension in nuclease-free water for subsequent digestion. Prior to digestion, a fraction of DNA from each sample was removed to which [$^{15}N_5$]-dG was added for quantiation of dG. Following cellular DNA digestion, samples were subjected to solid-phase extraction using Oasis® HLB extraction cartridges (Waters, Tauton, MA). The resulting eluent was dried under a stream of nitrogen and resuspended in water prior to LC-MS/MS analysis. dG and [$^{15}N_5$]-dG were detected with selected reaction monitoring with the following transitions, *m/z* 268→152 and *m/z* 273→157, respectively. M_1dG, 6-oxo-M_1dG, and their respective internal standards were detected as described above.

Reaction of purified α-KG-dependent enzymes with M_1dG-containing dsDNA. For reactions involving alkylation repair homolog enzymes, purified AlkB (200 nM), ALKBH2 (500 nM), or ALKBH3 (750 nM) was incubated with either 5 μM m1A-containing ssDNA (5'-GAAGACCTm1AGGCGTCC-3') or 5 μM M_1dG-containing dsDNA in a solution consisting of 47 mM HEPES (pH 8.0), 70 μM $(NH_4)_2Fe(SO_4)_2•6H_2O$, 0.93 mM α-KG, and 1.9 mM ascorbate. Reactions were allowed to proceed at 37°C for 1 h, prior to quenching with 10 mM EDTA and heat-inactivation at 95°C for 5 min. Samples were then treated as in experiments with nuclear lysates; the DNA was subsequently precipitated, digested, and adducts quantified via LC-MS/MS, but with added selected reaction monitoring for m1A (*m/z* 266→150). For reactions involving Jumonji C domain-containing enzymes, purified JMJD2A (Cayman Chemical, Ann Arbor, MI, 0.01 U), JMJD2E (Cayman Chemical, 500 nM), KDM3A (Active Motif, Carlsbad, CA, 50 nM), KDM5B (Active Motif, 100 nM), or KDM4B (Active Motif, 25 nM) was incubated with either 5 μM

peptide substrate H3K9me3 (Cayman Chemical), H3K9me3, H3K9me1 (AnaSpec, Fremont, CA), H3K4me3 (AnaSpec), and H3K9me3, respectively, or 5 μM M_1dG-containing dsDNA. Reactions with JMJD2A or JMJD2E were performed in 50 mM HEPES (pH 7.5), 50 mM NaCl, 1 mM ascorbate, 50 μM $(NH_4)_2Fe(SO_4)_2 \bullet 6H_2O$, and 1 mM α-KG at 37°C for 2 h. Reactions with KDM3A, KDM5B, or KDM4B were carried out in 50 mM HEPES (pH 7.5), 0.02% (v/v) Triton X-100, 100 μM α-KG, 100 μM ascrobate, 50 μM $(NH_4)_2Fe(SO_4)_2 \bullet 6H_2O$, and 1 mM tris(2-carboxyethyl)phosphine at room temperature for 2 h. Peptide-containing sample reactions were stopped via heat-inactivation at 95°C for 10 min. These samples were then digested to single amino acids and substrate remaining quantified by stable-isotope dilution LC-MS/MS, as recently reported (159). DNA-containing sample reactions were quenched by the addition of 1/10th volume 3 M sodium acetate (pH 5.5), followed by addition of 200 μL ice-cold ethanol. Precipitated DNA subsequently was digested and adducts quantified via LC-MS/MS as described above.

siRNA knockdown of α-KG-dependent enzymes. RKO cells were plated at a density of 3 x 10^6 cells/150 mm plate in RPMI + 10% FBS (23 mL medium per plate). After plating, a pre-mixed mixture consisting of 40 μL Lipofectamine 2000 (Life Technologies), non-targeting (AllStars Negative Control siRNA, Qiagen, Germantown, MD) or targeted siRNA (siGENOME individual or pooled human siRNAs, Dharmacon, Lafayette, CO) (Table 1), and 2 mL Opti-Minimal Essential Medium (Opti-MEM) was added immediately to each plate to give a final medium concentration of 10 nM siRNA. After 24 h, the medium was removed and replaced

with serum-free RPMI and the cells were allowed to incubate at 37°C for an additional 24 h. Once again, the existing medium was removed and replaced with fresh serum-free RPMI containing 400 μM adenine propenal. Cells were incubated at 37°C for 1 h, at which point the adenine propenal-containing medium was removed and replaced with fresh serum-free RPMI. Cells were harvested, as described above, after an additional 24 h in the new medium.

Table 1. Target sequence(s) for siRNAs directed against enzyme candidates.

Enzyme Candidate	Target Sequence (5'→3')
ALKBH3	GAACAGCUUUGUCAAGAUG
	UCAGAGAGGAUAUAACUUA
	GAGAACUUCCUUACACUUA
	CAUGGGACCUUGUUAAUCA
ALKBH5	GCCUGUUAGGGCUGAAGAA
ALKBH8	GCAUUGAGACAGUAUCCUA
HIF1AN	GAAAUUUCAUGAGUUCGUU
	CACAUAGAGUCAUUACUAA
	UCAUGGACUUCUUAGGUUU
	AGUUAUAGCUUCCCGACUA
JHDM1D	GCACAGACAUGACUACACA
JMJD6	GAACUGGGAUUCACAUCGA
KDM2B	GCAAUAAGGUCACUGAUCA
	GACCUCAGCUGGACCAAUA
	GGGAGUCGAUGCUUAUUGA
	CAGCAUAGACGGCUUCUCU
KDM4C	ACGAAGAUUUGGAGCGCAA
	GCAUAUAUGAUGAGGGUGU
	UUGCAUACAUGGAGUCUAA
	GGCAAAUAUUGUACUCCAA
KDM4D	GGAAGAACCGCAUCUAUAA
	AGAGAGACCUAUGAUAAUA
	CCCAGAAUCCAAAUUGUAA
	UGUCAUAGAAGGCGUCAAU
KDM5C	GAGCGGAGGUUUCCUAAUA
	GUGGACAACUUCAGGUUUA
	GCAAGGAUAUGCCUAAGGU
	GAGUGAAACUGAACUACUU
MINA	GUACAUAACUCCCGCAGGA
	GUAAGCAGAUGAAGUUAGA
	GGGCAACGAUUCAGUUUCA
	UCACAGUACUGCCGGAUCA
NO66	GCGAAGAACCGCUUUCAUG
	CCCGAGACUUCAUGGAUUA
	GUGCACCGCGCAACACUUA
	GACCAGCUGUCCUUGGCAA
PHF2	GCAAGCGCCUGACGUCAAG
	AGGAGUUUGUGGACUAUUA
	ACGGGAAACUACUCCUUUA
	CGCCCGACAUCGACAUAUA
EGLN1	GCGAUAAGAUCACCUGGAU
	GCUCAUCGCUGUUCCAGGA
	GAACAAGCACGGCAUCUGU
	CUUCAGAUUCGGUCGGUAA

RT-qPCR analysis of siRNA knockdown efficiency. RNA isolation from cells was performed using the TRIzol reagent protocol provided by the manufacturer (Life Technologies). Isolated RNA was resuspended in nuclease-free water and quantified using a NanoDrop™ spectrophotometer (Thermo Fisher Scientific, Waltham, MA). Reverse transcriptase reactions were performed using the iScript™ cDNA Synthesis Kit (Bio-Rad) according to the manufactuer's directions. qPCR was performed using iQ™ SYBR® Green Supermix (Bio-Rad) and primers purchased from either Eurofins MWG Operon or Sigma-Aldrich using the iCycler iQ® Multicolor Real-Time PCR Detection System (Bio-Rad) (Table 2). GAPDH was used as reference gene because its expression showed stability (consistent Ct values).

Table 2. Forward and reverse primers for qPCR-based amplification and quantitation of enzyme candidate (and GAPDH reference gene) mRNA levels.

Enzyme Candidate		Primer Sequence (5'→3')
ALKBH3	Forward	CAAATCCTCACTGGCACCCT
	Reverse	AGGTCAGGTTCACTCTCGGT
ALKBH8	Forward	CTGAGCCGAAGCGGAGTTTG
	Reverse	CCAGGCTCTGAGTGGCATAG
HIF1AN	Forward	CTAGGCCCATTCCGCGTCT
	Reverse	TCTTCCCTGTTGGACCTCGG
JHDM1D	Forward	GCAGGCAGACAGCAAAATGA
	Reverse	TCAGGGACCTCCACCAATTCA
JMJD6	Forward	GCACCAACTTCCCTGTGGTA
	Reverse	GCCTCCACAAGTGTCCCTAA
KDM2B	Forward	CCGGGAAACAAAAGCGTGG
	Reverse	TGGGGCTTCTCGTATTTCCG
KDM4C	Forward	CAGCCTCTGACATGCGATTTG
	Reverse	CAGGGTCGGCCACATATTCA
KDM4D	Forward	TGTTCTTCCTACCGGACCCT
	Reverse	TGGCCCAGAGGATGGTAGTT
KDM5C	Forward	GTGCTTCCATCACCAGTCAGT
	Reverse	TAGAGTCGGGGGAGGATCAG
MINA	Forward	GGAGGGAGAGAAACACTGGC
	Reverse	GGGGTATGCCGGTCCGTA
NO66	Forward	TTTGTGAGAGTGGGGGACCT
	Reverse	TGGCAGCGGAGAATCACTAC
PHF2	Forward	CGTGAAGGACAGTTACACCGA
	Reverse	CCGGCCTGATGAGATAGAAGG
EGLN1	Forward	GTCTGACCGTCGCAACCC
	Reverse	CCTCACACCTTTTTCACCTGT
GAPDH	Forward	AATGGGCAGCCGTTAGGAAA
	Reverse	GCGCCCAATACGACCAAATC

Photoaffinity capture of α-KG-dependent enzymes. RKO nuclear lysates were prepared as described above and pre-cleared of endogenously biotinylated proteins by end-over-end incubation with streptavidin beads overnight at 4°C. The unbound protein fraction was then removed and subjected to bicinchoninic acid (BCA) assay-based protein quantitation. For detection of endogenous nuclear α-KG-dependent enzymes and DR025 competition with 8-

hydroxy-5-quinolinecarboxylic acid (IOX1), 50 µg of pre-cleared nuclear lysate was coincubated with various concentrations of DR025 and IOX1 (added to the solution from 100x stocks in DMSO) in the presence of 15 µM $MnCl_2$ in a total solution volume of 40 µL for 45 min at room temperature. At this time, samples were placed on ice in open Eppendorf tubes positioned approximately 2 cm from an ultraviolet light and irradiated at 365 nm for 20 min. Following irradiation, sample loading buffer was added to each sample followed by SDS-PAGE, transfer to nitrocellulose, and detection of DR025-bound proteins by streptavidin-linked fluorophore. For experiments involving small molecule competition with DR025, RKO nuclear lysates were pre-cleared and quantified as described. Then 45 µg of pre-cleared nuclear lysate was preincubated with various concentrations of competing small molecules (IOX1, M_1dG, control oligo, M_1dG oligo) in the presence of 15 µM $MnCl_2$ in a total solution volume of 50 µL for 15 min at room temperature. After 15 min, DR025 was added to each sample for a final solution concentration of 10 µM, and samples were incubated an additional 45 min at room temperature followed by irradiation and sample analysis as described above.

Stable Isotope Labeling by Amino Acids in Cell Culture (SILAC)-based identification of M_1dG-associated α-KG-dependent enzymes. Isotopically light and heavy RKO cell lines were generated by continuous passaging of cells in RPMI containing 10% SILAC FBS and supplemented with [$^{12}C_6{}^{14}N_2$]-L-lysine and [$^{12}C_6{}^{14}N_4$]-L-arginine or [$^{13}C_6{}^{15}N_2$]-L-lysine and [$^{13}C_6{}^{15}N_4$]-L-arginine, respectively, with final amino acid medium concentrations of 0.1 mg/mL. Complete medium was sterile-filtered prior to use. Full cellular incorporation of labeled amino acids was

confirmed by digestion of cell protein samples to single amino acids and detection of both light and heavy lysine and arginine by LC-MS/MS, as recently reported (159). RKO cell lines used in this study were passaged five times in their respective light or heavy medium prior to harvesting as described above. Light and heavy RKO nuclear lysates were prepared as described above, complete with pre-clearing and BCA assay-based determination of protein concentration. Light nuclear lysates (135 µg) were preincubated with 10 µM control oligo in the presence of 15 µM $MnCl_2$ in a total solution volume of 200 µL for 15 min at room temperature. Heavy nuclear lysates (135 µg) were preincubated with 10 µM M_1dG oligo in the presence of 15 µM $MnCl_2$ in a total solution volume of 200 µL for 15 min at room temperature. After 15 min, DR025 was added to both light and heavy samples to give a final solution concentration of 10 µM and samples were incubated an additional 45 min at room temperature followed by irradiation as described above. Following irradiation, light and heavy samples were combined in equal volumes (i.e. equal protein amounts), mixed, and subjected to end-over-end incubation with streptavidin beads overnight at 4°C. Supernatant (unbound) proteins were removed and streptavidin beads were subjected to a series of washes (2 x 1 mL washes each with following solutions: (1) 1% SDS in PBS; (2) 4 M urea in PBS; (3) 1 M NaCl in PBS; (4) PBS; and (5) H_2O). After removal of the final wash solution, the streptavidin beads were boiled in 40 µL of 2x Laemmli buffer containing 6% β-mercaptoethanol for 15 min with occasional vortexing. Streptavidin beads were then removed and the supernatant stored at -20°C prior to SDS-PAGE, in-gel tryptic digestion, and LC-MS/MS analysis of peptides.

Results

Nuclear lysates enzymatically convert M_1dG to 6-oxo-M_1dG in dsDNA. Our previous findings suggested the presence of an activity in RKO cell nuclear lysates that can carry out the conversion of M_1dG to 6-oxo-M_1dG in dsDNA (126). To further characterize this activity and potentially isolate it using traditional protein purification methodology, we prepared nuclear lysates from fresh rat livers. Consistent with our previous findings, rat liver nuclear lysates also converted M_1dG to 6-oxo-M_1dG in dsDNA (Fig. 1*A*). This activity was abolished upon heat-denaturation of nuclear lysates prior to incubation with M_1dG-containing dsDNA (Fig. 1*A*). Since previous work from our lab has demonstrated a role for XO in the oxidation of free nucleoside M_1dG to 6-oxo-M_1dG (121), we also incubated rat liver nuclear lysates with the XO inhibitor allopurinol. Allopurinol treatment had no effect on nuclear lysate-dependent oxidation of M_1dG to 6-oxo-M_1dG in dsDNA (Fig. 1*A*), consistent with the absence of any contaminating cytosolic XO from the prepared nuclear lysates (Fig. 1*B*).

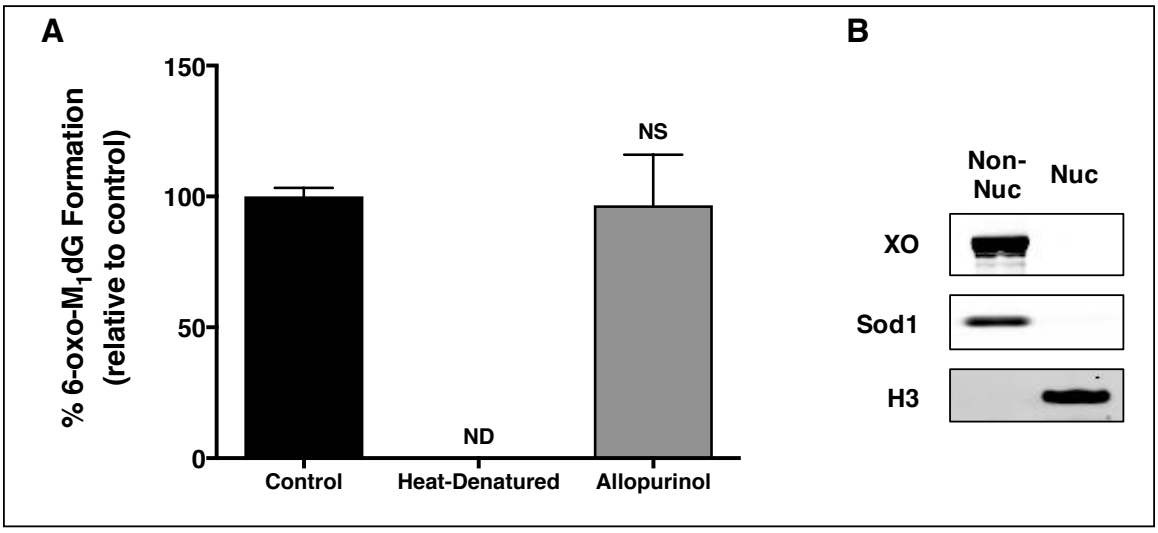

Figure 1. Rat liver nuclear lysate-promoted conversion of M_1dG to 6-oxo-M_1dG in dsDNA is heat-sensitive and XO-independent. (*A*) Nuclear lysates were either heat-denatured or treated with 50 μM allopurinol prior to reaction with M_1dG-containing dsDNA (~150 pmol M_1dG in ~640 μg DNA). The amount of 6-oxo-M_1dG was quantified via stable isotope dilution mass spectrometry and depicted as percent formed with respect to control (~3 pmol). Statistical significance was determined using one-way Anova. (*B*) Western blot analysis of nuclear (Nuc) and extranuclear (Non-Nuc) lysates reveals the absence of cytosolic proteins, including XO, in the nuclear lysate.

While experiments with fresh rat liver nuclear lysates confirmed the presence of the oxidase activity, variability in lysate preparation activity and a loss of activity upon liver freezing precluded this route as a practical method for activity isolation. Therefore, we also assessed whether a similar activity was present in the various cell lines in which we recently reported detection of 6-oxo-M_1dG in the genome. Indeed, oxidation was observed in lysate from three of the four cell lines tested, and this activity was heat-sensitive (Fig. 2*A*). Furthermore, this activity was unique to the nuclear fraction, as the non-nuclear (extranuclear) fraction failed to convert M_1dG to 6-oxo-M_1dG in dsDNA (Fig. 2*B*).

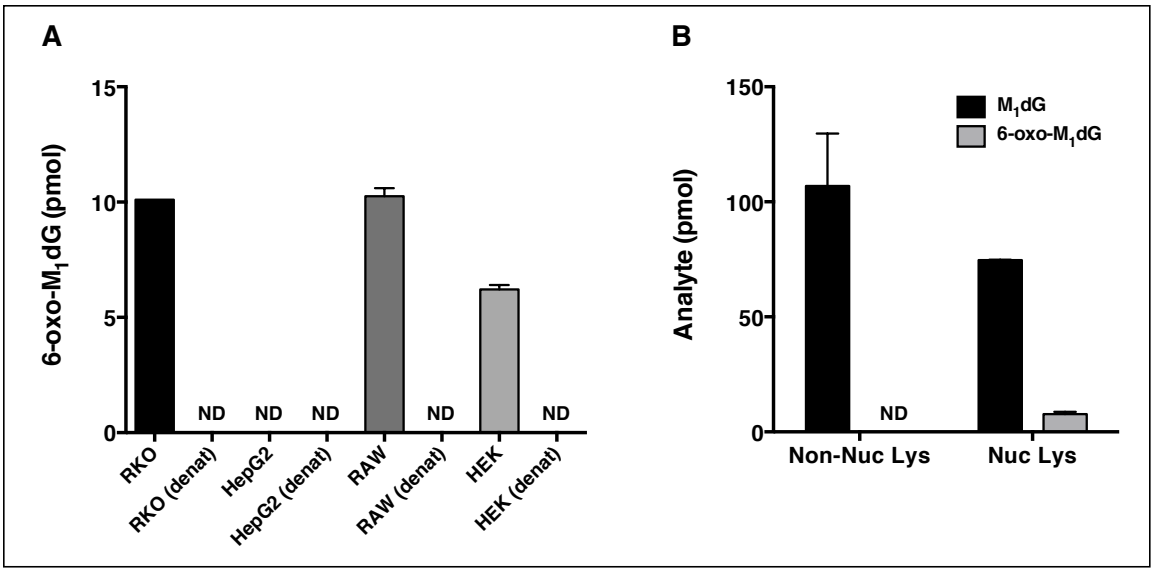

Figure 2. Cellular nuclear lysate-promoted conversion of M_1dG to 6-oxo-M_1dG in dsDNA is heat-sensitive and unique to the nuclear fraction. (*A*) Nuclear lysates prepared from various cell lines were either untreated or heat-denatured prior to reaction with M_1dG-containing dsDNA. The amount of 6-oxo-M_1dG was quantified via stable isotope dilution mass spectrometry. (*B*) Comparison of RAW264.7 cell extranuclear (Non-Nuc) versus nuclear (Nuc) lysate reaction with M_1dG-containing dsDNA.

The heat-sensitive nature of this activity suggested an enzyme is likely responsible for M_1dG oxidation, a notion supported by the fact that pretreatment of cell nuclear lysates with Proteinase K also abolished 6-oxo-M_1dG formation (Fig. 3). Finally, to assess whether the reaction is carried out by an enzyme directly or indirectly, for example, by enzymatically driven release of reactive oxygen species, we incubated cell nuclear lysates in the presence of free radical scavengers, *N*-acetylcysteine (NAC) or 4-hydroxy-2,2,6,6-tetramethylpiperidin-1-oxyl (TEMPOL), or catalase. None of these reagents affected 6-oxo-M_1dG formation (Fig. 3), suggesting that oxidation of M_1dG to 6-oxo-M_1dG in dsDNA is the result of direct oxidation by a nuclear enzyme.

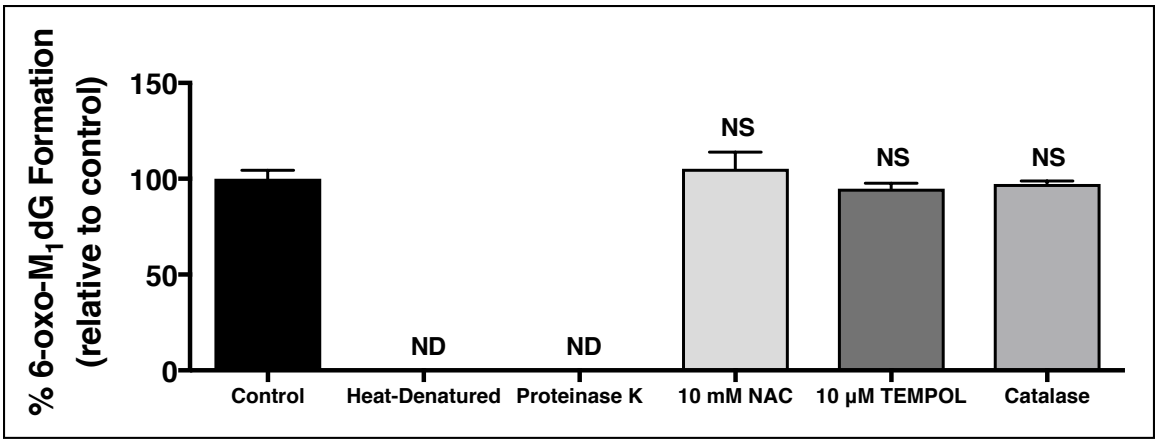

Figure 3. RAW264.7 cell nuclear lysate-promoted conversion of M_1dG to 6-oxo-M_1dG in dsDNA is enzymatically catalyzed. Nuclear lysates were pretreated as indicated prior to reaction with M_1dG-containing dsDNA. The amount of 6-oxo-M_1dG was quantified via stable isotope dilution mass spectrometry and depicted as percent formed with respect to control. Statistical significance was determined using one-way Anova.

Cofactor studies provide support for a Fe(II)/α-KG-dependent-enzyme.

The literature is rife with examples of oxidases that rely on metal cofactors for their catalytic activity. Consequently, we sought to assess the effect of various divalent metals on cell nuclear lysate-mediated conversion of M_1dG to 6-oxo-M_1dG in dsDNA. Metal chelation by EDTA or addition of various divalent metals known to displace Fe^{2+} from enzyme active sites reduced 6-oxo-M_1dG formation (Fig. 4). Several Fe(II)/α-KG-dependent enzymes have been reported to oxidize alkylated or otherwise modified DNA bases similar to M_1dG (160, 161). This led us to hypothesize that the M_1dG oxidase might also belong to this enzyme family. In support of this hypothesis, addition of Fe^{2+}, but not Fe^{3+}, to cell nuclear lysates potentiated 6-oxo-M_1dG formation, as did addition of α-KG (Fig. 5). Furthermore, addition of *N*-oxalylglycine (*N*-OG), an amide analog of α-KG and competitive inhibitor of Fe(II)/α-KG-dependent enzymes, reduced 6-oxo-M_1dG formation (Fig. 5). Finally, addition of IOX1, a broad-spectrum inhibitor of Fe(II)/α-KG-dependent

enzymes, reduced 6-oxo-M_1dG formation in a concentration-dependent manner (Fig. 6*A*). Collectively, these data suggest a Fe(II)/α-KG-dependent enzyme may be responsible for oxidation of M_1dG to 6-oxo-M_1dG in dsDNA.

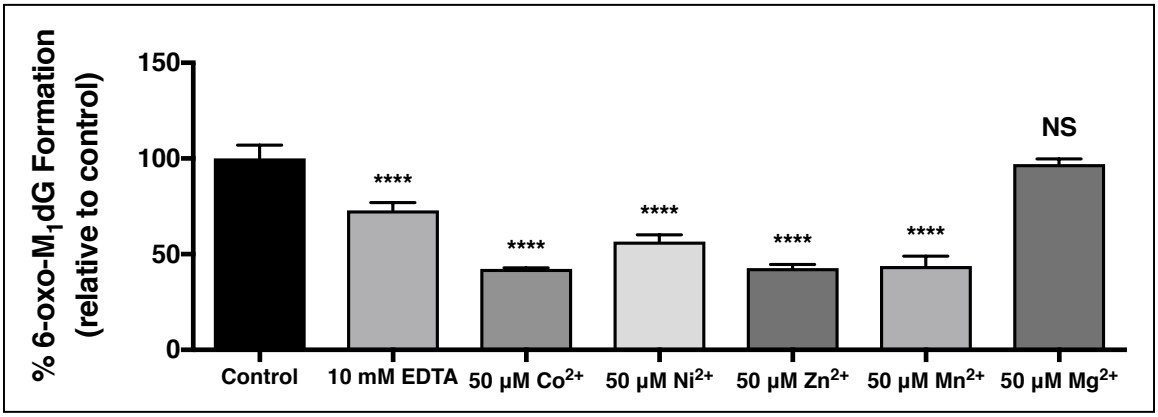

Figure 4. Nuclear lysate conversion of M_1dG to 6-oxo-M_1dG in dsDNA is inhibited by metal chelation and preincubation with divalent metals known to displace iron from enzyme active sites. The amount of 6-oxo-M_1dG was quantified via stable isotope dilution mass spectrometry and depicted as percent formed with respect to control. Statistical significance was determined using one-way Anova (**** $p < 0.0001$ compared to control).

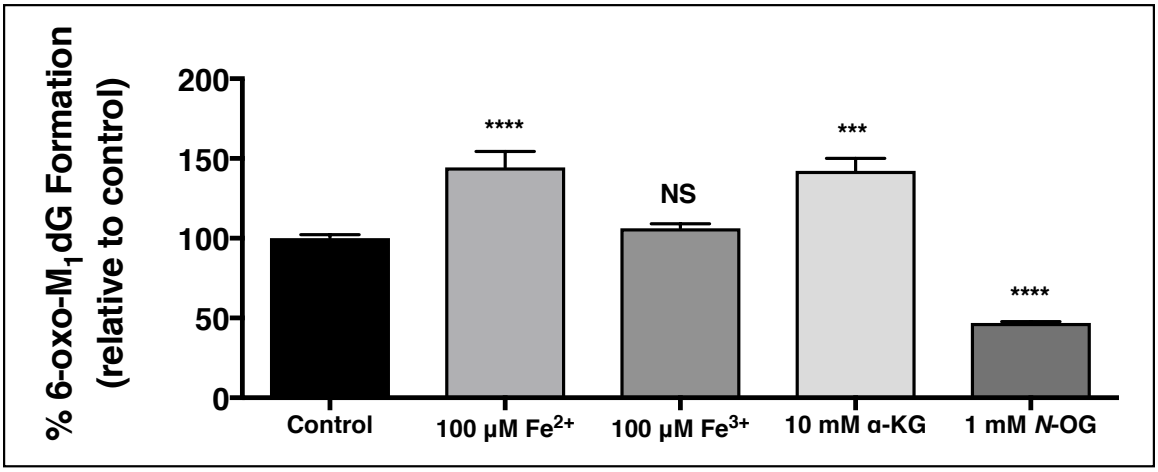

Figure 5. Nuclear lysate conversion of M_1dG to 6-oxo-M_1dG in dsDNA is altered by small molecules that affect Fe(II)/α-KG-dependent oxidase activity. The amount of 6-oxo-M_1dG was quantified via stable isotope dilution mass spectrometry and is depicted as percent formed with respect to control. Statistical significance was determined using one-way Anova (*** $p < 0.001$, **** $p < 0.0001$ compared to control).

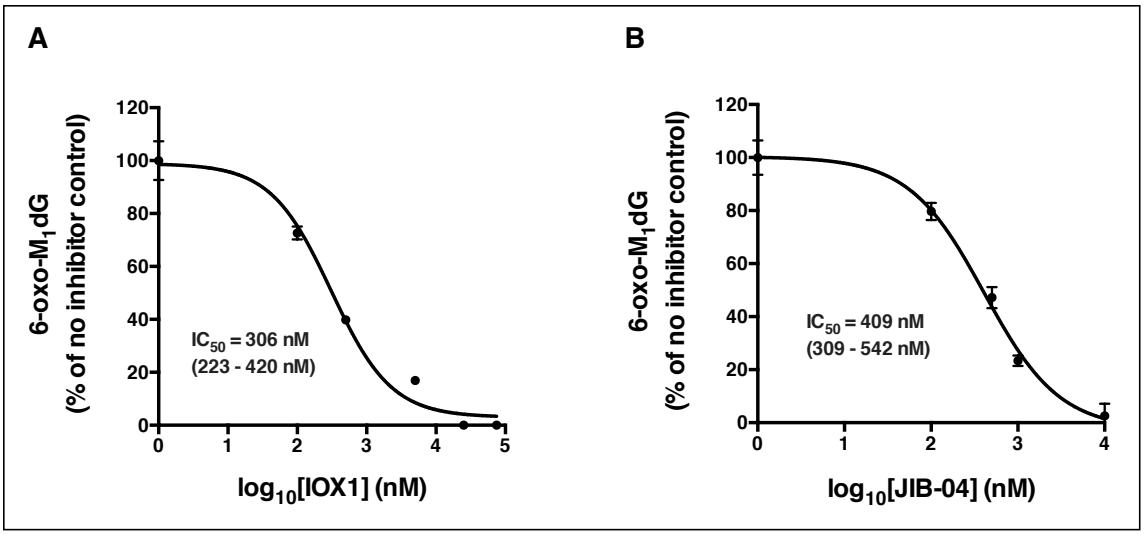

Figure 6. Nuclear lysate conversion of M_1dG to 6-oxo-M_1dG in dsDNA is inhibited in a concentration-dependent manner by broad-spectrum (*A*) and subfamily-specific (*B*) inhibitors of Fe(II)/α-KG-dependent enzymes. The amount of 6-oxo-M_1dG was quantified via stable isotope dilution mass spectrometry and depicted as percent formed with respect to control.

Jumonji C domain-containing protein inhibitor decreases 6-oxo-M_1dG formation both in vitro and in intact cells. Few inhibitors that are specific for one family of Fe(II)/α-KG-dependent enzymes over others exist. However, Wang, L. et al. recently developed an inhibitor of Jumonji C domain-containing proteins, a family of enzymes responsible for catalyzing the oxidative demethylation of histone lysines and arginines (162). Though they did not provide exhaustive proof of the compound (JIB-04)'s specificity, they did present *in vitro* data suggesting JIB-04 is inactive against the ten-eleven translocation (TET) family of enzymes which carry out the oxidative demethylation of 5-methylcytosine (161). Addition of JIB-04 to cell nuclear lysates reduced 6-oxo-M_1dG formation in a concentration-dependent manner (Fig. 6*B*). In order to determine whether JIB-04 also inhibits M_1dG oxidation to 6-oxo-M_1dG in cellular genomic DNA, RKO cells were treated with adenine propenal for 1 h to increase levels of M_1dG and then with either

DMSO (vehicle) or 500 nM JIB-04, a concentration sufficient to cause significant inhibition of histone demethylation (Fig. 7*A*). Cells were harvested over a period of 24 h, and genomic DNA was isolated and analyzed for M_1dG and 6-oxo-M_1dG. JIB-04 treatment resulted in an increase in genomic levels of M_1dG (Fig. 7*B*) as well as a decrease in genomic levels of 6-oxo-M_1dG (Fig. 7*C*). These data put forward Jumonji C domain-containing enzymes as possible oxidase candidates.

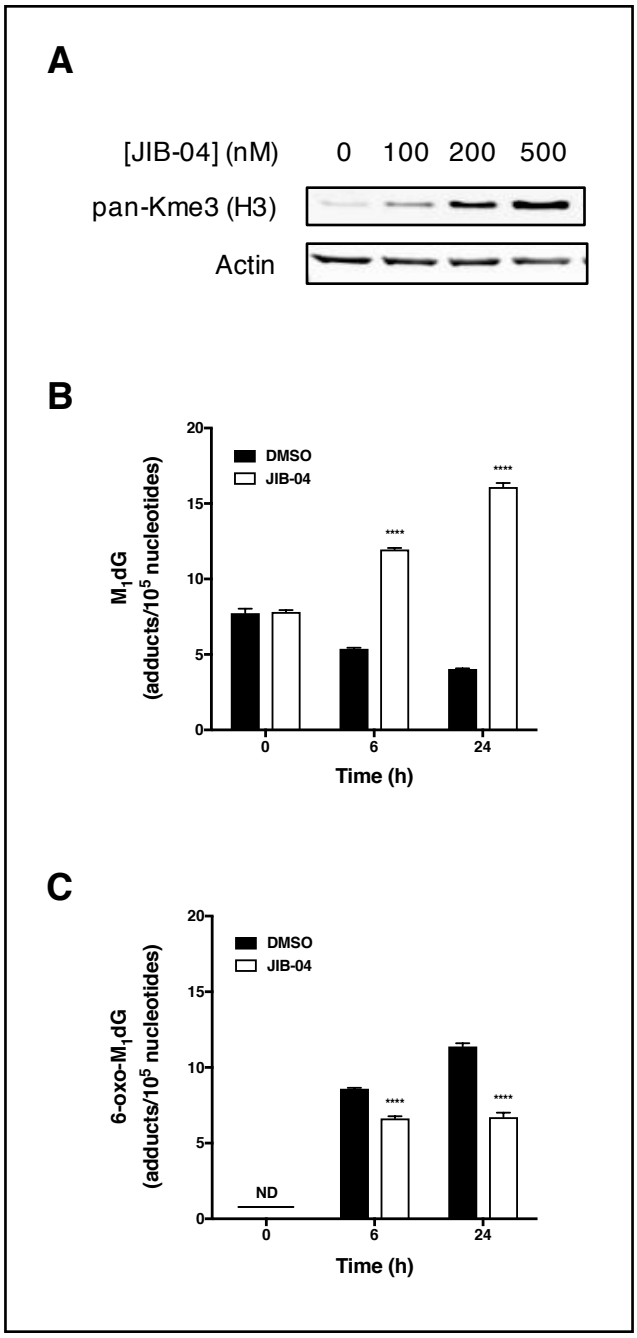

Figure 7. JIB-04 inhibits M_1dG oxidation to 6-oxo-M_1dG in RKO genomic DNA. (*A*) JIB-04 increases histone H3 lysine trimethylation in a concentration-dependent manner, as assessed by western blot. LC-MS/MS-based quantitation of (*B*) M_1dG and (*C*) 6-oxo-M_1dG levels in genomic DNA of RKO cells treated with DMSO (vehicle) or 500 nM JIB-04 for various lengths of time. Statistical differences between DMSO- and JIB-04-treated cellular genomic levels of M_1dG and 6-oxo-M_1dG at each time were determined using Student's t-test (**** $p < 0.0001$ compared to control).

Targeted analysis of putative M_1dG oxidases. The results of the above described studies led us to narrow down our search to a nuclear Fe(II)/α-KG-dependent enzyme, of which there are approximately forty as annotated in the UniProt database (www.uniprot.org) (Table 3).

Table 3. UniProt database search summary of annotated nuclear Fe(II)/α-KG-dependent enzymes categorized by enzyme family.

Enzyme Family	Nucleus-Localized Members
Alkylation Repair Homologs (AlkB)	ALKBH2, ALKBH3, ALKBH4, ALKBH5, ALKBH6, ALKBH8, FTO
Ten-Eleven Translocation Enzymes (TET)	TET1, TET2, TET3
Jumonji C Domain-Containing Proteins (JmjC)	HIF1AN, HR, JHDM1D, JMJD1C, JMJD2A, JMJD3, JMJD6, KDM2A, KDM2B, KDM3A, KDM3B, KDM4B, KDM4C, KDM4D, KDM4E, KDM5A, KDM5B, KDM5C, KDM5D, KDM8, MINA, NO66, PHF2, PHF8, UTX
Other α-KG-Dependent Enzymes	EGLN1, EGLN2, PHYHD1

Given that M_1dG oxidation to 6-oxo-M_1dG in dsDNA was inhibited by JIB-04 treatment, we posited that the TET enzymes were less likely candidates. We obtained some of the remaining enzyme candidates as generous gifts or by commercial purchases and tested them directly for activity in oxidizing M_1dG to 6-oxo-M_1dG in dsDNA *in vitro*. While all were active against their canonical substrates, none showed activity against M_1dG-containing dsDNA (Fig. 8 *A*-*H*).

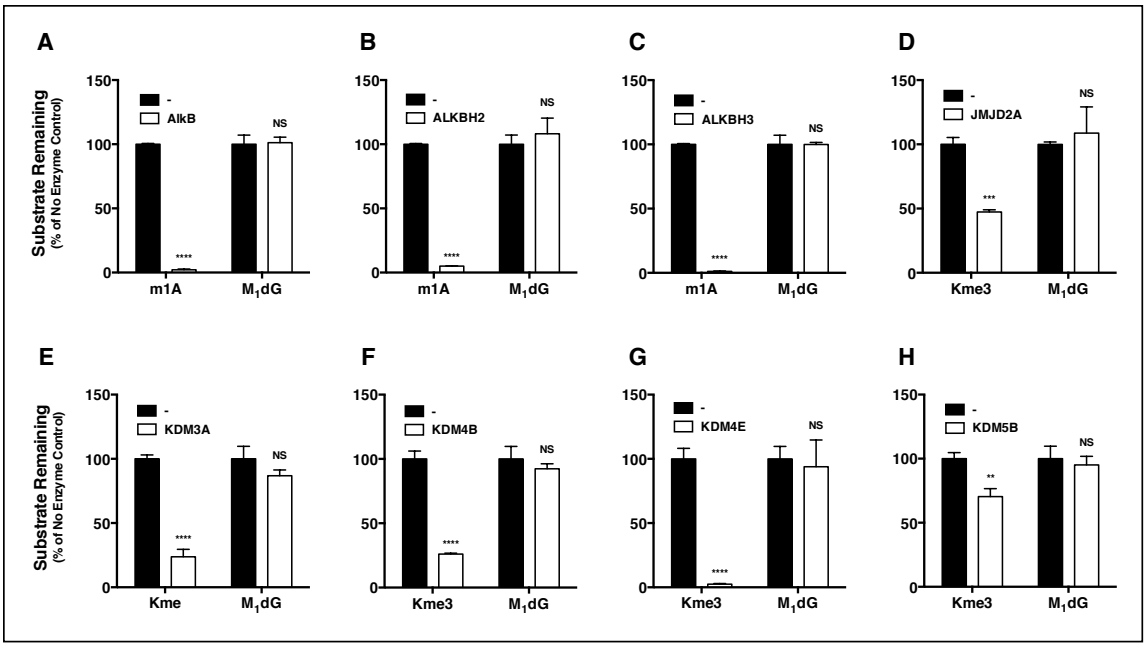

Figure 8. Activity of purified Fe(II)/α-KG-dependent enzymes AlkB (*A*), ALKBH2 (*B*), ALKBH3 (*C*), JMJD2A (*D*), KDM3A (*E*), KDM4B (*F*), KDM4E (*G*), and KDM5B (*H*) on their respective canonical substrates and on M_1dG-containing dsDNA. Substrate levels were determined by LC-MS/MS and are depicted as percent substrate remaining with respect to the no enzyme control. Statistical differences in substrate levels between no enzyme and enzyme samples were determined by Student's t-test (** $p < 0.01$, *** $p < 0.001$, **** $p < 0.0001$ compared to control).

Given our data suggesting Jumonji C domain-containing proteins were likely candidates, we investigated the cellular effect of one recently developed subclass (JMJD3 and UTX)-specific inhibitor, GSK-J4 (163). Cell treatment with GSK-J4 revealed a concentration dependent increase in H3K27me3, consistent with inhibition of JMJD3 and UTX (Fig. 9*A*). However, unlike JIB-04, GSK-J4 had no effect on genomic levels of M_1dG or 6-oxo-M_1dG (Fig. 9*B*).

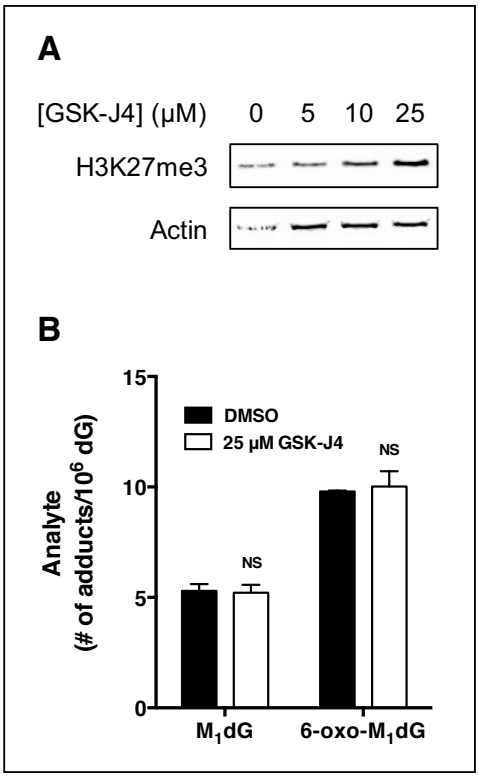

Figure 9. GSK-J4 has no effect on the oxidation of M_1dG to 6-oxo-M_1dG in RKO genomic DNA. (*A*) GSK-J4 increases H3K27 trimethylation in a concentration-dependent manner, as assessed by western blot. (*B*) LC-MS/MS-based quantitation of M_1dG and 6-oxo-M_1dG levels in genomic DNA of RKO cells treated with DMSO (vehicle) or 25 μM GSK-J4 for 24 h. Statistical differences between DMSO- and GSK-J4-treated cellular genomic levels of M_1dG and 6-oxo-M_1dG were determined using Student's t-test.

We decided to test the remaining enzyme candidates using an RNA interference screening approach. Non-targeting siRNA or siRNA targeted against individual protein candidates was transfected into RKO cell lines, and cellular genomic DNA was isolated for quantitation of M_1dG and 6-oxo-M_1dG. Fig. 10*A* depicts enzyme candidates for which siRNA knockdown resulted in 25% or less of enzyme mRNA expression remaining relative to the non-targeting siRNA control. Despite efficient knockdown of multiple enzyme candidates, no change in genomic 6-oxo-M_1dG was observed in any cells (Fig. 10*B*).

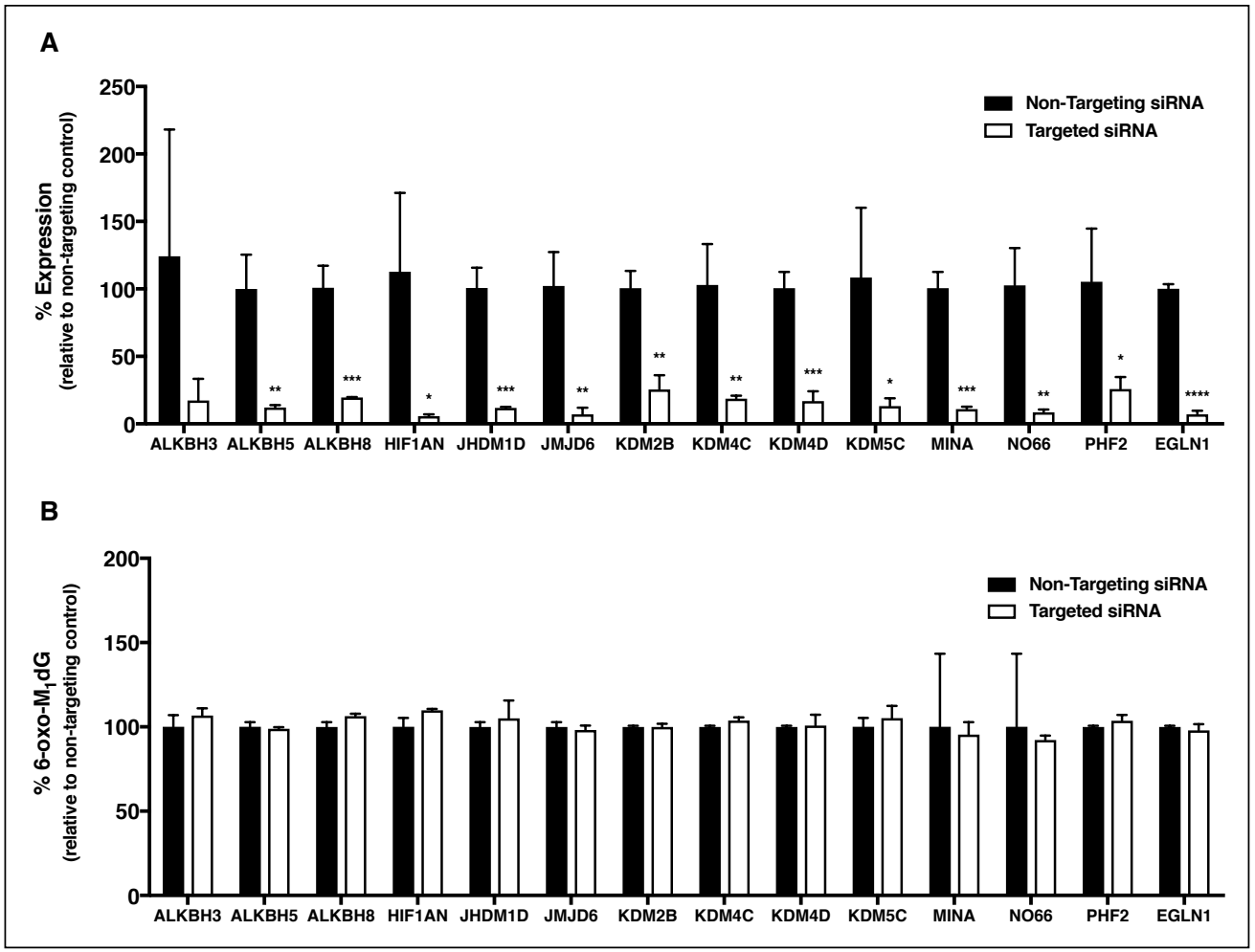

Figure 10. siRNA knockdown screen of nuclear Fe(II)/α-KG-dependent enzymes. (*A*) Extent of enzyme knockdown as assessed by RT-qPCR (ALKBH3, ALKBH8, HIF1AN, JHDM1D, JMJD6, KDM2B, KDM4C, KDM4D, KDM5C, MINA, NO66, PHF2, and EGLN1) or western blot (ALKBH5). (*B*) Levels of RKO cell genomic 6-oxo-M_1dG as assessed by LC-MS/MS. Statistical differences between non-targeting and targeted siRNA samples for each enzyme were determined using Student's t-test (* $p < 0.05$, ** $p < 0.01$, *** $p < 0.001$, **** $p < 0.0001$ compared to control).

Photoreactive probe-based identification of M_1dG-associated α-KG-dependent enzymes. Given apparent gridlock with regard to our targeted approaches, we considered the possibility that the M_1dG oxidase could be an unannotated Fe(II)/α-KG-dependent enzyme that might only be found using untargeted methodologies. Rotili, D. et al. recently developed a photoreactive probe (DR025), based upon IOX1, that allows for irradiation-dependent binding and streptavidin pulldown of all Fe(II)/α-KG-dependent enzymes in a sample (Fig. 11*A*) (164).

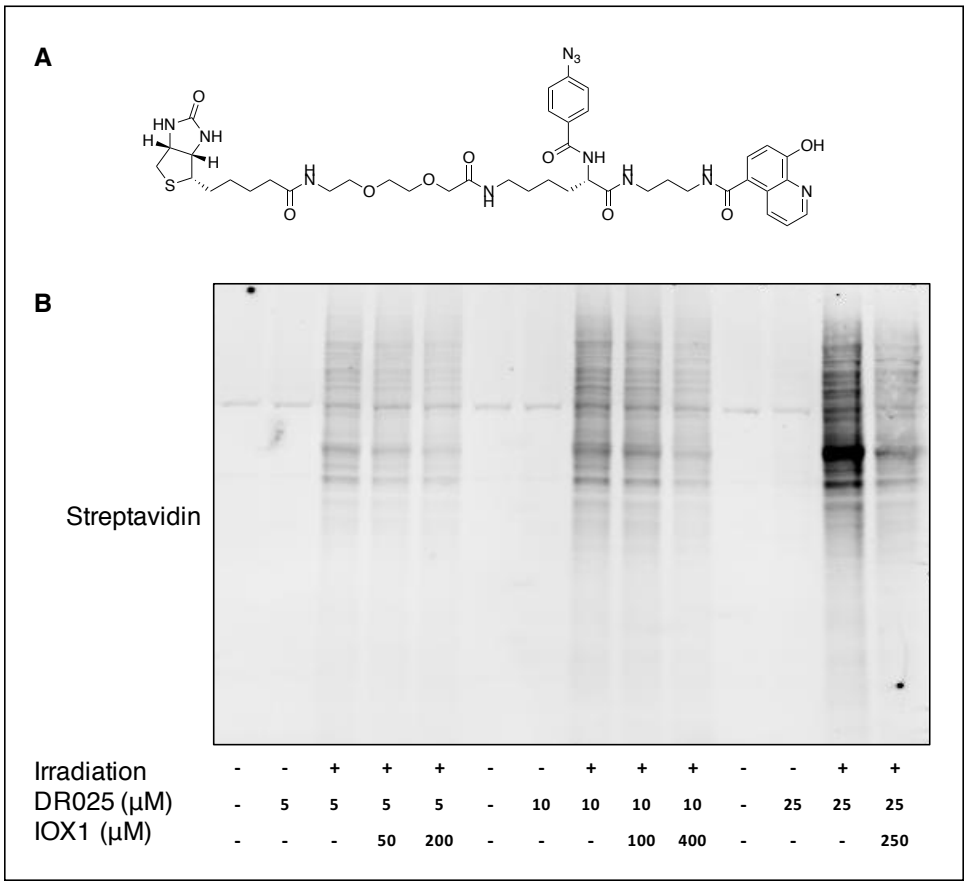

Figure 11. Photoaffinity labeling of endogenous Fe(II)/α-KG-dependent enzymes in RKO nuclear lysates. Nuclear lysates were incubated in the presence of various concentrations of DR025 (*A*) and IOX1 prior to irradiation. Reaction mixtures were then subjected to SDS-PAGE, transferred to nitrocellulose, and visualized via streptavidin-linked fluorophore (*B*).

We first validated the effectiveness of DR025 in our own hands by incubating cell nuclear lysates in the presence of various concentrations of the probe either with or without competitor IOX1. DR025 effectively labeled nuclear enzymes in an irradiation- and concentration-dependent manner (Fig. 11*B*) Furthermore, DR025 was efficiently competed out by IOX1 in a concentration-dependent fashion (Fig. 11*B*), suggesting selective binding of nuclear Fe(II)/α-KG-dependent enzymes. To assess which of these enzymes might also bind M_1dG, we preincubated cell nuclear lysates with either IOX1 (as a positive competition control), free nucleoside M_1dG, control oligonucleotide, or a M_1dG-containing oligonucleotide, followed by addition of DR025 and irradiation. Analysis of these samples revealed a concentration-dependent loss of specific protein bands in the presence of competitor M_1dG-containing oligonucleotide but not in the presence of the control oligonucleotide (Fig. 12). These data suggest the presence of one or more nuclear Fe(II)/α-KG-dependent enzymes that preferentially bind M_1dG-containing oligonucleotides over canonical oligonucleotides.

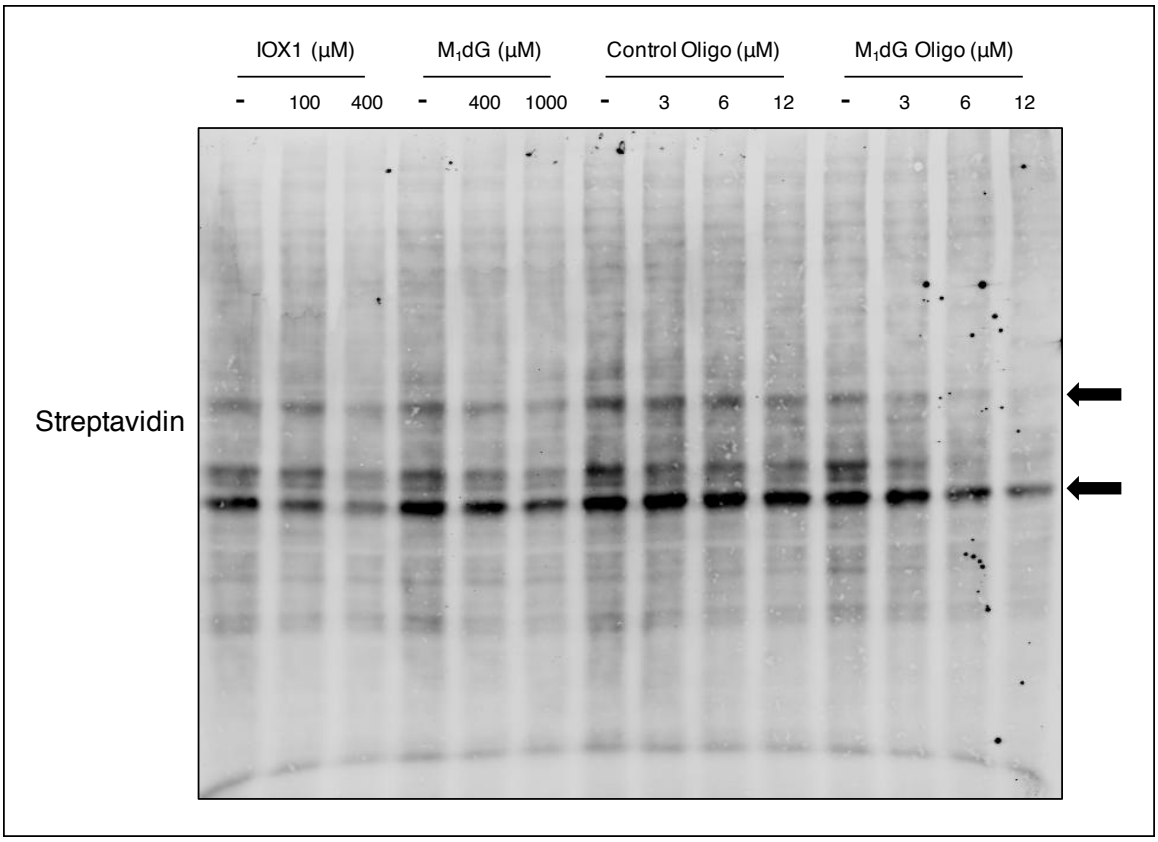

Figure 12. Competition between DR025 and small molecules for endogenous Fe(II)/α-KG-dependent enzymes in RKO nuclear lysates. Nuclear lysates were preincubated with the indicated concentrations of small molecule competitors prior to addition of DR025. Following irradiation, reaction mixtures were subjected to SDS-PAGE, transferred to nitrocellulose, and visualized via streptavidin-linked fluorophore.

In order to identify these enzymes and quantify their changes in the presence of competitor M_1dG-containing oligonucleotides, we employed a SILAC-based approach (Fig. 13). The previously described experiment was modified such that isotopically light nuclear lysates were preincubated with control oligonucleotide, whereas isotopically heavy nuclear lysates were preincubated with M_1dG-containing oligonucleotide prior to addition of DR025 and irradiation. Following irradiation, samples were combined in equal protein amounts, bound to streptavidin beads, eluted, digested, and subjected to LC-MS/MS analysis. Protein

targets with H/L ratios less than 1 indicate proteins successfully competed off of photoaffinity probe binding by M_1dG-containing dsDNA.

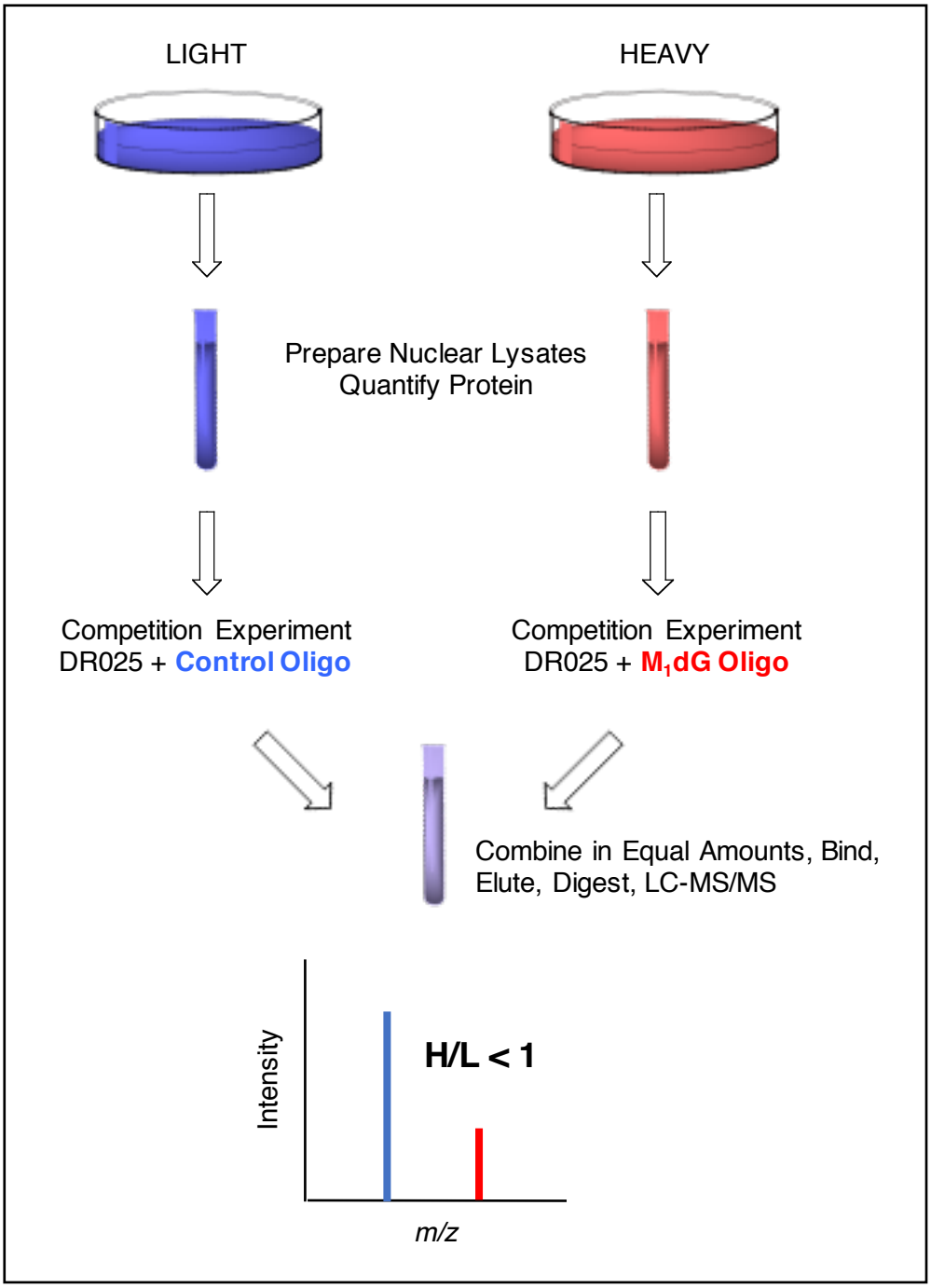

Figure 13. Workflow for SILAC-based identification of M_1dG-associated Fe(II)/α-KG-dependent enzymes present in RKO nuclear lysates.

Proteomic analysis of the sample described above revealed ~830 unique proteins of which ~160 had H/L ratios < 0.80, indicating proteins with substantially reduced DR025 binding in the presence of M_1dG-containing oligonucleotide. Manual analysis of this list revealed no Fe(II)/α-KG-dependent dioxygenases. Notably, we only detected one Fe(II)/α-KG-dependent dioxygenase in this experiment (JMJD1C, H/L = 1.10), despite the fact that our qPCR results suggest that many other such enzymes exist in the nuclei of RKO cells. Therefore, it is possible that failure to detect some nuclear Fe(II)/α-KG-dependent dioxygenases may be attributable to low abundances. Of interest was the finding that several of the differentially pulled-down proteins are involved in DNA and/or RNA binding (Table 4). It could be that these proteins were pulled down in complex with an Fe(II)/α-KG-dependent dioxygenase and thus might provide insight into the identity of the M_1dG oxidase. Repeat of the described SILAC experiment and/or western blot analysis of pulled-down proteins will be necessary to test their validity as differential binders.

Table 4. Select proteins with reduced binding to DR025 in the presence of M_1dG-containing oligonucleotide (H/L ratio < 0.80) and their UniProt-annotated functions.

Protein Symbol	Protein Name	Molecular Weight (kDa)	Function	H/L Ratio
RMXL1	RNA binding motif protein, X-linked-like 1	42	Pre-mRNA splicing	0.18
ATRX	Transcriptional regulator ATRX	283	Transcriptional regulator, thought to play role in DNA damage, repair, transcription	0.35
IF2B2/IF2B3	Insulin-like growth factor 2 mRNA-binding protein 2/3	66/64	mRNA transport	0.58/0.64
GNL3	Guanine nucleotide-binding protein-like 3	62	GTP and RNA binding functions	0.59
PAIRB	Plasminogen activator inhibitor 1 RNA-binding protein	45	Regulation of mRNA stability	0.63
SYF1	Pre-mRNA-splicing factor SYF1	100	Involved in transcription-coupled NER	0.65
SRS11	Serine/arginine-rich splicing factor 11	54	Pre-mRNA splicing	0.67
CEBPB	CCAAT/enhancer-binding protein β	36	Regulates genes involved in immune & inflammatory response	0.67
ZHX1	Zinc fingers and homeoboxes protein 1	98	Transcriptional repressor, associates with DNMT3B	0.69
PRP19	Pre-mRNA-processing factor 19	55	Ub-protein ligase, core component of complexes involved in pre-mRNA splicing and DNA repair	0.77

Discussion

While the identity of the oxidase responsible for conversion of M_1dG to 6-oxo-M_1dG in dsDNA is still unknown, the data presented here suggest that this oxidation reaction is indeed enzymatically catalyzed. Furthermore, we have garnered evidence that the enzyme is likely a Fe(II)/α-KG-dependent dioxygenase. Purified enzyme testing and siRNA studies in RKO cells render certain putative oxidase candidates less likely; however, they do not completely exclude the possibility that one or more of these enzymes might be involved.

Limitations of purified enzyme testing include the inability to account for cellular cofactors, coenzymes, or protein-protein interactions required for catalysis. This question could be addressed by spiking purified proteins into cellular nuclear lysates and performing analogous experiments. Another limitation of these experiments is that we have assumed that fully duplexed M_1dG-containing DNA is the appropriate substrate for enzymatic oxidation. While this is consistent with the ability of cellular nuclear lysates to oxidize M_1dG to 6-oxo-M_1dG in dsDNA, it is possible that the true substrate is an alternative sort of DNA, such as a forked duplex or ssDNA, a small fraction of which our M_1dG-containing dsDNA substrate might contain. (The M_1dG-containing dsDNA was prepared by reacting adenine propenal with duplexed 21-mer DNA, as described above, hence there was no control over the number or location of M_1dG adducts nor the potential structural impact multiple adducts might have on the dsDNA.) Future studies involving incubation of cellular nuclear lysates with site-specifically incorporated M_1dG-containing DNA (both ssDNA and dsDNA) might help address this current

experimental shortcoming.

Many of the limitations of direct *in vitro* testing of purified enzymes were circumvented via siRNA knockdown of candidate enzymes. For example, since these experiments were performed in cells, we did not have to concern ourselves with ensuring that all relevant cofactors or interacting enzymes would be present. Likewise, concerns over the specific nature of M_1dG-containing DNA became irrelevant. As with direct purified protein testing, however, siRNA-knockdown-based enzyme identification has its own limitations. Despite relatively efficient knockdown of enzyme candidates (< 25% expression remaining), the target enzyme was still expressed in the cells in all cases (Fig. 10). Thus, if only a small amount of the target enzyme is needed to catalyze the reaction, siRNA-mediated reduction of enzyme expression may have been insufficient to result in lower levels of genomic 6-oxo-M_1dG. Futhermore, knockdown efficiency was assessed (in most cases) by RT-qPCR which speaks only to mRNA, and not protein, levels. (Western blot analysis of protein levels, due to a lack of suitable antibodies for most of the tested enzymes, was technically intractable.) Additionally, the possibility exists that more than one enzyme is capable of carrying out this oxidation. In this case, knockdown of one genuine M_1dG oxidase may have been masked by the presence and/or upregulation of another M_1dG oxidase. Although knockout studies might help address the former shortcoming of the siRNA knockdown approach, they would not help address (and might even exacerbate) the latter pitfall.

The photoaffinity probe approach, specifically in regard to the competition experiments, shows some promise. This approach enables direct binding of Fe(II)/α-KG-dependent enzymes, via the IOX1-based moiety, and protein pull-down, via the streptavidin moiety. Upon incubation of cellular nuclear lysates in the presence of both a fixed concentration of DR025 and increasing concentrations of M_1dG-containing dsDNA, we observed a concentration-dependent decrease in select protein bands (Fig. 12). These bands represent Fe(II)/α-KG-dependent enzymes which display binding affinity for M_1dG-containing dsDNA and are therefore putative M_1dG oxidase candidates. Proteomic analysis of SILAC samples, prepared as described in Fig. 13, revealed numerous DNA and/or RNA-binding proteins that differentially bound DR025 in the presence of M_1dG-containing oligonucleotide (Table 4). Though none are annotated as Fe(II)/α-KG-dependent enzymes, it is possible that these proteins associate with such enzymes and thus may provide clues as to the identity of the M_1dG oxidase(s). The proteins of interest identified in this experiment will be validated by repeat SILAC experiment and/or western blot analysis.

CHAPTER IV

CONCLUSION

Significance and Future Directions (Part A)

In Chapter II, I presented data revealing that 2-AG allosterically potentiates AA oxygenation by COX-2, whereas AA allosterically inhibits 2-AG oxygenation by the enzyme. Furthermore, I reported an inverse correlation between cellular AA levels and PG-G production, suggesting that substrate-dependent allosteric regulation may also occur in intact cells. Beyond the relatively straightforward implications discussed previously, this work has three more broad-sweeping ramifications.

First, these studies necessitated the development of optimal conditions for fixed time-point kinetics assays. Since AA and 2-AG oxygenation are indistinguishable via oxygen consumption measurement, traditional continuous kinetics assays employing an oxygen electrode proved unsuitable. Therefore, we optimized conditions for a fixed time-point kinetics assay followed by LC-MS/MS detection of multiple oxygenation products in a single sample. As aforementioned, PPHP was added along with substrate to ensure complete enzyme activation, and reaction times were minimized in order to limit substrate turnover and enzyme inactivation. These conditions enable accurate fixed time-point COX-2 kinetics experiments with any combination of substrates and/or inhibitors. Furthermore, LC-MS/MS detection of products enables identification of product profile changes

undetectable with an oxygen electrode (165). The described assay is now routinely used for all kinetics studies performed in the Marnett laboratory.

Second, this work provides additional rationale for the low cellular and *in vivo* levels of PG-Gs. The detection of PGE_2-G from rat hind paw homogenates by Hu et al. remains the only published *in vivo* report of PG-Gs to date (80). Our work suggests that PG-G production may be limited due to the fact that AA can allosterically inhibit 2-AG turnover. Consequently, one might hypothesize that reduction of AA and/or elevation of 2-AG levels in tissues that express COX-2 might permit PG-G detection *in vivo*. In collaboration with the laboratory of Sachin Patel (Vanderbilt University Medical Center), Phil Kingsley (Marnett laboratory) analyzed levels of AA, 2-AG, PGs, and PG-Gs in the brains of COX-2-overexpressing transgenic mice treated with JZL 184, a selective inhibitor of MAGL (166) (the major 2-AG hydrolase in the brain) (72). Consistent with literature reports of its activity, JZL 184 reduced levels of AA and elevated levels of 2-AG in the brains of both wild-type and COX-2 transgenic mice. Interestingly, PG-Gs (specifically PGD_2-G, PGE_2-G, and $PGF_{2\alpha}$-G) were only detected in the JZL 184-treated COX-2 transgenic mice, and these products were eliminated upon co-administration of the COX-2-selective inhibitor lumiracoxib. These unpublished studies are illuminated by our *in vitro* and cellular work and, collectively, the data suggest insight into the potential physiological detection and role of PG-Gs might be gained through the study of tissues/organs expressing high levels of COX-2 (either basally or induced) and low levels of AA.

Third, the systems-level methodology developed here for understanding interactions between the two COX-2 subunits and the substrates AA and 2-AG is more broadly applicable to the study of multimeric enzymes in general. Our computational biology collaborator in this study, Erin Shockley (Carlos F. Lopez laboratory, Vanderbilt University), recently published the computational details of this novel method that was pioneered using COX-2 as a case study model enzyme (167). The methodology enables analysis of any reaction network in which there are multiple competing interactions. Currently, the Lopez laboratory is using the data gathered from our studies with COX-2, AA, and 2-AG, and the corresponding interactions model (CORM), for probabilistic network pathways analyses; these studies analyze the flux of a given substrate through a system. Results from this work may shed light on methods that may be used to modulate network activity toward a desired product and thus have relevance for drug target design.

While the described work has revealed much about how substrates can allosterically regulate COX-2, the structural basis for this regulation remains unknown. This question is not only important for understanding how substrates allosterically interact with COX-2, but also for understanding how compounds like 13-methylarachidonic acid potentiate 2-AG oxygenation and various inhibitors prevent AA and/or 2-AG oxygenation (87). Some insight into this question is provided by X-ray crystal structures of COX generated using substoichiometric amounts of NSAIDs in which inhibitor is only bound to one subunit of the enzyme (84, 168). The structures reveal movement of amino acid residues 121-129 upon inhibitor binding. As these residues are positioned at the dimer interface, the data

suggest that cross-talk between COX subunits might be occurring there. Our lab has generated some COX-2 enzymes with site-directed mutations of residues involved in subunit-subunit interactions, including Gln372, Gln374, and Tyr544, and we are currently assessing the effect of those mutations on ligand (substrate, potentiator, or inhibitor) binding.

In the broader context of inflammation, our results suggest that substrates, as well as inhibitors and non-substrate fatty acids, can compete for both the catalytic and allosteric sites of COX-2. From a clinical perspective, this could mean that under settings of high substrate release, NSAIDs might not be as effective as anticipated. Additionally, the identified role of 2-AG in potentiating AA turnover suggests that increasing endocannabinoid tone, particularly through monoacylglycerol lipase inhibition, might also modulate PG production and thus the extent of inflammatory response in that tissue. These data also suggest that the physiological consequences of such drugs as giripladib may not only be due to inhibition of AA release, but also to the relatively uncharacterized action of various PG-G species. Collectively, our findings along with those of Smith and colleagues suggest that changes in fatty acid and fatty acid derivatives in the cellular milieu may greatly affect the ratio of products produced in inflammation and NSAID potency. Differences in the cellular lipid composition may help account for the differential effects of NSAIDs among the general public.

Significance and Future Directions (Part B)

In Chapter III, I demonstrated that M_1dG in dsDNA is converted to 6-oxo-M_1dG by rat liver or cellular nuclear lysates via direct enzymatic oxidation. Studies with cofactors and inhibitors, both *in vitro* and in intact cells, suggest that the responsible enzyme(s) belong to the family of Fe(II)/α-KG-dependent enzymes. Though the identity of the M_1dG oxidase remains unknown, several notable steps have been made toward that goal.

First, by determining the family (Fe(II)/α-KG-dependent) to which the responsible enzyme(s) belong, we have substantially narrowed the pool of candidates. Of the 200+ annotated nuclear oxidases, only about 40 of them are Fe(II)/α-KG-dependent enzymes. Therefore, identification of the major class to which the enzyme(s) belong made the direct testing techniques (described herein) feasible. These studies also uncovered important enzyme cofactors. If future efforts to identify the protein involve direct purification attempts, incorporation of these cofactors into the purification and/or assay buffers may be important for maintaining enzyme activity.

Second, we have developed a direct, photoaffinity probe-based method for identification of the target enzyme(s). In collaboration with the VICB Chemical Synthesis Core, we have made DR025, a photoaffinity probe for detection of Fe(II)/α-KG-dependent enzymes (164), and validated it in our own hands. Furthermore, we have designed and implemented competition experiments in which both DR025 and M_1dG-containing dsDNA were incubated with cellular nuclear lysates. Initial results revealed a reduction in DR025 binding of select

proteins in the presence of increasing concentrations of M_1dG-containing dsDNA. A SILAC-based experiment designed to identify and quantify these proteins revealed several DNA and/or RNA-binding proteins that will now be validated by repeat experiment and/or western blot. Furthermore, the probe-competitor-type experiment employed here is, at least in theory, also applicable for the identification of substrates, including DNA adducts or amino acid posttranslational modifications, of other Fe(II)/α-KG-dependent enzymes.

Although 6-oxo-M_1dG has been detected in genomic DNA isolated from multiple cell lines, detection of the adduct *in vivo* has not yet been reported. Recently, however, Bin Ma (Irina Stepanov laboratory, University of Minnesota) presented data regarding a new method he had developed for simultaneous detection of M_1dG and 6-oxo-M_1dG in human leukocyte DNA. Sample analysis revealed the presence of both adducts, at comparable levels, in human leukocyte DNA. These unpublished findings support our cellular findings and provide impetus to our current efforts to understand 6-oxo-M_1dG formation and its functional consequences.

As aforementioned, when opposite dC in duplex DNA, M_1dG ring-opens to form the less mutagenic adduct, N^2-(3-oxo-1-propenyl)-dG (115-118, 169). The structure of 6-oxo-M_1dG renders such analogous ring-opening unlikely. The addition of an oxygen atom to M_1dG also adds steric bulk to the adduct, potentially making replication bypass even more difficult. Furthermore, unlike the AlkB oxidation product of M_1dG, which decomposes to dG (125), 6-oxo-M_1dG appears

stable over time (126). Therefore, we hypothesize that 6-oxo-M_1dG may be more mutagenic than M_1dG.

In order to characterize the mutagenic potential of 6-oxo-M_1dG, we are collaborating with Plamen Christov (VICB Chemical Synthesis Core) to generate oligonucleotides with site-specifically incorporated 6-oxo-M_1dG adducts. *In vitro* replication bypass assays will be performed to assess the efficiency and fidelity with which different Y-family polymerases, which play a role in the mutation spectrum of M_1dG (115, 170), perform translesion synthesis on DNA templates containing 6-oxo-M_1dG. These experiments will be executed in collaboration with the Fred Guengerich laboratory, which has published extensively in this area and with whom we previously collaborated for analysis of M_1dG mutagenicity (171-173). In addition, studies in *E. coli* will be performed to determine the cellular mutagenicity of 6-oxo-M_1dG; these experiments will be completed in the John Essigman laboratory (Massachusetts Institute of Technology) using their previously optimized competitive replication of adduct bypass (CRAB) and restriction endonuclease and postlabeling (REAP) assays (174).

In conclusion, our finding that M_1dG is oxidized to 6-oxo-M_1dG is, to our knowledge, the first example of enzymatic oxidation of an exocyclic DNA adduct in genomic DNA that results in a unique, stable adduct. Thus, this finding has led to a series of questions which we now seek to answer: What is the effect of this enzymatic transformation on DNA replication and adduct turnover/repair? Are other similar adducts affected in an analogous fashion? What enzyme(s) are involved and how are they recruited to the sites of damage? If, as we

hypothesize, M_1dG oxidation represents “activation” of a DNA adduct, we may be able to provide new insight into how lipid and DNA peroxidation resulting from an inflammatory response can give rise not only to initial mutations but also to potentially more mutagenic species via endogenous oxidative activation. Conversely, if enzymatic oxidation represents a cellular attempt to repair DNA adducts such as M_1dG, we may uncover novel enzymes or novel functions of enzymes important for preventing mutations. In either case, such enzymes, especially if they act on multiple DNA adduct substrates, might be viable targets for therapeutic intervention.

REFERENCES

1. Ricciotti E & FitzGerald GA (2011) Prostaglandins and inflammation. *Arterioscler Thromb Vasc Biol* 31(5):986-1000.

2. Taghizadeh K*, et al.* (2008) Quantification of DNA damage products resulting from deamination, oxidation and reaction with products of lipid peroxidation by liquid chromatography isotope dilution tandem mass spectrometry. *Nat Protoc* 3(8):1287-1298.

3. Funk CD (2001) Prostaglandins and leukotrienes: advances in eicosanoid biology. *Science* 294(5548):1871-1875.

4. Lee SH*, et al.* (1992) Selective expression of mitogen-inducible cyclooxygenase in macrophages stimulated with lipopolysaccharide. *The Journal of biological chemistry* 267(36):25934-25938.

5. Tsatsanis C, Androulidaki A, Venihaki M, & Margioris AN (2006) Signalling networks regulating cyclooxygenase-2. *Int J Biochem Cell Biol* 38(10):1654-1661.

6. Eliopoulos AG, Dumitru CD, Wang CC, Cho J, & Tsichlis PN (2002) Induction of COX-2 by LPS in macrophages is regulated by Tpl2-dependent CREB activation signals. *EMBO J* 21(18):4831-4840.

7. Vane JR (1971) Inhibition of prostaglandin synthesis as a mechanism of action for aspirin-like drugs. *Nature New Biology* 231:232-235.

8. Langenbach R, Loftin C, Lee C, & Tiano H (1999) Cyclooxygenase knockout mice: models for elucidating isoform-specific functions. *Biochem Pharmacol* 58(8):1237-1246.

9. Rossi F (1986) The O2- -forming NADPH oxidase of the phagocytes: nature, mechanisms of activation and function. *Biochimica et biophysica acta* 853(1):65-89.

10. Marletta MA (1988) Mammalian synthesis of nitrite, nitrate, nitric oxide, and N-nitrosating agents. *Chem Res Toxicol* 1(5):249-257.

11. Radi R, Beckman JS, Bush KM, & Freeman BA (1991) Peroxynitrite-induced membrane lipid peroxidation: the cytotoxic potential of superoxide and nitric oxide. *Arch Biochem Biophys* 288(2):481-487.

12. Ferrer-Sueta G & Radi R (2009) Chemical biology of peroxynitrite: kinetics, diffusion, and radicals. *ACS Chem Biol* 4(3):161-177.

13. Porter NA, Caldwell SE, & Mills KA (1995) Mechanisms of free radical oxidation of unsaturated lipids. *Lipids* 30(4):277-290.

14. Liebler DC (1993) The role of metabolism in the antioxidant function of vitamin E. *Crit Rev Toxicol* 23(2):147-169.

15. Hamberg M & Samuelsson B (1973) Detection and isolation of an endoperoxide intermediate in prostaglandin biosynthesis. *Proceedings of the National Academy of Sciences of the United States of America* 70(3):899-903.

16. Hamberg M, Svensson J, Wakabayashi T, & Samuelsson B (1974) Isolation and structure of two prostaglandin endoperoxides that cause platelet aggregation. *Proceedings of the National Academy of Sciences of the United States of America* 71(2):345-349.

17. Nugteren DH & Hazelhof E (1973) Isolation and properties of intermediates in prostaglandin biosynthesis. *Biochimica et biophysica acta* 326(3):448-461.

18. Laneuville O*, et al.* (1995) Fatty acid substrate specificities of human prostaglandin-endoperoxide H synthase-1 and -2. Formation of 12-hydroxy-(9Z, 13E/Z, 15Z)- octadecatrienoic acids from alpha-linolenic acid. *The Journal of biological chemistry* 270(33):19330-19336.

19. Kozak KR, Rowlinson SW, & Marnett LJ (2000) Oxygenation of the endocannabinoid, 2-arachidonylglycerol, to glyceryl prostaglandins by cyclooxygenase-2. *The Journal of biological chemistry* 275(43):33744-33749.

20. Yu M, Ives D, & Ramesha CS (1997) Synthesis of prostaglandin E2 ethanolamide from anandamide by cyclooxygenase-2. *The Journal of biological chemistry* 272(34):21181-21186.

21. Prusakiewicz JJ, Kingsley PJ, Kozak KR, & Marnett LJ (2002) Selective oxygenation of N-arachidonylglycine by cyclooxygenase-2. *Biochem Biophys Res Commun* 296(3):612-617.

22. Xie WL, Chipman JG, Robertson DL, Erikson RL, & Simmons DL (1991) Expression of a mitogen-responsive gene encoding prostaglandin synthase is regulated by mRNA splicing. *Proceedings of the National Academy of Sciences of the United States of America* 88(7):2692-2696.

23. Kujubu DA, Fletcher BS, Varnum BC, Lim RW, & Herschman HR (1991) TIS10, a phorbol ester tumor promoter-inducible mRNA from Swiss 3T3 cells, encodes a novel prostaglandin synthase/cyclooxygenase homologue. *The Journal of biological chemistry* 266(20):12866-12872.

24. O'Banion MK, Winn VD, & Young DA (1992) cDNA cloning and functional activity of a glucocorticoid-regulated inflammatory cyclooxygenase. *Proceedings of the National Academy of Sciences of the United States of America* 89(11):4888-4892.

25. Arber N*, et al.* (2006) Celecoxib for the prevention of colorectal adenomatous polyps. *N Engl J Med* 355(9):885-895.

26. Baron JA*, et al.* (2006) A randomized trial of rofecoxib for the chemoprevention of colorectal adenomas. *Gastroenterology* 131(6):1674-1682.

27. Bertagnolli MM*, et al.* (2006) Celecoxib for the prevention of sporadic colorectal adenomas. *N Engl J Med* 355(9):873-884.

28. Bresalier RS*, et al.* (2005) Cardiovascular events associated with rofecoxib in a colorectal adenoma chemoprevention trial. *N Engl J Med* 352(11):1092-1102.

29. Solomon SD*, et al.* (2005) Cardiovascular risk associated with celecoxib in a clinical trial for colorectal adenoma prevention. *N Engl J Med* 352(11):1071-1080.

30. Picot D, Loll PJ, & Garavito RM (1994) The X-ray crystal structure of the membrane protein prostaglandin H2 synthase-1. *Nature* 367(6460):243-249.

31. Kurumbail RG*, et al.* (1996) Structural basis for selective inhibition of cyclooxygenase-2 by anti-inflammatory agents. *Nature* 384(6610):644-648.

32. Luong C*, et al.* (1996) Flexibility of the NSAID binding site in the structure of human cyclooxygenase-2. *Nat Struct Biol* 3(11):927-933.

33. Smith WL, Garavito RM, & DeWitt DL (1996) Prostaglandin endoperoxide H synthases (cyclooxygenases)-1 and -2. *The Journal of biological chemistry* 271(52):33157-33160.

34. Kulmacz RJ & Lands WE (1984) Prostaglandin H synthase. Stoichiometry of heme cofactor. *The Journal of biological chemistry* 259(10):6358-6363.

35. Van der Ouderaa FJ, Buytenhek M, Nugteren DH, & Van Dorp DA (1977) Purification and characterization of prostaglandin endoperoxide synthetase from sheep vesicular glands. *Biochimica et biophysica acta* 487(2):315-331.

36. van der Ouderaa FJ, Buytenhek M, Slikkerveer FJ, & van Dorp DA (1979) On the haemoprotein character of prostaglandin endoperoxide synthetase. *Biochimica et biophysica acta* 572(1):29-42.

37. Vecchio AJ, Simmons DM, & Malkowski MG (2010) Structural basis of fatty acid substrate binding to cyclooxygenase-2. *The Journal of biological chemistry* 285(29):22152-22163.

38. Spencer AG, Woods JW, Arakawa T, Singer, II, & Smith WL (1998) Subcellular localization of prostaglandin endoperoxide H synthases-1 and -2 by immunoelectron microscopy. *The Journal of biological chemistry* 273(16):9886-9893.

39. Van D, Beerthuis RK, Nugteren DH, & Vonkeman H (1964) The biosynthesis of prostaglandins. *Biochimica et biophysica acta* 90:204-207.

40. Bergstroem S, Danielsson H, & Samuelsson B (1964) The enzymatic formation of prostaglandin E2 from arachidonic acid. Prostaglandins and related factors 32. *Biochimica et biophysica acta* 90:207-210.

41. Hamberg M & Samuelsson B (1967) On the mechanism of the biosynthesis of prostaglandins E-1 and F-1-alpha. *The Journal of biological chemistry* 242(22):5336-5343.

42. Hamberg M & Samuelsson B (1967) Oxygenation of unsaturated fatty acids by the vesicular gland of sheep. *The Journal of biological chemistry* 242(22):5344-5354.

43. Samuelsson B (1965) On the incorporation of oxygen in the conversion of 8, 11, 14-eicosatrienoic acid to prostaglandin E1. *J Am Chem Soc* 87:3011-3013.

44. Marnett LJ (2000) Cyclooxygenase mechanisms. *Curr Opin Chem Biol* 4(5):545-552.

45. Koppenol WH, Moreno JJ, Pryor WA, Ischiropoulos H, & Beckman JS (1992) Peroxynitrite, a cloaked oxidant formed by nitric oxide and superoxide. *Chem Res Toxicol* 5(6):834-842.

46. Landino LM, Crews BC, Timmons MD, Morrow JD, & Marnett LJ (1996) Peroxynitrite, the coupling product of nitric oxide and superoxide, activates prostaglandin biosynthesis. *Proceedings of the National Academy of Sciences of the United States of America* 93(26):15069-15074.

47. Marnett LJ, Wright TL, Crews BC, Tannenbaum SR, & Morrow JD (2000) Regulation of prostaglandin biosynthesis by nitric oxide is revealed by targeted deletion of inducible nitric-oxide synthase. *The Journal of biological chemistry* 275(18):13427-13430.

48. Markey CM, Alward A, Weller PE, & Marnett LJ (1987) Quantitative studies of hydroperoxide reduction by prostaglandin H synthase. Reducing substrate specificity and the relationship of peroxidase to cyclooxygenase activities. *The Journal of biological chemistry* 262(13):6266-6279.

49. Miyamoto T, Ogino N, Yamamoto S, & Hayaishi O (1976) Purification of prostaglandin endoperoxide synthetase from bovine vesicular gland microsomes. *The Journal of biological chemistry* 251(9):2629-2636.

50. Dietz R, Nastainczyk W, & Ruf HH (1988) Higher oxidation states of prostaglandin H synthase. Rapid electronic spectroscopy detected two spectral intermediates during the peroxidase reaction with prostaglandin G2. *Eur J Biochem* 171(1-2):321-328.

51. Karthein R, Dietz R, Nastainczyk W, & Ruf HH (1988) Higher oxidation states of prostaglandin H synthase. EPR study of a transient tyrosyl radical in the enzyme during the peroxidase reaction. *Eur J Biochem* 171(1-2):313-320.

52. Cook HW & Lands WE (1975) Evidence for an activating factor formed during prostaglandin biosynthesis. *Biochem Biophys Res Commun* 65(2):464-471.

53. Hemler ME, Cook HW, & Lands WE (1979) Prostaglandin biosynthesis can be triggered by lipid peroxides. *Arch Biochem Biophys* 193(2):340-345.

54. Hemler ME, Graff G, & Lands WE (1978) Accelerative autoactivation of prostaglandin biosynthesis by PGG2. *Biochem Biophys Res Commun* 85(4):1325-1331.

55. Kulmacz RJ (1987) Prostaglandin G2 levels during reaction of prostaglandin H synthase with arachidonic acid. *Prostaglandins* 34(2):225-240.

56. Dong L*, et al.* (2011) Human cyclooxygenase-2 is a sequence homodimer that functions as a conformational heterodimer. *The Journal of biological chemistry* 286(21):19035-19046.

57. Smith WL & Lands WE (1972) Oxygenation of polyunsaturated fatty acids during prostaglandin biosynthesis by sheep vesicular gland. *Biochemistry* 11(17):3276-3285.

58. Wu G, Vuletich JL, Kulmacz RJ, Osawa Y, & Tsai AL (2001) Peroxidase self-inactivation in prostaglandin H synthase-1 pretreated with cyclooxygenase inhibitors or substituted with mangano protoporphyrin IX. *The Journal of biological chemistry* 276(23):19879-19888.

59. Wu G, Wei C, Kulmacz RJ, Osawa Y, & Tsai AL (1999) A mechanistic study of self-inactivation of the peroxidase activity in prostaglandin H synthase-1. *The Journal of biological chemistry* 274(14):9231-9237.

60. Vanderhoek JY & Lands WE (1973) Acetylenic inhibitors of sheep vesicular gland oxygenase. *Biochimica et biophysica acta* 296(2):374-381.

61. Lecomte M, Lecocq R, Dumont JE, & Boeynaems JM (1990) Covalent binding of arachidonic acid metabolites to human platelet proteins. Identification of prostaglandin H synthase as one of the modified substrates. *The Journal of biological chemistry* 265(9):5178-5187.

62. Boutaud O*, et al.* (2001) Characterization of the lysyl adducts of prostaglandin H-synthases that are derived from oxygenation of arachidonic acid. *Biochemistry* 40(23):6948-6955.

63. Rouzer CA & Marnett LJ (2005) Structural and functional differences between cyclooxygenases: fatty acid oxygenases with a critical role in cell signaling. *Biochem Biophys Res Commun* 338(1):34-44.

64. Devane WA*, et al.* (1992) Isolation and structure of a brain constituent that binds to the cannabinoid receptor. *Science* 258(5090):1946-1949.

65. Mechoulam R*, et al.* (1995) Identification of an endogenous 2-monoglyceride, present in canine gut, that binds to cannabinoid receptors. *Biochem Pharmacol* 50(1):83-90.

66. Sugiura T*, et al.* (1995) 2-Arachidonoylglycerol: a possible endogenous cannabinoid receptor ligand in brain. *Biochem Biophys Res Commun* 215(1):89-97.

67. Matsuda LA, Lolait SJ, Brownstein MJ, Young AC, & Bonner TI (1990) Structure of a cannabinoid receptor and functional expression of the cloned cDNA. *Nature* 346(6284):561-564.

68. Munro S, Thomas KL, & Abu-Shaar M (1993) Molecular characterization of a peripheral receptor for cannabinoids. *Nature* 365(6441):61-65.

69. Kozak KR, Prusakiewicz JJ, Rowlinson SW, Schneider C, & Marnett LJ (2001) Amino acid determinants in cyclooxygenase-2 oxygenation of the endocannabinoid 2-arachidonylglycerol. *The Journal of biological chemistry* 276(32):30072-30077.

70. Bisogno T*, et al.* (2006) Development of the first potent and specific inhibitors of endocannabinoid biosynthesis. *Biochimica et biophysica acta* 1761(2):205-212.

71. Prescott SM & Majerus PW (1983) Characterization of 1,2-diacylglycerol hydrolysis in human platelets. Demonstration of an arachidonoyl-monoacylglycerol intermediate. *The Journal of biological chemistry* 258(2):764-769.

72. Blankman JL, Simon GM, & Cravatt BF (2007) A comprehensive profile of brain enzymes that hydrolyze the endocannabinoid 2-arachidonoylglycerol. *Chem Biol* 14(12):1347-1356.

73. Xie S*, et al.* (2010) Inactivation of lipid glyceryl ester metabolism in human THP1 monocytes/macrophages by activated organophosphorus insecticides: role of carboxylesterases 1 and 2. *Chem Res Toxicol* 23(12):1890-1904.

74. Kozak KR*, et al.* (2002) Metabolism of the endocannabinoids, 2-arachidonylglycerol and anandamide, into prostaglandin, thromboxane, and prostacyclin glycerol esters and ethanolamides. *The Journal of biological chemistry* 277(47):44877-44885.

75. Rouzer CA & Marnett LJ (2005) Glycerylprostaglandin synthesis by resident peritoneal macrophages in response to a zymosan stimulus. *The Journal of biological chemistry* 280(29):26690-26700.

76. Musee J & Marnett LJ (2012) Prostaglandin H synthase-2-catalyzed oxygenation of 2-arachidonoylglycerol is more sensitive to peroxide tone than oxygenation of arachidonic acid. *The Journal of biological chemistry* 287(44):37383-37394.

77. Manna JD*, et al.* (2014) Identification of the major prostaglandin glycerol ester hydrolase in human cancer cells. *The Journal of biological chemistry* 289(49):33741-33753.

78. Nirodi CS, Crews BC, Kozak KR, Morrow JD, & Marnett LJ (2004) The glyceryl ester of prostaglandin E2 mobilizes calcium and activates signal transduction in RAW264.7 cells. *Proceedings of the National Academy of Sciences of the United States of America* 101(7):1840-1845.

79. Bruser A*, et al.* (2017) Prostaglandin E2 glyceryl ester is an endogenous agonist of the nucleotide receptor P2Y6. *Sci Rep* 7(1):2380.

80. Hu SS, Bradshaw HB, Chen JS, Tan B, & Walker JM (2008) Prostaglandin E2 glycerol ester, an endogenous COX-2 metabolite of 2-arachidonoylglycerol, induces hyperalgesia and modulates NFkappaB activity. *British journal of pharmacology* 153(7):1538-1549.

81. Vecchio AJ & Malkowski MG (2011) The structural basis of endocannabinoid oxygenation by cyclooxygenase-2. *The Journal of biological chemistry* 286(23):20736-20745.

82. Dong L, Sharma NP, Jurban BJ, & Smith WL (2013) Pre-existent asymmetry in the human cyclooxygenase-2 sequence homodimer. *The Journal of biological chemistry* 288(40):28641-28655.

83. Prusakiewicz JJ, Duggan KC, Rouzer CA, & Marnett LJ (2009) Differential sensitivity and mechanism of inhibition of COX-2 oxygenation of arachidonic acid and 2-arachidonoylglycerol by ibuprofen and mefenamic acid. *Biochemistry* 48(31):7353-7355.

84. Rimon G*, et al.* (2010) Coxibs interfere with the action of aspirin by binding tightly to one monomer of cyclooxygenase-1. *Proceedings of the National Academy of Sciences of the United States of America* 107(1):28-33.

85. Yuan C*, et al.* (2009) Cyclooxygenase allosterism, fatty acid-mediated cross-talk between monomers of cyclooxygenase homodimers. *The Journal of biological chemistry* 284(15):10046-10055.

86. Duggan KC*, et al.* (2011) (R)-Profens are substrate-selective inhibitors of endocannabinoid oxygenation by COX-2. *Nature chemical biology* 7(11):803-809.

87. Kudalkar SN*, et al.* (2015) 13-Methylarachidonic acid is a positive allosteric modulator of endocannabinoid oxygenation by cyclooxygenase. *The Journal of biological chemistry* 290(12):7897-7909.

88. Diczfalusy U, Falardeau P, & Hammarstrom S (1977) Conversion of prostaglandin endoperoxides to C17-hydroxy acids catalyzed by human platelet thromboxane synthase. *FEBS Lett* 84(2):271-274.

89. VanderVeen LA, Hashim MF, Shyr Y, & Marnett LJ (2003) Induction of frameshift and base pair substitution mutations by the major DNA adduct of the endogenous carcinogen malondialdehyde. *Proceedings of the National Academy of Sciences of the United States of America* 100(24):14247-14252.

90. Mukai FH & Goldstein BD (1976) Mutagenicity of malonaldehyde, a decomposition product of peroxidized polyunsaturated fatty acids. *Science* 191(4229):868-869.

91. Basu AK & Marnett LJ (1983) Unequivocal demonstration that malondialdehyde is a mutagen. *Carcinogenesis* 4(3):331-333.

92. Yau TM (1979) Mutagenicity and cytotoxicity of malonaldehyde in mammalian cells. *Mech Ageing Dev* 11(2):137-144.

93. Spalding JW (1988) Toxicology and carcinogenesis studies of malonaldehyde, sodium salt (3-hydroxy-2-propenal, sodium salt) in F344/N rats and B6C3F1 mice. in *National Toxicology Program Technical*

Report Series (U.S. Department of Health and Human Services, Research Triangle Park, NC), pp 1-182.

94. Chaudhary AK, Reddy GR, Blair IA, & Marnett LJ (1996) Characterization of an N6-oxopropenyl-2'-deoxyadenosine adduct in malondialdehyde-modified DNA using liquid chromatography/electrospray ionization tandem mass spectrometry. *Carcinogenesis* 17(5):1167-1170.

95. Stone K, Ksebati MB, & Marnett LJ (1990) Investigation of the adducts formed by reaction of malondialdehyde with adenosine. *Chem Res Toxicol* 3(1):33-38.

96. Stone K, Uzieblo A, & Marnett LJ (1990) Studies of the reaction of malondialdehyde with cytosine nucleosides. *Chem Res Toxicol* 3(5):467-472.

97. Benamira M*, et al.* (1995) Induction of mutations by replication of malondialdehyde-modified M13 DNA in Escherichia coli: determination of the extent of DNA modification, genetic requirements for mutagenesis, and types of mutations induced. *Carcinogenesis* 16(1):93-99.

98. Dedon PC, Plastaras JP, Rouzer CA, & Marnett LJ (1998) Indirect mutagenesis by oxidative DNA damage: formation of the pyrimidopurinone adduct of deoxyguanosine by base propenal. *Proceedings of the National Academy of Sciences of the United States of America* 95(19):11113-11116.

99. Grollman AP, Takeshita M, Pillai KM, & Johnson F (1985) Origin and cytotoxic properties of base propenals derived from DNA. *Cancer Res* 45(3):1127-1131.

100. Fang JL, Vaca CE, Valsta LM, & Mutanen M (1996) Determination of DNA adducts of malonaldehyde in humans: effects of dietary fatty acid composition. *Carcinogenesis* 17(5):1035-1040.

101. Rouzer CA*, et al.* (1997) Analysis of the malondialdehyde-2'-deoxyguanosine adduct pyrimidopurinone in human leukocyte DNA by gas chromatography/electron capture/negative chemical ionization/mass spectrometry. *Chem Res Toxicol* 10(2):181-188.

102. Vaca CE, Fang JL, Mutanen M, & Valsta L (1995) 32P-postlabelling determination of DNA adducts of malonaldehyde in humans: total white blood cells and breast tissue. *Carcinogenesis* 16(8):1847-1851.

103. Kaneko H*, et al.* (1998) Inhibition of post-ischemic reperfusion injury of the kidney by diamine oxidase. *Biochimica et biophysica acta* 1407(3):193-199.

104. Munnia A*, et al.* (2006) Bronchial malondialdehyde DNA adducts, tobacco smoking, and lung cancer. *Free Radic Biol Med* 41(9):1499-1505.

105. Chaudhary AK*, et al.* (1994) Detection of endogenous malondialdehyde-deoxyguanosine adducts in human liver. *Science* 265(5178):1580-1582.

106. Pang B*, et al.* (2007) Lipid peroxidation dominates the chemistry of DNA adduct formation in a mouse model of inflammation. *Carcinogenesis* 28(8):1807-1813.

107. Cai Q, Tian L, & Wei H (1996) Age-dependent increase of indigenous DNA adducts in rat brain is associated with a lipid peroxidation product. *Exp Gerontol* 31(3):373-385.

108. Chaudhary AK, Nokubo M, Marnett LJ, & Blair IA (1994) Analysis of the malondialdehyde-2'-deoxyguanosine adduct in rat liver DNA by gas chromatography/electron capture negative chemical ionization mass spectrometry. *Biol Mass Spectrom* 23(8):457-464.

109. Jeong YC, Nakamura J, Upton PB, & Swenberg JA (2005) Pyrimido[1,2-a]-purin-10(3H)-one, M1G, is less prone to artifact than base oxidation. *Nucleic Acids Res* 33(19):6426-6434.

110. Jeong YC*, et al.* (2008) Accumulation of M1dG DNA adducts after chronic exposure to PCBs, but not from acute exposure to polychlorinated aromatic hydrocarbons. *Free Radic Biol Med* 45(5):585-591.

111. Singh R*, et al.* (2001) Lobe-specific increases in malondialdehyde DNA adduct formation in the livers of mice following infection with Helicobacter hepaticus. *Carcinogenesis* 22(8):1281-1287.

112. Bonassi S*, et al.* (2017) 3-(2-deoxy-beta-d-erythro-pentafuranosyl)pyrimido[1,2-alpha]purin-10(3H)-one deoxyguanosine adducts of workers exposed to asbestos fibers. *Toxicol Lett* 270:1-7.

113. Munnia A, Amasio ME, & Peluso M (2004) Exocyclic malondialdehyde and aromatic DNA adducts in larynx tissues. *Free Radic Biol Med* 37(6):850-858.

114. Wang M*, et al.* (1996) Lipid peroxidation-induced putative malondialdehyde-DNA adducts in human breast tissues. *Cancer Epidemiol Biomarkers Prev* 5(9):705-710.

115. Fink SP, Reddy GR, & Marnett LJ (1997) Mutagenicity in Escherichia coli of the major DNA adduct derived from the endogenous mutagen malondialdehyde. *Proceedings of the National Academy of Sciences of the United States of America* 94(16):8652-8657.

116. Mao H, Schnetz-Boutaud NC, Weisenseel JP, Marnett LJ, & Stone MP (1999) Duplex DNA catalyzes the chemical rearrangement of a malondialdehyde deoxyguanosine adduct. *Proceedings of the National Academy of Sciences of the United States of America* 96(12):6615-6620.

117. Riggins JN, Daniels JS, Rouzer CA, & Marnett LJ (2004) Kinetic and thermodynamic analysis of the hydrolytic ring-opening of the malondialdehyde-deoxyguanosine adduct, 3-(2'-deoxy-beta-D-erythro-pentofuranosyl)- pyrimido[1,2-alpha]purin-10(3H)-one. *J Am Chem Soc* 126(26):8237-8243.

118. Riggins JN, Pratt DA, Voehler M, Daniels JS, & Marnett LJ (2004) Kinetics and mechanism of the general-acid-catalyzed ring-closure of the malondialdehyde-DNA adduct, N2-(3-oxo-1-propenyl)deoxyguanosine (N2OPdG-), to 3-(2'-Deoxy-beta-D-erythro-pentofuranosyl)pyrimido[1,2-alpha]purin- 10(3H)-one (M1dG). *J Am Chem Soc* 126(34):10571-10581.

119. Johnson KA, Fink SP, & Marnett LJ (1997) Repair of propanodeoxyguanosine by nucleotide excision repair in vivo and in vitro. *The Journal of biological chemistry* 272(17):11434-11438.

120. Hoberg AM, Otteneder M, Marnett LJ, & Poulsen HE (2004) Measurement of the malondialdehyde-2'-deoxyguanosine adduct in human urine by immuno-extraction and liquid chromatography/atmospheric pressure chemical ionization tandem mass spectrometry. *J Mass Spectrom* 39(1):38-42.

121. Otteneder MB*, et al.* (2006) In vivo oxidative metabolism of a major peroxidation-derived DNA adduct, M1dG. *Proceedings of the National Academy of Sciences of the United States of America* 103(17):6665-6669.

122. Knutson CG, Skipper PL, Liberman RG, Tannenbaum SR, & Marnett LJ (2008) Monitoring in vivo metabolism and elimination of the endogenous DNA adduct, M1dG {3-(2-deoxy-beta-D-erythro-pentofuranosyl)pyrimido[1,2-alpha]purin-10(3H)-one}, by accelerator mass spectrometry. *Chem Res Toxicol* 21(6):1290-1294.

123. Knutson CG, Wang H, Rizzo CJ, & Marnett LJ (2007) Metabolism and elimination of the endogenous DNA adduct, 3-(2-deoxy-beta-D-erythropentofuranosyl)-pyrimido[1,2-alpha]purine-10(3H)-one, in the rat. *The Journal of biological chemistry* 282(50):36257-36264.

124. Akingbade D*, et al.* (2012) Selection of monoclonal antibodies against 6-oxo-M(1)dG and their use in an LC-MS/MS assay for the presence of 6-oxo-M(1)dG in vivo. *Chem Res Toxicol* 25(2):454-461.

125. Singh V*, et al.* (2014) Mechanism of repair of acrolein- and malondialdehyde-derived exocyclic guanine adducts by the alpha-

ketoglutarate/Fe(II) dioxygenase AlkB. *Chem Res Toxicol* 27(9):1619-1631.

126. Wauchope OR*, et al.* (2015) Nuclear oxidation of a major peroxidation DNA adduct, M1dG, in the genome. *Chem Res Toxicol* 28(12):2334-2342.

127. Rouzer CA*, et al.* (2006) Zymosan-induced glycerylprostaglandin and prostaglandin synthesis in resident peritoneal macrophages: roles of cyclooxygenase-1 and -2. *The Biochemical journal* 399(1):91-99.

128. Rowlinson SW, Crews BC, Lanzo CA, & Marnett LJ (1999) The binding of arachidonic acid in the cyclooxygenase active site of mouse prostaglandin endoperoxide synthase-2 (COX-2). A putative L-shaped binding conformation utilizing the top channel region. *The Journal of biological chemistry* 274(33):23305-23310.

129. McKew JC*, et al.* (2008) Indole cytosolic phospholipase A2 alpha inhibitors: discovery and in vitro and in vivo characterization of 4-{3-[5-chloro-2-(2-{[(3,4-dichlorobenzyl)sulfonyl]amino}ethyl)-1-(diphenylmethyl)-1H-indol-3-yl]propyl}benzoic acid, efipladib. *Journal of medicinal chemistry* 51(12):3388-3413.

130. Johnson KA, Simpson ZB, & Blom T (2009) Global kinetic explorer: a new computer program for dynamic simulation and fitting of kinetic data. *Analytical biochemistry* 387(1):20-29.

131. Johnson KA, Simpson ZB, & Blom T (2009) FitSpace explorer: an algorithm to evaluate multidimensional parameter space in fitting kinetic data. *Analytical biochemistry* 387(1):30-41.

132. Johnson KA (2009) Fitting enzyme kinetic data with KinTek Global Kinetic Explorer. *Methods in enzymology* 467:601-626.

133. Lopez CF, Muhlich JL, Bachman JA, & Sorger PK (2013) Programming biological models in Python using PySB. *Molecular systems biology* 9:646.

134. ter Braak C, Vrugt, JA (2008) Differential Evolution Markov Chain with snooker updater and fewer chains. *Statistics and Computing* 18(4):435-446.

135. Patil A, Huard D, & Fonnesbeck CJ (2010) PyMC: Bayesian stochastic modelling in Python. *Journal of statistical software* 35(4):1-81.

136. Eydgahi H*, et al.* (2013) Properties of cell death models calibrated and compared using Bayesian approaches. *Molecular systems biology* 9:644.

137. Geweke J (1992) *Evaluating the accuracy of sampling-based approaches to calculating posterior moments.* (Clarendon Press, Oxford).

138. Gelman AR & Rubin DB (1992) *A single series from the Gibbs sampler provides a false sense of security* (Clarendon Press, Oxford).

139. Rouzer CA*, et al.* (2006) Lipid profiling reveals arachidonate deficiency in RAW264.7 cells: structural and functional implications. *Biochemistry* 45(49):14795-14808.

140. Kingsley PJ & Marnett LJ (2003) Analysis of endocannabinoids by Ag+ coordination tandem mass spectrometry. *Analytical biochemistry* 314(1):8-15.

141. Kingsley PJ, Rouzer CA, Saleh S, & Marnett LJ (2005) Simultaneous analysis of prostaglandin glyceryl esters and prostaglandins by electrospray tandem mass spectrometry. *Analytical biochemistry* 343(2):203-211.

142. Gijon MA & Leslie CC (1999) Regulation of arachidonic acid release and cytosolic phospholipase A2 activation. *Journal of leukocyte biology* 65(3):330-336.

143. Gijon MA, Spencer DM, Siddiqi AR, Bonventre JV, & Leslie CC (2000) Cytosolic phospholipase A2 is required for macrophage arachidonic acid release by agonists that do and do not mobilize calcium. Novel role of mitogen-activated protein kinase pathways in cytosolic phospholipase A2 regulation. *The Journal of biological chemistry* 275(26):20146-20156.

144. Hirabayashi T & Shimizu T (2000) Localization and regulation of cytosolic phospholipase A(2). *Biochimica et biophysica acta* 1488(1-2):124-138.

145. Fujishima H*, et al.* (1999) Cytosolic phospholipase A2 is essential for both the immediate and the delayed phases of eicosanoid generation in mouse bone marrow-derived mast cells. *Proceedings of the National Academy of Sciences of the United States of America* 96(9):4803-4807.

146. Magrioti V & Kokotos G (2010) Phospholipase A2 inhibitors as potential therapeutic agents for the treatment of inflammatory diseases. *Expert opinion on therapeutic patents* 20(1):1-18.

147. Rouzer CA & Marnett LJ (2003) Mechanism of free radical oxygenation of polyunsaturated fatty acids by cyclooxygenases. *Chemical reviews* 103(6):2239-2304.

148. DeGroot MH & Schervish MJ (2002) *Probability and Statistics* (Addison-Wesley) Third Ed.

149. Swinney DC, Mak AY, Barnett J, & Ramesha CS (1997) Differential allosteric regulation of prostaglandin H synthase 1 and 2 by arachidonic acid. *The Journal of biological chemistry* 272(19):12393-12398.

150. Chen W, Pawelek TR, & Kulmacz RJ (1999) Hydroperoxide dependence and cooperative cyclooxygenase kinetics in prostaglandin H synthase-1 and -2. *The Journal of biological chemistry* 274(29):20301-20306.

151. Zou H*, et al.* (2012) Human cyclooxygenase-1 activity and its responses to COX inhibitors are allosterically regulated by nonsubstrate fatty acids. *Journal of lipid research* 53(7):1336-1347.

152. Dong L*, et al.* (2016) Interactions of 2-O-arachidonylglycerol ether and ibuprofen with the allosteric and catalytic subunits of human COX-2. *Journal of lipid research* 57(6):1043-1050.

153. Dong L*, et al.* (2016) Different Fatty Acids Compete with Arachidonic Acid for Binding to the Allosteric or Catalytic Subunits of Cyclooxygenases to Regulate Prostanoid Synthesis. *The Journal of biological chemistry* 291(8):4069-4078.

154. Marnett LJ (1999) Lipid peroxidation-DNA damage by malondialdehyde. *Mutat Res* 424(1-2):83-95.

155. Basu AK*, et al.* (1988) Identification of adducts formed by reaction of guanine nucleosides with malondialdehyde and structurally related aldehydes. *Chem Res Toxicol* 1(1):53-59.

156. Diel IJ*, et al.* (1992) Detection of tumor cells in bone marrow of patients with primary breast cancer: a prognostic factor for distant metastasis. *J Clin Oncol* 10(10):1534-1539.

157. Fink SP & Marnett LJ (2001) The relative contribution of adduct blockage and DNA repair on template utilization during replication of 1,N2-propanodeoxyguanosine and pyrimido. *Mutat Res* 485(3):209-218.

158. Johnson F, Pillai KM, Grollman AP, Tseng L, & Takeshita M (1984) Synthesis and biological activity of a new class of cytotoxic agents: N-(3-oxoprop-1-enyl)-substituted pyrimidines and purines. *J Med Chem* 27(8):954-958.

159. Galligan JJ*, et al.* (2017) Quantitative analysis and discovery of lysine and arginine modifications. *Anal Chem* 89(2):1299-1306.

160. Fedeles BI, Singh V, Delaney JC, Li D, & Essigmann JM (2015) The AlkB family of Fe(II)/alpha-ketoglutarate-dependent dioxygenases: repairing nucleic acid alkylation damage and beyond. *The Journal of biological chemistry* 290(34):20734-20742.

161. Rasmussen KD & Helin K (2016) Role of TET enzymes in DNA methylation, development, and cancer. *Genes Dev* 30(7):733-750.

162. Wang L*, et al.* (2013) A small molecule modulates Jumonji histone demethylase activity and selectively inhibits cancer growth. *Nat Commun* 4:2035.

163. Kruidenier L*, et al.* (2012) A selective jumonji H3K27 demethylase inhibitor modulates the proinflammatory macrophage response. *Nature* 488(7411):404-408.

164. Rotili D*, et al.* (2011) A photoreactive small-molecule probe for 2-oxoglutarate oxygenases. *Chem Biol* 18(5):642-654.

165. Beavers WN*, et al.* (2014) omega-Alkynyl lipid surrogates for polyunsaturated fatty acids: free radical and enzymatic oxidations. *J Am Chem Soc* 136(32):11529-11539.

166. Long JZ*, et al.* (2009) Selective blockade of 2-arachidonoylglycerol hydrolysis produces cannabinoid behavioral effects. *Nature chemical biology* 5(1):37-44.

167. Shockley EM, Vrugt JA, & Lopez CF (2017) PyDREAM: High-dimensional parameter inference for biological models in Python. *Bioinformatics*.

168. Sidhu RS, Lee JY, Yuan C, & Smith WL (2010) Comparison of cyclooxygenase-1 crystal structures: cross-talk between monomers comprising cyclooxygenase-1 homodimers. *Biochemistry* 49(33):7069-7079.

169. Hashim MF*, et al.* (2004) In vitro bypass of malondialdehyde-deoxyguanosine adducts: differential base selection during extension by the Klenow fragment of DNA polymerase I is the critical determinant of replication outcome. *Biochemistry* 43(37):11828-11835.

170. Walsh JM, Hawver LA, & Beuning PJ (2011) Escherichia coli Y family DNA polymerases. *Front Biosci (Landmark Ed)* 16:3164-3182.

171. O'Flaherty DK & Guengerich FP (2014) Steady-state kinetic analysis of DNA polymerase single-nucleotide incorporation products. *Curr Protoc Nucleic Acid Chem* 59:7 21 21-13.

172. Maddukuri L*, et al.* (2010) In vitro bypass of the major malondialdehyde- and base propenal-derived DNA adduct by human Y-family DNA polymerases kappa, iota, and Rev1. *Biochemistry* 49(38):8415-8424.

173. Stafford JB*, et al.* (2009) Translesion DNA synthesis by human DNA polymerase eta on templates containing a pyrimidopurinone deoxyguanosine adduct, 3-(2'-deoxy-beta-d-erythro-pentofuranosyl)pyrimido-[1,2-a]purin-10(3H)-one. *Biochemistry* 48(2):471-480.

174. Delaney JC & Essigmann JM (2006) Assays for determining lesion bypass efficiency and mutagenicity of site-specific DNA lesions in vivo. *Methods in enzymology* 408:1-15.